# Mechanisms of early hemato-endothelial development from human pluripotent stem cells

A DISSERTATION
SUBMITTED TO
THE FACULTY OF THE GRADUATE SCOOL
OF THE UNIVERSITY OF MINNESOTA
BY

Mathew George Angelos

IN PARTIAL FULFILLMENT OF THE REQUIREMENTS
FOR THE DEGREE OF
DOCTOR OF PHILOSOPHY

Dan S. Kaufman, MD, PhD, Advisor

September 2016

**Acknowledgements**

There are many people that I would like to thank who have altruistically contributed to my growth as a physician-scientist. First, I thank my advisor, Dan Kaufman, for providing me the tools, guidance, and opportunity to carry out my graduate studies. Dan allowed me to explore my own interests in hematology. He has been open and supportive to every new endeavor that I wished to pursue, and has been patient in allowing me to make (many) mistakes as a part of the scientific process. Dan always challenged me to be critical about my research and, in the process, made me a better scientist.

I would especially like to thank Mike Verneris for also playing an active role in my training and stepping in to support me when I needed it. Mike has an unparalleled inquisitiveness and enthusiasm for discovery, and I have thoroughly enjoyed our engaging scientific and personal conversations. I would also like to thank Jakub Tolar and Chris Pennell for serving on my thesis committee and especially for their help in crafting my pre-doctoral fellowship.

I also thank George Truskey (Duke) and Elise Kohn (NIH). George graciously allowed me to work in his lab as a freshman in college and discover what high-level science was all about. Elise opened my eyes to what a career as a physician-scientist was really like. I certainly would have never made it to this point without their initial support.

I thank the members of both the Kaufman and Verneris labs for providing a positive working environment. Thanks to Patrick Ferrell in helping me get started and George Scaria for his assistance along the way. Thanks to Laura Bendzick and Caitlin Ryan for their help and friendship. I also want acknowledge all the undergraduate students

(especially Paige Ruh) that have assisted me in my research efforts. One of my goals is to be an effective mentor and educator, so I hope I was able to impart some useful advice as you continue on your own endeavors.

I thank the Medical Scientist Training Program (especially Yoji Shimizu, Pete Bitterman, Marshall Hertz, Susan Shurson, and Nick Berg) for their help throughout this process. The MiCAB program (Steve Jameson, Louise Shand) has been equally supportive. Special thanks to Dr. Peter Southern, who always had nothing but positive words of support and reassurance since the start of medical school.

Lastly, I would like to thank all my colleagues in the MSTP and MiCAB programs for your comradery, advice, and encouragement. And, to Steve, you're pretty great.

## Dedication

This thesis is dedicated to my mother, Susan, and my father, Albert.

Thank you for your love and support as I follow my crazy dreams.

## Abstract

Hemogenic endothelium is a highly specialized population of vascular endothelial cells that produces hematopoietic stem cells (HSCs) during embryonic development. This process, referred to as the endothelial-to-hematopoietic transition (EHT), is critical to establish a functional hematopoietic system that persists throughout adulthood. The underlying genetic and cell signaling mechanisms that regulate human EHT remain poorly defined. Human pluripotent stem cells, including embryonic stem cells (hESCs) and induced pluripotent stem cells (hiPSCs) provide a well-defined cellular platform that can be used to study these mechanisms. In this work, functional human hemogenic endothelium was identified and isolated from the earliest hemato-endothelial cells differentiated from hESCs. Analysis of hemogenic endothelial cells at a single-cell resolution found hESC-derived hemogenic endothelium was transcriptionally distinct from vascular endothelial cells lacking hematopoietic potential. Novel genetic markers distinguishing human hemogenic endothelium are also presented. Contributions from the aryl hydrocarbon receptor (AHR), an important cell signaling molecule in HSC biology, were also assessed at the level of human EHT. Small molecule inhibition and gene deletion of *AHR* significantly improved functional hematopoietic stem and progenitor cell development from hESCs. Importantly, a novel role for AHR in the development of hESC-derived innate lymphoid cells is also presented. Collectively, this dissertation identifies and describes key transcriptional and signaling mechanisms that support human EHT. This information will be useful to optimize the development of HSCs and other hematopoietic lineages that are suitable for future clinical application.

## Table of Contents

## List of Tables

## List of Figures

**Disclosure of Publications and Author Contributions**

The work presented in this dissertation is a compilation of previously published manuscripts, manuscripts under peer-review at the time of submission, and manuscripts to be submitted for publication. Chapters of this dissertation have been modified, reformatted, and/or adapted from the following manuscripts. Versions of the finalized manuscripts can be referenced in the proceeding citations:

1. **Angelos MG**, Kidwai F, and, Kaufman DS. 2014. Pluripotent Stem Cells and Gene Therapy. In Jeffrey Laurence, ed. *Translating Gene Therapy to the Clinic.* Elsevier Press.

   M.G.A. designed, wrote, and edited the manuscript; F.K. wrote the manuscript, D.S.K. edited the manuscript.

2. **Angelos MG** and Kaufman DS. Advancements in pluripotent stem cell applications for regenerative medicine. *Current Opinion in Organ Transplantation.* 2015 Dec; 20(6): 663-70. PMCID: PMC4635470.

   M.G.A. designed, wrote, and edited the manuscript; D.S.K. edited the manuscript.

3. **Angelos MG**, Ruh P, Webber B, Ryan C, Bendzick LB, Verneris MR, and Kaufman DS. Aryl hydrocarbon receptor antagonism promotes early hemato-lymphoid development from human pluripotent stem cells. 2016 July. *In revision. (Blood).*

   M.G.A. designed the experimental plan, performed the experiments, analyzed the data, and wrote the manuscript; B.R.W. designed the CRISPR gRNA and performed hESC nucleofection; P.R., C.R. and L.B. performed the experiments and provided technical assistance; M.R.V edited the manuscript, and D.S.K. designed the experimental plan, wrote, and edited the manuscript. We thank Anna Kim for technical assistance and Jason Motl and the University of Minnesota Flow Cytometry Core Facility for assistance with FACS.

4. **Angelos MG,** Abrahante JE, and Kaufman DS. Single-cell resolution of human hemato-endothelial cells reveals distinct transcriptional signatures of hemogenic endothelium. 2016 September. *Submitted (eLife).*

   M.G.A. designed the experimental plan, performed the experiments, analyzed the data, and wrote the manuscript; J.E.A. formatted the data for analysis and edited the manuscript; D.S.K. designed the experimental plan, wrote, and edited the manuscript. We thank Jerry Daniel and the University of Minnesota Genomics Core for assistance with the Fluidgm C1 capture experiments and single-cell RNASeq. We also thank Gene Yeo (UCSD) for the helpful discussions.

# CHAPTER 1

## *Background and Significance:*

## *Human hematopoietic development and hemato-endothelial differentiation from human pluripotent stem cells*

**Overview of hematopoiesis and the birth of hematopoietic stem cells**

Hematopoiesis (αίμα: blood; ποιέω: to make) is a multi-factorial process that consists of temporally and spatially ordered phases over the course of human development. The first phase, termed the "primitive wave," occurs exclusively within the extraembryonic yolk sac and is the only site of hematopoietic development between days 21-28 of human gestation[1–3]. Primitive hematopoiesis begins with the differentiation of mesodermal cells into progenitor cells that are bi-potent for hematopoietic and/or endothelial fates[4]. These primitive cells are referred to as hemangioblasts. When hemangioblasts differentiate, they form luminal outpouches into the exocoelomic cavity classified as blood islands[2]. The blood islands house the earliest hematopoietic cells prior to the development of the embryological vasculature network.

Primitive hematopoiesis is largely dominated by the development of a transient population of immature erythroid cells enriched for the expression of embryonic globin genes, such as ε- and γ-globin[3]. In the mouse, these cells are termed primitive erythroid colony-forming cells ($Ery^P$-CFC) due to their ability to form colonies of large nucleated erythroid cells in semi-solid media culture. Importantly, $Ery^P$-CFCs quickly expand within the conceptus between embryological day (E) 7.25-8.25, but cease to exist after E9.0. These findings led to the consensus that primitive hematopoiesis is a transient wave of hematopoietic development and simply functions to generate oxygen-carrying erythroid cells to meet the high metabolic demands of embryogenesis[4]. Furthermore, while there is an abundance of $Ery^P$-CFC within the blood islands, significant numbers of megakaryocytic (Meg-CFC) and macrophage (Mac-CFC) colony-forming cells of

undefined function have also been identified[2]. This led to the idea that a short-lived, multipotent hematopoietic stem cell with limited self-renewal capability (termed ST-HSC) exists within blood islands, but are not able to support the entire range of hematopoietic cell phenotypes found in the mature adult.

Definitive hematopoiesis occurs as a second phase after the onset of primitive hematopoiesis. In mice, definitive hematopoiesis begins at E11.0, while in humans this process begins on Day 28[5]. In both species, hematopoietic stem cells (HSCs) with 1) the ability to differentiate into every terminal hematopoietic cell phenotype, and 2) the ability to permanently engraft into an immunodeficient mouse model, is the hallmark of definitive hematopoiesis. HSCs arise directly from specialized vascular beds of endothelial cells referred to as hemogenic endothelium (HE). HE was first characterized from the ventral wall of the dorsal aorta-gonad-mesonephros (AGM) region[6–8], but has secondarily been identified from the placental vasculature bed[9–11], vitelline arteries[12–14], and umbilical arteries[13,15,16]. In these sites, HE undergo a specialized process known as the endothelial-to-hematopoietic transition (EHT). Live-cell *in vivo* imaging studies in both the mouse and zebrafish AGM using reporter genes to trace hematopoietic cells provided direct evidence of a phenotypic switch from adherent endothelium to non-adherent hematopoietic cells[17–19]. These newly appearing cells were found to directly bud off from HE and enter the systemic circulation. On a molecular level, there are several gene and signaling networks that contribute to EHT (described below). Macroscopically, EHT is thought to, in part, be initiated by the onset of blood flow within the developing embryo. At the AGM, HE can sense fluid shear stress associated with blood flow, which in turn stimulates HSC

development[20–23]. This is induced by the upregulation of nitric oxide (NO) as a consequence of biomechanical stimulation, which has also been correlated to HSC specification[21,23]. Indeed, studies investigating definitive hematopoiesis using heartbeat-less mouse and zebrafish models (*Ncx1*$^{-/-}$) have demonstrated a dramatic reduction in hematopoietic clusters sprouting from the AGM[24]. Once initial HSCs emerge, they are carried within the circulation for further expansion and differentiation to the fetal liver (FL), thymus, spleen, and ultimately to the bone marrow where life-long hematopoiesis occurs[25].

**Regulatory mechanisms of the endothelial-to-hematopoietic transition (EHT) from hemogenic endothelium**

The specification of functional HSCs from HE is a multifactorial process dependent on intrinsic gene expression and extracellular cues provided by the developing hematopoietic niche. The Notch signaling pathway has emerged as a major regulator of EHT and definitive hematopoiesis[26–29]. In brief, Notch signaling consists of four distinct Notch receptors (Notch 1-4), of which only Notch 1 and 4 contribute to definitive hematopoietic development[30,31]. These transmembrane receptors bind and respond to Delta (DLL1, DLL3, DLL4) or Jagged (JAG1, JAG2) ligand families presented on neighboring cells. This interaction triggers cleavage of the intracellular Notch domain (Nicd), which then translocates to the nucleus and heterodimerizes with recombining binding protein suppressor kappa (RBPjκ), that then functions as a transcription factor for many key hematopoietic genes[32]. AGM explants from *Notch1*$^{-/-}$ embryos were found to have reduced

hemato-endothelial potential as measured by colony-forming assays, but did not entirely abrogate HSC production[30]. This suggests that other complementary, Notch-independent pathways are also involved in EHT.

One of the most important hematopoietic transcription factors regulated by Notch signaling is RUNX1. Overexpression of RUNX1 in both zebrafish and mouse Notch signaling mutants rescues HSC development within the AGM[33,34]. This finding supports that RUNX1 is, in part, directly regulated by Notch. RUNX1 has been referred to as the "master regulator" of definitive hematopoietic development[35]. *RUNX1* is expressed in virtually all HSCs[36–40], HE residing in the AGM[41], and also some mesodermal progenitor cells[42]. In *Runx1*$^{-/-}$ embryos, primitive hematopoiesis develops normally, however, mid-gestational lethality arises due to a complete loss of AGM and subsequent HSC formation[41,43,44]. The requirement for RUNX1 in EHT has been best demonstrated in studies using a *Runx1* conditional knockout under the control of a tamoxifen-inducible VE-cadherin (endothelial cell-specific) Cre recombinase[37,45]. In this system, *Runx1* was not expressed in any blood cell where Cre recombinase was activated, confirming that RUNX1 was required for definitive blood formation. Furthermore, *Runx1* expression was redundant for hematopoietic stem and progenitor cell (HSPC) functionality once they initially formed from HE[37]. Similar function of RUNX1 in EHT has been further validated by Swiers, *et al*.[46] at the single cell level. Using a GFP-reporter mouse of *Runx1* gene expression, they demonstrated *Runx1*$^{+}$ HSCs arise directly from *Runx1*$^{+}$ HE. Moreover, *Runx1*$^{-}$ endothelial cells did not support a hemogenic program and failed to produce hematopoietic cells.

Together, these studies confirm the activity of RUNX1 is crucial for the establishment of a definitive hematopoietic program in vertebrate systems.

The *RUNX1* gene consists of two promoters: a distal (P1) promoter and proximal (P2) promoter that are separated by 160 kb. An evolutionarily conserved intra-promoter +23 hematopoietic enhancer sequence is necessary for *RUNX1* transcription[47]. The P1 promoter transcribes the *RUNX1c* isoform and encodes a 19-amino acid longer protein at the N-terminus, currently of unknown function. The P2 promoter transcribes the shorter *RUNX1a/b* isoform. Interestingly, each promoter has differential activity dependent on the phase of hematopoiesis[47–49]. The P2 promoter is first active in yolk sac mesoderm and is required for embryonic viability by inducing primitive hematopoietic programs. The P1 promoter becomes active later in development and is highly enriched within HSCs and definitive hematopoietic progenitor cells[38,40]. As such, acquisition of P1 promoter activity can be used as a "genetic switch" in tracking the exact moment when EHT begins.

The +23 *RUNX1* enhancer serves as a *cis*-regulatory element for several transcription factors with key roles in EHT[36]. Three prominent motifs include GATA, ETS, and E-BOX, which possess recognition sites for GATA2, FLI1 and SCL/TAL1, respectively[50]. *GATA2* functions similarly to *RUNX1* in that it is also, in part, driven by Notch1 activity. Haploinsufficiency of *Gata2* significantly decreases the total number of HSCs derived from the AGM and complete *Gata2* knockout results in lethality due to a lack of HSC production[51–54]. Recent evidence from the zebrafish model suggests that within HE, *gata2b* (a form of GATA2 that is restricted to HE exclusively in zebrafish) is required to initiate the expression of *runx1* in a Notch-dependent fashion[55]. *Fli1* functions

upstream of both *Gata2* and *Runx1*, and is one of the earliest genes expressed in the specification of HE[56]. *Fli1* expression is enriched within the AGM simultaneously as *Runx1* and is also observed in newly developed hematopoietic progenitors[57,58]. *Fli1*-deficient embryos generate almost identical phenotypes as *Runx1*-deficient and *Gata2*-deficient embryos, thus highlighting its important role in vascular and hematopoietic specification[59]. SCL/TAL1 also functions upstream of RUNX1 activity, however its role in definitive hematopoiesis is less clear[56]. SCL/TAL1 appears to be important for both primitive and definitive hematopoietic development, as *Scl*/*Tal1* knockouts fail to produce any hematopoietic cells, including primitive erythrocytes[60–62]. Furthermore, mesodermal progenitor cells lacking *Scl/Tal1* expression failed in forming blast colonies in methylcellulose assays, further indicating its crucial role in the establishment of functional HE [63].

Two families of homeobox proteins (Hox and Sox) have also been implicated in EHT. In particular, HOXA3 is an important negative regulator of mouse definitive hematopoiesis. Overexpression of *HoxA3* is associated with repression of *Runx1* and other hematopoietic-specific genes, while *HoxA3* repression is associated with increased *Runx1* expression and retention of an endothelial cell phenotype[64]. HOXB4 is suggested to function as a molecular switch in conferring lymphoid potential to otherwise primitive hematopoietic cells developed from mouse embryonic stem cells[65]. However, it seems HOXB4 is redundant in human cells, as expansion and long-term engraftment of hematopoietic cells derived from *HOXB4*-overexpressed human embryonic stem cells (hESCs) was not achieved[66]. *HOXA9* has been implicated in human EHT, but again, is not

sufficient on its own to confer long-term engraftment[67]. Dou *et al.*[68] recently implicated medial *HOXA* genes to be key regulators of HSC maintenance, but these genes were silenced in hESC-derived hematopoietic cells. This suggests the *HOXA* locus may be a key regulator in developed AGM to produce engraftable hematopoietic cells. In human EHT, *SOX17* has also recently been identified as a genetic marker of HE and that it is required for the development of the earliest hematopoietic progenitor cells in a Notch-dependent fashion[69–72].

Notch-independent signaling pathways have also been identified as important players in EHT. Wnt signaling is especially active in lateral plate mesoderm during embryogenesis and several key Wnt-associated molecules are overexpressed in the AGM[73–76]. Furthermore, addition of small molecules used to hyperactivate Wnt effector responses have increased the yield of HSPCs with lymphoid potential in zebrafish, mouse, and human models of hematopoiesis[77–79]. Bone morphogenic protein-4 (BMP4), a member of the TGF-β superfamily, has also been shown to support hemato-endothelial specification from the lateral plate mesoderm[80]. Addition of BMP4 to cell culture enhances hematopoietic activity, and does so by converging on both GATA2 and RUNX1 to promote a definitive hematopoietic program[80–82]. Taken together, EHT is a complex process that is dependent on many signaling and transcriptional modalities that function in a well-concerted manner during embryogenesis to produce the earliest hematopoietic cells (Figure 1-1).

**Modeling human hematopoiesis using human pluripotent stem cells**

Our understanding of the earliest events of human hematopoiesis has mostly developed from studies using mouse models. While the mouse hematopoietic system is similar to that of humans, there are several major differences between species that necessitate study with human cells to appropriately understand human hematopoietic development. First, the balance of adult blood leukocytes is significantly different. Mouse blood is skewed towards lymphocytes (75-90% B-, T-, and NK cells; 10-25% neutrophils), while human blood is skewed towards neutrophils (50-70% neutrophils; 30-50% lymphocytes)[83,84]. Second, surface antigens specific to HSC phenotypes are different (Mouse: $CD34^{-/lo}$c-$kit^{hi}CD38^{+}$Flt-$3^{-}$; Human: $CD34^{hi}$c-$kit^{lo}CD38^{-}$Flt-$3^{+}$) as well as the chronicity between HSC divisions[85,86]. Third, IL-7 receptor-mediated signaling is required for mouse B-cell lymphopoiesis, but it is dispensable in humans[83,87]. Fourth, as previously mentioned, HOXB4 overexpression expands mouse HSCs, but not human HSCs, suggesting HSC self-renewal is different between species[65,66,87]. Fifth, erythroid cell maturation differs in globin switching mechanisms[3]. Lastly, innate immune cell surface immunophenotype is highly variable between species, potentially lending to differences in function[87,88].

Human pluripotent stem cells, such as human embryonic stem cells (hESCs) and human induced pluripotent stem cells (hiPSCs), provide an excellent platform for studying the earliest events of human hematopoietic development and differentiation of HSPCs into terminal blood lineages. The first hematopoietic derivations from hESCs were demonstrated by Kaufman *et al.*, in which hESCs co-cultured with murine bone marrow stroma or yolk sac endothelial cells produced $CD34^{+}$ hematopoietic cells with myeloid,

erythroid, and megakaryocytic colony-forming potential[89]. Although this seminal study did not generate cells of lymphoid lineage, other groups have modified hESC conditions using various stromal cell co-culture and defined cytokine approaches to promote hemato-lymphoid development. Vodyanik *et al.*[90] and Choi *et al.*[91] co-cultured hESCs with the OP9 mouse bone marrow stromal cell line in the absence of additional hematopoietic cytokines. This method generated HSPCs with multilineage potential, including B-lymphocytes and natural killer (NK) cells. Timmermans *et al.*[92] expanded on this method using a OP9 cell line genetically engineered to overexpress DLL1 (OP9-DL1) to generate $CD3^+$ T-lymphocytes with functional T-cell receptors. To better recapitulate the AGM and developing hematopoietic niche, Gori *et al.*[93] recently utilized engineered endothelial cell lines that overexpressed two Notch-related ligands, JAG1 and DLL4, to differentiate non-human primate iPSCs into hematopoietic cells. Interestingly, these iPSCs generated massive quantities of $CD34^+CD45^+$ hematopoietic progenitor cells as compared to non-endothelial cell culture. They also found longer engraftment time of $CD34^+$ cells in secondary transplant recipients with multilineage potential, but they only assessed as far as 12 weeks. These data highlight the importance of recapitulating the developing human hematopoietic niche for the production of multilineage HSPCs from hESCs/hiPSCs.

Cytokines and small molecules have also been used to influence differentiation of definitive hematopoietic cells from human pluripotent stem cells. The addition of TGF-β/Activin/Nodal inhibitors has been one successful strategy. Since TGF-β/Activin/Nodal signaling is crucial for primitive erythropoiesis[94], inhibition of this pathway could skew hematopoietic development towards definitive lineages. Indeed, treatment of hESC

cultures with Activin/Nodal inhibitors minimized production of primitive progenitor cells and supported definitive hematopoietic development[77,78]. Wnt signaling has also been amplified using GSK-3 inhibitors (thus, increasing transcription of Wnt effector targets) to promote the development of hemato-lymphoid cells, suggesting enhanced definitive hematopoiesis lineage commitment[79,95]. New evidence using a combination of TGF-β/Activin/Nodal and GSK-3 inhibition further improved hemato-lymphoid potential from hiPSCs as compared to either treatment alone[96].

While various stromal cell platforms and defined additives have been employed, no *in vitro* method alone to date has developed true HSCs that are multipotent and capable of life-long, permanent engraftment from hESCs/hiPSCs. However, there are two published studies that demonstrate hiPSCs can yield transplantable HSCs[97,98]. In each case, undifferentiated hiPSCs were injected into immunocompromised mice and allowed to form self-assembled teratomas. HSPCs and mature lymphoid cells could be isolated from dissected teratomas, with some HSPCs capable of multilineage reconstitution. Hematopoiesis was enhanced with the co-injection of OP9 cells intra-teratomally. While these HSPCs cannot be used for clinical purposes due to xenotransplantation and inefficient yield, these studies provide crucial evidence on a basic level that hESCs/hiPSCs possess the intrinsic capacity to differentiate into HSPCs *ex utero*. However, these studies also shed light on their dependency of a local and embryological-like microenvironment to fully mature into functional hematopoietic cells.

**Innate lymphoid cell (ILC) development and differentiation from human pluripotent stem cells**

Innate lymphoid cells (ILCs) are a relatively newly defined grouping of lymphoid cells that contribute important factors to the innate immune response in blood and mucosal barriers[99,100]. In essence, ILC development, phenotype, and function in the innate immune response correlates to that of T-lymphocytes in the adaptive immune response[101]. Group 1 ILCs are comprised of conventional natural killer (cNK) cells (analogous to $CD8^+$ cytotoxic T-cells) and non-toxic ILCs (ILC1) that secrete TNF and IFNγ[102,103]. Group 2 ILCs (ILC2) are analogous to $CD4^+$ $T_H2$ helper cells in that they secrete IL-4, IL-5, IL-9, and IL-13 to facilitate Type 2 inflammatory responses[99]. Human Group 3 ILCs (ILC3) are a heterogeneous population that can be subdivided into two groups based upon expression of natural cytotoxicity receptor (NCR; NKp44 and NKp46). $NCR^+$ ILC3 can express and secrete IL-22[104–106]. Developmentally related to Group 3 ILCs are lymphoid tissue inducer (LTi) cells, which are required for secondary lymphoid organ development[107]. Confounding these classifications is an increasing body of evidence that suggest ILC subsets are plastic and may transform into other ILC phenotypes. As such, deconvoluting the heterogeneity of human ILCs remains an active area of research[99,102,103,107].

All lymphocytes stem from a common lymphoid progenitor (CLP) cell[4]. While B-lymphocyte development in the bone marrow and T-lymphocyte development in the thymus have been well-characterized, human ILC development remains unclear. The first specification of ILCs is dependent on TOX and NFIL3 (also referred to as E4BP4) to produce a combined NK/ILC progenitor cell that lacks B- and T-lymphocyte potential[108–

[110] . This cell, sometimes referred to as an α-lymphoid precursor (αLP) and interchangeable with the nomenclature "pre-NK cell", uniformly expresses CD34, CD45RA, CD117 and α4β7 integrin, but lacks other ILC developmental markers such as CD56 and CD94[99,102,111]. αLPs are thought to then specify either into NK cell progenitors (termed "iNK cell") or LTi/ILC progenitors in part by the activity of ID2 and GATA3. *GATA3* gene ablation in HSCs prevents the development of ILCs (mainly ILC2), but does not affect NK cell development[112–114]. iNK cells at this stage begin to acquire NK cell-like functionality in producing IL-5, IL-13, and tumor-necrosis factor-related apoptosis inducing ligand (TRAIL)[115]. Next, iNK cells continue to develop into matured NK cells, first becoming a cytotoxic $CD56^{bright}$ NK cell that begins to express mature NK cell surface antigens (CD94/NKG2A, NKG2D, NKp46), and ultimately transitioning into a $CD56^{dim}$ NK cell with full cytotoxic potential[116]. EOMES, T-BET, and ID2 have all been identified as key transcription factors mediating iNK maturation[117]. On the other hand, murine studies show that ILC/LTi progenitors can differentiate into LTi cells based on expression of *RORC* or can commit to ILC lineages based on expression of *PLZF*[99]. From here, specification into ILC1, ILC2, and ILC3 cells is predominantly under transcription factor control. ILC1 specification is dictated by T-BET, ILC2 by GATA3, and ILC3 by RORγt. The aryl hydrocarbon receptor (AHR) has also been shown to been indispensable for functional ILC3 differentiation[118,119].

The Kaufman lab has pioneered NK cell differentiation from human pluripotent stem cells. The initial report utilized a two-step culture method—first to differentiate $CD34^{+}CD45^{+}$ hematopoietic progenitor cells from hESCs on mouse stroma and then

defined conditions to support NK cell differentiation[120]. Here, cytokines that induced peripheral and umbilical cord blood $CD34^+$ differentiation into NK cells (Flt3-L, SCF, IL-3, IL-7, and IL-15) were used to generate $CD56^+CD45^+$ cells that co-expressed matured NK cell surface antigens, such as NKG2A, NKp44, NKp46, and KIR. These hESC-derived (and later hiPSC-derived) NK cells also possessed direct cytotoxic activity against leukemia, solid tumors, and HIV infected $CD4^+$ T-cells[120–124]. It was later found that co-culture using OP9-DL1 prevented differentiation towards T-lymphoid lineages and instead increased NK cell development[125]. Mature hESC- and hiPSC-derived NK cells once differentiated can also be expanded similar to peripheral blood-derived NK cells when cultured in the presence of IL-2 and stimulated with membrane bound IL-21 expressing antigen presenting cells[126,127].

**The aryl hydrocarbon receptor (AHR) and its role in human hematopoiesis**

The AHR is a member of the Per/Arnt/Sim (PAS) family of environment-sensing, basic helix-loop-helix transcriptional regulators[128–130]. AHR is a cytoplasmic receptor that normally is stabilized by co-chaperone protein HSP90, X-associated protein 2 (XAP2), and p23[131–133]. Following ligand binding to AHR, the HSP90:XAP2:p23 complex is removed and becomes stabilized by ARNT/HIF1β (aryl hydrocarbon nuclear translocator/hypoxia-inducible factor 1β), forming a functional heterodimer. This heterodimer subsequently binds to the 5'-GCGTG-3' consensus within xenobiotic responses element (XRE) that is located immediately upstream of several AHR target genes, such as *CYP1A1*, *CYP1B1*, *AHRR*, *IL-17*, and *IL-22* (Figure 1-2). AHR homology is evolutionarily conserved across

diverse species and has historically been studied for its role as a mediator of cellular toxicity in response to environmental pollutants[134].

Recent studies have shown AHR is expressed in many tissues during embryonic development and its signaling can have broad effects on genes that influence development, proliferation, differentiation, and the innate immune response[135–137]. Endogenous AHR-mediated signaling has been shown to play a potential role in developmental hematopoiesis. Genetic profiling studies and computational analyses from mouse models reveal *Ahr* is expressed in hematopoietic stem cells (HSCs)[130,138]. *Ahr* expression is highest in immature hematopoietic cells (including immature B-cells, T-cells, and bone-marrow derived $Sca^+$ HSCs) relative to terminally differentiated phagocytes, dendritic cells, erythroid cells, T-cells, and megakaryocytes[138]. AHR activation is also required for the development of $Th_{17}$ cells, regulatory T-cells, and ILC3[129,137,139,140]. A high-throughput screen to identify compounds that promote expansion of $CD34^+$ umbilical cord blood *ex vivo* discovered that StemReginin-1 (SR-1), a potent AHR antagonist, could increase the number of engraftable $CD34^+$ cells at least 17-fold and are suitable for transplant[141]. Indeed, Wagner *et al.*[142] recently transplanted expanded umbilical cord blood-derived $CD34^+$ cells treated with SR-1 in a Phase I/II clinical trial. SR-1 treated $CD34^+$ cells robustly expanded over 300-fold and conferred faster time to engraftment of neutrophils and platelets relative to patients treated with manipulated units. These breakthroughs demonstrate that AHR may also be a crucial mediator of HSC growth and differentiation. Indeed, $Ahr^{-/-}$ mice present with splenomegaly, altered numbers of erythrocytes and leukocytes, and a 2-fold enhancement in HSC-enriched $Lin^-Sca^+c\text{-}Kit^+$ cells in the bone

marrow compartment[143]. Furthermore, *Ahr*$^{-/-}$ mice are susceptible to lymphoma and other hematological malignancies[144]. Collectively, these data suggest that AHR may also serve as a critical regulator of definitive hematopoiesis. AHR expression is required to maintain HSC quiescence and hematopoietic progenitor cell differentiation, while AHR repression is necessary to promote expansion and maturation of HSCs and terminal hematopoietic cells. It remains unknown what, if any, specific role AHR plays earlier in the process of early human hematopoietic lineage commitment. It is also unclear whether AHR signaling is important for the specification of mesoderm-derived cells into primitive and/or definitive hematopoietic cells via EHT mechanisms.

**Thesis Statement**

The experiments described in this dissertation contribute novel information to our understanding of human endothelial and hematopoietic development. Previous knowledge of these processes has largely been derived from studies that are dependent on non-human animal models, which do not perfectly correlate with human biology. By using human pluripotent stem cells to model the earliest events of hematopoiesis, we can identify unique biological features of the endothelial-to-hematopoietic transition (EHT) and the maturation of adult blood cells that are specific to human development. Furthermore, these data can be extrapolated to optimize the production of HSPCs that may be suitable for treating patients with hematological and immunological pathologies.

In Chapter 2, we first establish an approach to define functional human hemogenic endothelial cells using a combination of endothelial cell surface antigens and

the expression of *RUNX1c*, a key EHT gene. With this schema, we analyzed the transcriptional signatures of individual cells from three distinct populations simultaneously derived from hESCs: hemogenic endothelial cells, vascular endothelial cells that lack hematopoietic potential, and early hematopoietic progenitor cells. Here, we determined human hemogenic endothelial cells have a similar transcriptional signature as the earliest hematopoietic progenitor cells, but both populations are distinct from vascular endothelial cells lacking hematopoietic potential. We also present novel genetic candidates that distinguish hemogenic endothelium from non-hemogenic endothelium. These genes possessed high predictive value in conferring hemogenic endothelial and hematopoietic phenotype. As such, these genes serve as excellent candidates for future gain-or-loss of function studies to promote a uniform population of hemogenic endothelium from human pluripotent stem cells.

In Chapter 3, we expand on the current role of AHR in the normal physiology of human hematopoietic development. Here, we demonstrate AHR modulates hematopoietic potential at the level of EHT. AHR antagonism using small molecules and *AHR* gene deletion both enhanced early hemato-endothelial differentiation from hESCs. This is the first evidence that suggests AHR is functional prior to the development of a $CD34^+$ HSPC. We further utilize AHR inhibition as a method to enhance hemato-lymphoid differentiation from hESCs, specifically ILCs. We specifically demonstrate ILC3 dependency on AHR activity and, as such, is the first evidence of human ILC3 differentiation from human pluripotent stem cells. This method can serve as a platform in

future studies to better understand the developmental biology and function of human ILCs and other hemato-lymphoid cell subsets.

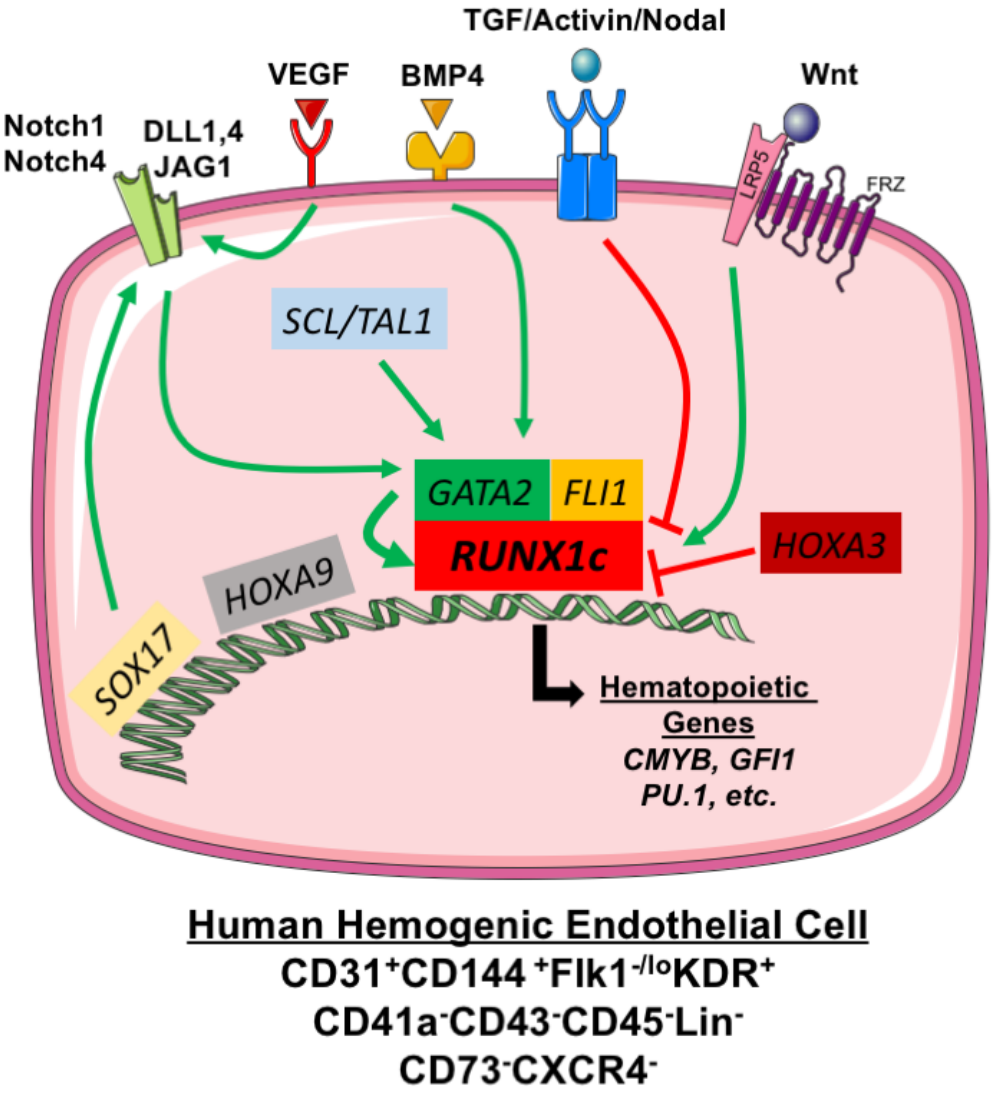


**Figure 1-1. Key cell signaling and transcriptional regulators of human hemogenic endothelial cells.** *RUNX1c* forms a transcriptional complex between *GATA2*, *FLI1*, and *SCL/TAL* to regulate the endothelial-to-hematopoietic transition (EHT). Upstream activation of Notch, VEGF, BMP4, and Wnt signaling promote the activity of *RUNX1c* (green arrows), while the TGFβ/activin/nodal signaling pathway inhibits *RUNX1c* activity (red arrows). Some Hox/Sox transcription factors further contribute to the activity of *RUNX1c*-mediated EHT.

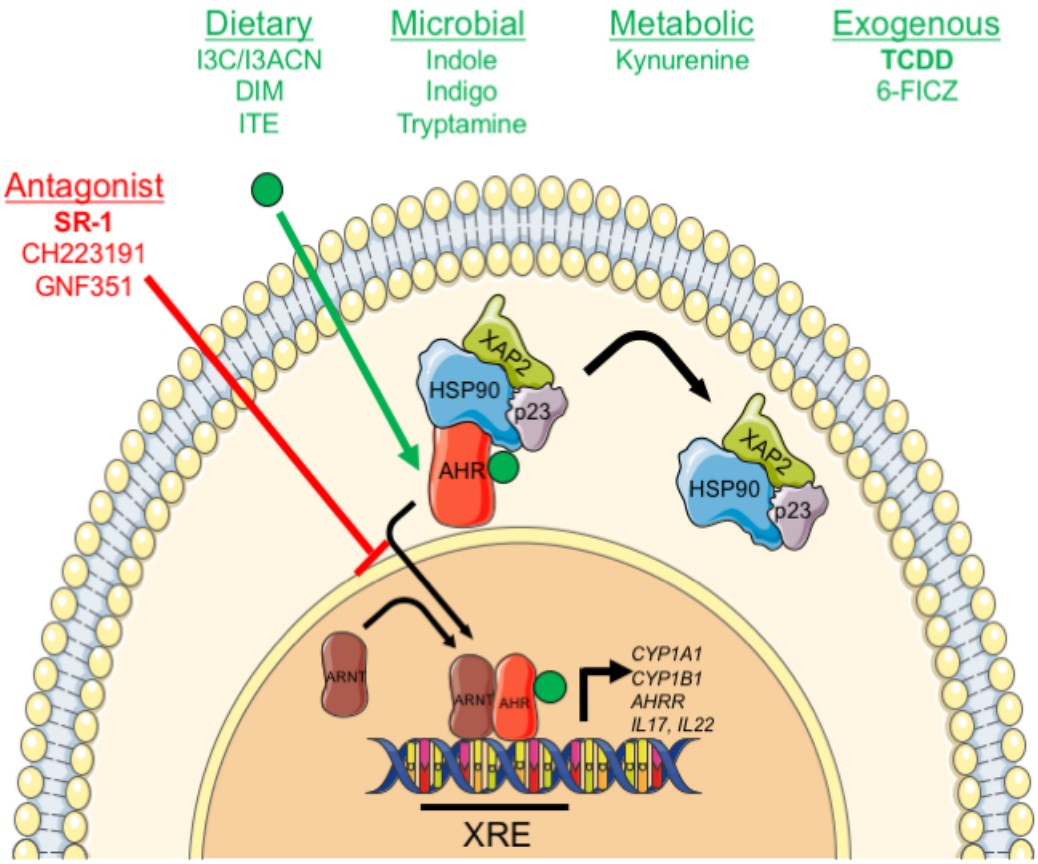


**Figure 1-2. Canonical AHR signaling.** AHR agonist ligands (green) are derived from dietary, microbial metabolism, human metabolism, or exogenous/environmental sources. AHR antagonists (red) are exogenously produced. SR-1 and TCDD (bold) possess the most potent activity in either class. Upon AHR activation, AHR disassociates from a cytoplasmic HSP90:XAP2:p23 co-chaperone complex and translocates into the nucleus. Here, AHR forms a heterodimer with ARNT and binds to xenogenic-response elements (XRE) to affect downstream gene transcription. AHR can be sequestered in the cytoplasm using AHR antagonists, thereby preventing effector gene target transcription. Adapted and modified from references [131,145,146].

# CHAPTER 2

***Single cell resolution of human pluripotent stem cell derived hemato-endothelial cells reveals distinct transcriptional signatures of hemogenic endothelium***

**ABSTRACT**

The endothelial-to-hematopoietic transition (EHT) mediated by hemogenic endothelium is an important stage in definitive hematopoietic development. Although EHT has been visualized both *in vitro* and *in vivo*, a thorough understanding of the genetic mechanisms underlying hemogenic endothelial cell fate remains poorly understood, especially in the humans. Using human pluripotent stem cells as a model for EHT, we hypothesized human hemogenic endothelium is phenotypically and transcriptionally distinct from other vascular endothelial cells and the earliest hematopoietic progenitor cells. We employed defined culture methods to differentiate hemogenic endothelial cells (HE, defined as $CD31^{+}CD144^{+}CD41^{-}CD43^{-}CD45^{-}CD73^{-}$*RUNX1c*$^{+}$), vascular endothelial cells without hematopoietic potential (non-HE, defined as $CD31^{+}CD144^{+}CD41^{-}CD43^{-}CD45^{-}CD73^{-}$*RUNX1c*$^{-}$), and hematopoietic progenitor cells (HP, defined as $CD34^{+}CD43^{+}$*RUNX1c*$^{+}$) from hESCs engineered with a *RUNX1c*-tdTomato reporter. Using these defined cell populations, we performed single-cell RNASeq on 55 HE, 47 non-HE, and 35 HP cells. HE and HP were both highly enriched in genes implicated in known hemogenic endothelial transcriptional networks, such as *CDH5*, *ERG*, *GATA2*, and *FLI*. Using t-distributed stochastic neighbor embedding (t-SNE) analysis, we found transcriptional overlap between individual HE and HP cells; however, these populations were distinct from two, separate groupings of non-HE. Further analysis revealed novel biomarkers for human HE/HP cells, such as *TIMP3*, *ESAM*, *RHOJ*, and *DLL4*. One subset of non-HE cells was enriched for several extracellular matrix genes and suggestive of a previously reported endothelial-to-mesenchymal transition (EndMT). Taken together, we

demonstrate that hESC-derived HE and HP share a common developmental pathway, while non-HE are heterogeneous and transcriptionally distinct. Our findings provide a novel strategy to test new genetic targets and optimize the production of definitive hematopoietic cells from human pluripotent stem cells.

## INTRODUCTION

Hemogenic endothelium is a rare and highly specialized subset of vascular endothelial cell that functions as a precursor population to blood development[17,18,28,147]. In mammals, hematopoiesis occurs in two sequential phases in a defined temporo-spatial manner[2,3,148]. Hemogenic endothelium is associated with the definitive phase of embryological hematopoiesis, which is characterized by the life-long development of multipotent hematopoietic stem and progenitor cells (HSPCs)[4,149]. One of the hallmarks of definitive hematopoiesis is the endothelial-to-hematopoietic transition (EHT), a process where hemogenic endothelial cells phenotypically switch from a stationary endothelial cell state to a detached and free-moving HSPC. Although EHT has been visualized both *in vitro* and *in vivo* at specific anatomical landmarks via lineage tracing studies[18,150,151], the regulation of this fate change at both a cellular and molecular level remains unclear. Confounding this knowledge further is an absence of unique cell surface markers allowing phenotypic identification and isolation of hemogenic endothelium from other developmentally related cell types[46,152]. Furthermore, specific hemogenic endothelial cell genetic identifiers from humans have yet to be adequately defined.

One candidate identifier of human hemogenic endothelium is *RUNX1c*, an isoform of the *RUNX1* gene. Expression of the +24 intronic enhancer, which drives *RUNX1c* expression via the P1 promoter, has been shown to be restricted to a subset of endothelial cells where *de novo* generation of HSPCs occurs in both zebrafish and mouse models[36,46]. *RUNX1c* expression has also been correlated exclusively to human definitive hematopoietic cells, including $CD34^+$ umbilical cord blood and hematopoietic stem cells[37–

[40,153,154]. Our lab, and others, have previously described human EHT using a human *RUNX1c* pluripotent stem cell reporter system[77,95]. As such, *RUNX1c* can serve as a genetic basis for selecting human hemogenic endothelial cells from other developing endothelial and hematopoietic cell populations.

Human pluripotent stem cells, such as human embryonic stem cells (hESCs) and induced pluripotent stem cells (hiPSCs) serve as a useful platform to understand basic mechanisms underlying human EHT. We, and others, have previously shown differentiation of early hematopoietic progenitor cells from hESC-derived bi-potent endothelial cells capable of developing into cells of the erythroid[155,156], myeloid[89,157–159], and lymphoid lineages[78,160,161]. However, production of functional and long-term engraftable HSPCs from hESCs/hiPSCs *in vitro* has yet to be achieved. One hypothesis is that hESCs are biased toward primitive hematopoietic lineages, and fail to adequately generate hemogenic endothelial cells that produce definitive hematopoietic cells[158,162–164]. To assess this degree of heterogeneity from an hESC/hiPSCs system, single-cell RNA sequencing has emerged as an invaluable tool to discover novel and rare cellular subsets otherwise obscured in bulk RNASeq experiments[165–168].

In the present study, we utilized hESCs previously engineered to express a *RUNX1c*-tdTomato reporter construct[77] to investigate the transcriptional signatures of human hemogenic endothelial cells (HE), vascular endothelial cells that lack hematopoietic potential (non-HE), and the earliest definitive hematopoietic progenitor cells (HP). We sequenced and analyzed 137 individual cells and performed comprehensive biostatistical analyses to reveal that endothelial cells derived from hESCs are heterogeneous in nature.

Human hemogenic endothelial cells and early hematopoietic progenitors shared similar gene expression signatures, suggesting a common developmental lineage. Intriguingly, vascular endothelial cells were found to be distinct from HE and HP, with a unique population of cells transformed into a mesenchymal/fibroblast-like cell phenotype. These studies now allow us to define novel genetic biomarkers to distinguish HE from non-HE and serve as a unique strategy to optimize definitive hematopoietic cell differentiation from human pluripotent stem cells.

## MATERIALS AND METHODS

### Human embryonic stem cell (hESC) culture

hESC-*RUNX1c*-tdTomato reporter cells were previously engineered and validated in our lab[77]. In brief, a 1 kb fragment of the human *RUNX1c* P1 promoter and 250 bp conserved intronic region of the +24 enhancer were flanked by tdTomato. Upstream, a constitutively active GFP:zeo fusion protein permitted identification of cells differentiated from hESCs with stable reporter integration. hESC-*RUNX1c*-tdTomato were TrypLE adapted for single cell culture and maintained on irradiated mouse embryonic fibroblasts (MEF) in ES growth media consisting of Dulbecco's Modified Eagle's Media (DMEM)/Ham's F-12 Media (F12) (ThermoFischer Scientific, Carlsbad, CA), 15% Knockout Serum Replacement (ThermoFischer Scientific), 1mM L-glutamine (ThermoFischer Scientific), 0.1 mM β-mercaptoethanol (ThermoFischer Scientific), 1% minimum essential medium nonessential amino acids (ThermoFischer Scientific), 1% penicillin-streptomycin (ThermoFischer Scientific), and 4 ng/mL basic fibroblast growth

factor (R&D Systems, Minneapolis, MN). Cells were cultured in a 37°C air humidified incubator supplemented with 5% $CO_2$ until 70-80% confluency, at which point they were passaged using 1x TrypLE Select (ThermoFischer Scientific). All hESCs used in subsequent experiments did not exceed single-cell adaption transfer number 35.

**Spin embryoid body (Spin-EB) formation and hemato-endothelial differentiation**

Single-cell adapted hESCs were harvested with 1x TrypLE Select and aggregated as spin embryoid bodies, as previously described[169,170]. In brief, hESCs were plated at 3,000 cells/100 μL in a round-bottom 96-well plate using serum-free BPEL media supplemented with 20 ng/mL BMP4 (R&D Systems), 40 ng/mL SCF (R&D Systems), and 20 ng/mL VEGF (R&D Systems) (Stage I media). Cells were centrifuged for 5 minutes at 1500 rpm to form embryoid bodies (Day 0) and were incubated for 6 additional days to promote mesoderm induction. To differentiate early hemato-endothelial cells, Day 6 spin-EBs were transferred to pre-gelatinized 24-well plates (approx. 8-16 EBs/well) with BEL media supplemented with 40 ng/mL SCF, 40 ng/mL VEGF, 30 mg/mL thrombopoietin (R&D Systems), 30 ng/mL IL-3 (PeproTech, Rocky Hill, NJ), and 30 ng/mL IL-6 (PeproTech) (Stage II media). For long-term culture, media was exchanged every 3-4 days with cytokine supplementation. To harvest endothelial cells for analysis, non-adherent (hematopoietic) cell fractions were removed while the remaining adherent fractions were washed and treated with 0.05% trypsin containing 2% chicken serum for 5 minutes. Adherent cells were collected, vortexed, and filtered to generate single-cell suspensions suitable for

analysis. To harvest hematopoietic cells, only non-adherent cell fractions were harvested and filtered to generate single-cell suspensions suitable for analysis.

**Immunofluorescent and fluorescent imaging**

To visualize surface antigens on developing endothelial and hematopoietic cells, cells were fixed with 3.7% paraformaldehyde for 10 minutes and subsequently permeabilized with 0.05% Triton X-100 for 5 minutes, both at room temperature. Following permeabilization, cells were initially blocked with immunofluorescence blocking buffer (5% goat serum, 1% glycerol, 0.1% bovine serum albumin, 0.1% fish skin gelatin, 0.04% sodium azide, pH=7.2) for 30 minutes and then incubated overnight with primary antibodies (see below) at 4°C. Cells were then washed and incubated with either AlexaFluor 568 or AlexaFluor 647 conjugated anti-mouse secondary antibody (ThermoFischer Scientific, Waltham, MA) for 1 hour at room temperature. Following subsequent washes, nuclei were counterstained with Hoescht 33342 (Cell Signaling Technologies, Danvers, MA) and immediately imaged. Cells were imaged on an Olympus IX71 epifluorescent inverted microscope (Olympus, Center Valley, PA). The following primary antibodies were used: anti-VWF (Clone 6994, Abcam, Cambridge, MA), anti-mouse-PECAM1 (Clone 89C2, Cell Signaling Technologies). For GFP and tdTomato detection, viable cells were directly imaged in a 24 well plate on an inverted epifluorescent microscope in culture medium.

**Flow Cytometry and Fluorescent-Activated Cell Sorting**

Single cells were harvested as previously described and resuspended at 100 cells/μL of FACS buffer (DPBS + 2% FBS + 0.1% sodium azide). Cells were then incubated with antibodies for 30 minutes at 4°C, washed, and resuspended in fresh FACS buffer containing Sytox Blue Live/Dead stain. Samples were analyzed immediately on an LSR Fortessa cytometer (BD Biosciences, San Jose, CA). The following antibodies were used in this study per manufacturer recommendation (all anti-human): CD31-APC (eBioscience, San Diego, CA), CD34-PECy7 (BD Biosciences), CD41a-APC (BD Biosciences), CD43-APC (BD Biosciences), CD45-APC (BD Biosciences), CD73-APC (BD Biosciences), CD144-APC (eBioscience). All gating was set relative to isotype controls of identical fluorophores. Data from flow cytometry was analyzed using FlowJo software (Treestar, Ashland, OR).

For cell sorting of hESC-derived hemogenic endothelium (HE) and vascular endothelial cells without hematopoietic potential (non-HE), Day 11 hESC-*RUNX1c*-tdTomato were differentiated and harvested as described above. Cells were stained with anti-human CD41a-APC (BD Biosciences), CD43-APC (BD Biosciences), CD45-APC (BD Biosciences), CD73-APC (BD Biosciences), CD144-PECy7 (eBioscience), and CD31-APC-eFluor 780 (eBioscience) in sterile FACS Buffer for 30 minutes at 4°C. Cells were washed with FACS buffer and dead cells were counterstained with Live/Dead Fixable Aqua (ThermoFisher Scientific) immediately prior to sorting. Live HE ($CD31^+CD144^+CD41a^-CD43^-CD45^-tdTomato^+$) and non-HE ($CD31^+CD144^+CD41a^-CD43^-CD45^-tdTomato^-$) populations were sorted using a FACSAria II (BD Biosciences) directly into BPEL media. Early human hematopoietic progenitor cells (HP) were

harvested from a parallel differentiation culture at matched time points. Non-adherent hESC-*RUNX1c*-tdTomato derived cells were harvested as described above and stained with anti-human CD34-PECy7 (BD Biosciences) and CD43-APC (BD Biosciences) for 30 minutes at 4°C. Cells were washed with FACS buffer and dead cells were counterstained with Sytox Blue (ThermoFisher Scientific) immediately prior to sorting. Live HP ($CD34^+CD43^+tdTomato^+$) were also sorted on a FACSAria II directly into BPEL media. Post-sort flow cytometry sample validation was performed on all samples.

**Post-sort HE and non-HE culture conditions**

Immediately following FACS, both HE and non-HE populations were washed and counted. To assess for endothelial cell morphology, $5x10^4$ cells were seeded onto fibronectin coated 24-well plates in Endothelial Basal Media (EBM2) supplemented with EGM-2 BulletKit (Lonza, Allendale, NJ). Following 5 days of culture, cells were washed and stained to assess for CD31 expression and morphological appearance using an epifluorescent inverted microscope. To assess for hematopoietic potential, $5x10^4$ cells were seeded in Stage II media in low-attachment 24-well plates. Following 2 days of cultures, cells were directly visualized using an epifluorescent microscope for non-adherent, $GFP^+tdTomato^+$ hematopoietic cells. Pre-sort cells were also prepared and similarly processed as a control for hematopoiesis.

**Single-cell capture and RNASeq**

Sorted HE, non-HE, and HP were stained with a Live/Dead viability/cytotoxicity kit (ThermoFisher Scientific) and resuspended at 50 cells/μL. Cells were captured on three, separate medium-sized (10-17 μm cell diameter) chips using the Fluidgm C1 Single-Cell Auto Prep System (Fluidgm, San Diego, CA) per the manufacturer protocol. Following capture, cells were visualized using phase-contrast and fluorescent microscopy using a Nikon Inverted Ti-E Deconvolution motorized Microscope (Nikon, Belmont, CA). At this point, only live, single, and $GFP^+$ cells were selected for cDNA library preparation. Additionally, for HE and HP sorted cells, tdTomato expression was also verified; cells absent for tdTomato signal were excluded. Following capture and validation, cDNA was prepared from each cell using the SMARTer Ultra Low RNA kit for the Fluidgm C1 system, according to the manufacturer recommendations (Clontech, Mountain View, CA). cDNA library concentrations were assessed using Quant-iT PicoGreen dsDNA assay Kit (ThermoFischer Scientific). cDNA concentrations that were less than 25 ng/μL were further excluded from subsequent sequencing. mRNA libraries were transcribed using the Illumina Nextera XT preparation kit (Illumina, San Diego, CA) according to the manufacturer protocol and sequenced on an Illumina HiSeq 2500. Sequencing was performed in rapid-mode using 50 bp paired-end reads to a depth of approximately $1.8x10^6$ reads/sample. In parallel from the same differentiation as single cell captures, bulk population RNA controls were also similarly processed and included in subsequent analyses.

**Bioinformatic analyses of single-cell RNASeq data**

Illumina reads were processed via a pipeline developed by the University of Minnesota Informatics Institute in collaboration with the Minnesota Supercomputing Institute and the University of Minnesota Genomics Center. Briefly, FastQ files were trimmed using Trimmomatic (Usadel Lab, Max Planck Institute, Germany; parameters used: -phred33 -threads 8, ILLUMINACLIP, LEADING:3 TRAILING:3 SLIDINGWINDOW:4:16 MINLEN:25). After trimming, mapping to the human genome was performed via TopHat (v. 2.0.13, Johns Hopkins University) and Bowtie (v. 2.2.4.0, Johns Hopkins University). Fraction per kilobases per million (FPKM) expression was calculated via cuffquant function in Cufflinks (Trapnell Lab, University of Washington). Log-transformed FPKM values were analyzed using the Seurat R toolkit developed by the Satija Lab (https://github.com/satijalab/seurat; New York Genome Center, NYU), which has been extensively published elsewhere[171–174]. Principal component analysis (PCA) and t-distributed stochastic neighbor embedding (t-SNE) analysis were performed in parallel with two gene lists in Seurat; one list of the total genome ("Total") mapped transcripts (26,257 genes) and another restricted list of blood and endothelial ("Blood & EC"; 2,556 genes) gene subsets. The Blood & EC gene list was exported from a list of genes tagged to "hematopoiesis" and "endothelial" categorizers within Ingenuity Pathway Analysis (IPA) software (Qiagen, Valencia, CA). For t-SNE analyses, only statistically significant principal components (defined as $p<0.05$, see Supplemental Figure 2-5) for each gene list were used as function input. Differentially expressed genes between cell populations and clusters were assessed using "ROC" and "t-test" functions in the Seurat package using the default settings. Isoform level quantification of *RUNX1c* was mapped using Salmon (Patro

Lab, Stony Brook University)[175]. FPKM values were averaged between HE and non-HE groups and compared to assess *RUNX1c* enrichment. Gene ontology enrichment analysis of the total mapped genes between HE and non-HE was performed using IPA.

### Additional Statistical Analyses

Differences between groups were compared either with student's t-test using Prism 6 (GraphPad Software, San Diego, CA). Results were considered statistically significant at p-values $< 0.05$.

## RESULTS

### hESC-*RUNX1c*-tdTomato cells differentiate into early hemato-endothelial cells in chemically-defined and xenogenic-free culture conditions

We first assessed the kinetics of hESC-*RUNX1c*-tdTomato differentiation into early hemato-endothelial cells using defined culture and cytokine conditions (Figure 2-1A). Here, we expanded on our previously published data to better identify the emergence of endothelial progenitor cells[77]. hESC-*RUNX1c*-tdTomato cells differentiated into adherent cells with endothelial characteristics as early as Day 9 of culture. Endothelial cells propagated around the perimeter of each embryoid body, and were positive for two specific endothelial cell markers: CD144 (VE-Cadherin) and von Willebrand Factor (vWF) (Figure 2-1B, top panels). At Day 12 of differentiation, rounded, non-adherent hematopoietic progenitor cells could be seen (Figure 2-1B, bottom panels). These hematopoietic cells all expressed a constitutively active GFP:zeo fusion protein, while a fraction of the them also

dually expressed tdTomato, suggesting these cells are of the definitive hematopoietic lineage and developed from EHT.

We next quantified the development of endothelial and hematopoietic cells by flow cytometry. At Day 9 of culture, a majority of the differentiated cells were endothelial cells, defined as $CD34^+CD31^+$ (27.5%±6.6) and $CD34^+CD144^+$ (22.0%±7.3) with limited numbers of hematopoietic progenitor cells, defined by $CD34^+CD41a^+$ (2.3%±0.4), $CD34^+CD43^+$ (6.3%±1.4), and $CD34^+CD45^+$ (1.2%±0.6) (Figures 2-1C & 2-1D). By Day 12, the endothelial cell populations declined, accompanied by a reciprocal increase in hematopoietic progenitor cells. By Day 15, a majority of cells were hematopoietic, with statically significant gains in the percentage of $CD34^+CD41a^+$ (7.16%±2.7, $p<0.05$), $CD34^+CD43^+$ (16.17%±3.3, $p<0.01$), and $CD34^+CD45^+$ (11.8%±1.6, $p<0.01$) phenotypes. To parallel hematopoietic development, tdTomato (*RUNX1c*) was detected in appreciable quantity at Day 12 (14.7%±4.1), with a majority of the cells later expressing *RUNX1c* after blood development occurred at Day 15 (69.5%±6.4, $p<0.01$) (Figures 2-1E & 2-1F). As such, hESC-*RUNX1c*-tdTomato cells serve as an excellent platform to allow us to isolate defined endothelial cell populations that are suitable for single-cell genetic analyses.

**Combined endothelial cell surface antigen and *RUNX1c* expression delineate human hemogenic endothelium from vascular endothelium lacking hematopoietic potential**

We next assessed for the presence of human hemogenic endothelium from differentiating hESC-*RUNX1c*-tdTomato cells by using a combination of endothelial cell-specific surface markers and $tdTomato^+$ expression. Because Day 11 was just prior to the

onset of detectable *RUNX1c* hematopoietic cells, we characterized adherent hESC-derived cells at this time point. Here, approximately 10% of the total cells were $CD144^{+}CD31^{+}$ and negative for CD41a and CD43 expression (Figure 2-2A, top panels). When sub-gating on these populations, we found approximately 40% of the cells were dually $tdTomato^{+}$, suggestive of a hemogenic endothelium phenotype (Figure 2-2A, bottom panels). We next FACS-sorted three populations: 1) putative hemogenic endothelial cells (HE; defined as $CD31^{+}CD144^{+}CD41^{-}CD43^{-}CD45^{-}CD73^{-}tdTomato^{+}$); 2) vascular endothelial cells lacking hematopoietic potential (non-HE; defined as $CD31^{+}CD144^{+}CD41^{-}CD43^{-}CD45^{-}CD73^{-}$ $tdTomato^{-}$) and 3) early hematopoietic progenitor cells (HP; defined as $CD34^{+}CD43^{+}tdTomato^{+}$), and further assessed their phenotypic responses in both endothelial cell and hematopoietic cell culture conditions (Figure 2-2B and Supplemental Figure 2-1). Here, we demonstrate HE cells retain endothelial morphology in the absence of pro-hematopoietic growth conditions. hESC-derived HE seeded onto fibronectin coated wells in endothelial growth media were able to generate a confluent, cobblestone monolayer that fully expressed CD31 (PECAM1) at the cellular junctions (Figure 2-2C). The morphological and phenotypic appearance was similar to that of control human umbilical vein endothelial cells (HUVEC). We next assessed whether HE and/or non-HE would generate $tdTomato^{+}$ hematopoietic cells in pro-hematopoietic culture conditions. In the span of two days, HE robustly produced non-adherent, $tdTomato^{+}$ cells similar to pre-sorted cells from the same hESC differentiation (Figure 2-2D). Additionally, non-HE cells failed to produce comparable quantities of $tdTomato^{+}$ cells, as these cells adhered and retained an endothelial-like morphology. Taken together, these results demonstrate that

phenotypic HE and non-HE can be sorted and distinguished from hESCs based on this combination of endothelial surface antigen and *RUNX1c* expression.

**Single-cell RNASeq reveals similarities in HE and HP gene signatures, but both are transcriptionally distinct from non-HE**

Using characterized hESC-derived HE, non-HE, and HP cell populations, we next defined each cell population on a single cell transcriptional level. To do so, we performed single-cell RNASeq to assess individual cells and determine the developmental similarities of each population. We used the Fluidgm C1 Single-Cell Autoprep system in conjunction with Illumina Next Generation Sequencing to analyze 55 HE, 47 non-HE, and 35 HP single cells (Supplemental Figure 2-2A & 2-2B). To ensure correct identification of single-cells, we validated that individual HE and HP cells captured were tdTomato$^{+}$ within the microfluidic capture chamber, while non-HE cells were tdTomato$^{-}$ (Supplemental Figure 2-2A). We performed sequencing to a depth of approximately $1.8x10^{6}$ reads/sample to further verify enrichment of *RUNX1c* at the isoform level and provide a complete gene expression profile for each individual cell. We first confirmed the representativeness of single-cell transcripts to the expression level of the bulk cell populations. As a function of fraction per kilobase per million mapped fragments (FPKM), we found a strong correlation between gene expression averaged across individual cells as compared to the bulk populations ($R^2$=0.90) (Supplemental Figure 2-2C). While we did not see statistically significant differences in the expression of all combined transcript variants of the *RUNX1* gene across populations, we confirmed HE possessed higher log-transformed FPKM

expression of the *RUNX1c* specific isoform compared to non-HE (9.23±2.61 vs. 1.22±0.67, $p<0.01$) (Supplemental Figure 2-2D). We next assessed the ontological pathways significantly enriched between hESC-derived HE and non-HE using Ingenuity Pathway Analysis software. Several of the highest statistically significant ontological pathways were specific to embryological development and hematopoiesis, including "Hematological System Development and Function" (log $p<10^{-15}$), "Tissue Development" (log $p<10^{-8}$), "Embryonic Development" (log $p<10^{-7}$), and "Hematopoiesis" (log $p<10^{-6}$).

By generating violin plots of log-transformed FPKM values, we next analyzed the expression of key genes known to be associated with vascular endothelial cells, hemogenic endothelium, and hematopoietic progenitor cell phenotype. These plots provide complementary data regarding total gene expression and the frequency of expression across individual cells in a given population. We found that both HE and HP possessed similar expression and distribution of several endothelial and hemogenic endothelial genes that was higher than those of non-HE. For example, *KDR*, *NR2F2*, *LMO2*, *PECAM1*, and *EFNB2* were significantly increased vascular endothelial cell-related genes in the HE and HP groups as compared to the non-HE group (Figure 2-3A). *SOX17*, *CDH5*, *ERG*, *ESAM*, *FLI1*, *FOXF1*, *KIT*, and *MECOM* were also significantly increased hemogenic endothelium-related genes in HE and HP as compared to non-HE. We also observed HP cells to have overexpression of key hematopoietic genes as compared to HE and non-HE, including *IL7R*, *ITGA2B*, *RAG1*, and *WNT5A*, while some genes such as *HOXB5*, *GATA2, GATA3, and MEIS1* were also overexpressed in HE. We further confirmed that genes associated with cardiac development and terminal erythroid, myeloid, and lymphoid cell

differentiation were not appreciably expressed, while endogenous housekeeper genes, such as *GAPDH*, *ACTB*, and *GPI* possessed uniform expression across all three populations (Supplemental Figure 2-3). Genes characteristically associated with pluripotency (*POU5F1/OCT4*, *NANOG, DPPA2*), primitive streak development (*MIXL1, T*), lateral plate mesoderm (*FOXF1*, *IRX3*), ectoderm (*PAX6*, *SOX1*, *SOX10*), and endoderm (*FOXA1A*, *GATA4*) did not yield any detectable FPKM expression (data not shown).

We next sought to investigate wide-scale transcriptional profile similarities between HE, non-HE, and HP populations. Using Seurat, we performed principal component analysis to reduce the dimensionality of FPKM expression values using: 1) the total mapped gene list (26,257 genes; "Total") and 2) a hematopoietic and endothelial restricted gene list (2,556 genes; "Blood & EC"). In both analyses, we found at least 3 distinct groups of cells when plotted against the first two most statistically significant principal components (Figure 2-3B). In either analysis, many of the HE and HP single cells overlapped within a common principal component area, while two clusters primarily composed of non-HE cells were distinctly located in separate areas. We further resolved the composition of these clusters by performing t-distributed stochastic neighbor embedding (t-SNE) analysis using genes assigned only to statistically significant principal components for both the Total (Supplemental Figures 2-5A & 2-6A) and Blood & EC (Supplemental Figures 2-5B & 2-6B) gene lists. Using this approach, clear resolution of one, centralized cluster of transcriptionally similar HE and HP populations could be ascertained, while a majority of the non-HE cells were segregated into two divergent clusters (Figure 2-3C). In applying Seurat's density parameter clustering functions, three

main clusters (Clusters 2, 3, and 4, with Cluster 1 representing statistical outlier single cells) were identified using the total gene list (Figure 2-3D). A similar identification was seen in the Blood & EC gene lists in marking Clusters 2, 3, and 5 (note: Cluster 1 represents statistical outlier single cells and Clusters 4 and 6 are comprised of ≤3 single cells). In analyzing the Total gene list, we observed Cluster 2 was mostly heterogeneous for HE (55.8%) and HP (27.91%), with few non-HE cells (16.28%) (Supplemental Figure 2-7). Clusters 3 and 4 were mainly composed of non-HE (75.76% and 69.23%, respectively). We further validated separation of non-HE from HE and HP by generating heat maps using unsupervised clustering of genes found within the statistically significant principal components (Figure 2-3E). Taken together, these data demonstrate that individual HE and HP are transcriptionally related to one another, while non-HE are heterogeneous and transcriptional distinct from both HE and HP.

**Clustering analysis identifies novel biomarkers of hESC-derived HE and HP with divergent developmental pathways of non-HE**

Using individual cells re-classified into transcriptionally distinct groups from the Total gene list, we identified distinguishing biomarkers between HE/HP single cells and the two subsets of non-ECs by performing receiver operating characteristic (ROC) curve analysis in Seurat. ROC analysis is a non-parametric method that is useful in providing the probability (power) that a gene is up- or down-regulated within given group[176]. Cluster 2 yielded 651 statistically significant identifier genes, with the most powerful predictors being previously known hemogenic endothelium related genes such as *CDH5* (DGE:

2.07)[177], *ERG* (DGE: 2.08)[178], *CLDN5* (DGE: 2.07)[179], and *TEK* (DGE: 2.01)[180] (Figure 2-4A). Cluster 3 and Cluster 4 yielded 916 and 928 statistically significant identifier genes, respectively. Here, we report the top 50 distinguishing genes between groups of cells assigned to Clusters 2, 3, and 4. We next confirmed the specificity of novel biomarkers of each cluster by mapping the gene expression to individual cells on the Total gene list t-SNE plots as shown in Figure 2-3C. We identified at least four novel gene markers with increased and specific expression to Cluster 2: *TIMP3* (DGE: 2.06), *ESAM* (DGE: 2.20), *RHOJ* (DGE: 2.27) and *DLL4* (DGE: 2.49) (Figure 2-4B). We also show that *TYROBP* (DGE: 3.78) and *CCL4* (DGE: 5.34) are specific in designating the Cluster 3 subset, which was largely composed of non-HE. Interestingly, Cluster 4 was mostly comprised of genes that encode extracellular matrix protein products. We found significant upregulation of *COL1A1* (DGE: 6.58), *COL1A2* (DGE: 4.63), *DCN* (DGE: 6.09), *LUM* (DGE: 4.87), *COL3A1* (DGE: 3.50), *VCAN* (DGE: 3.55), and several other extracellular matrix components/genes. This would suggest cells of this cluster transformed from an endothelial phenotype into a mesenchymal or fibroblast phenotype. To further validate the uniqueness of each cluster set, we generated a new heat map of gene expression across individual cells using a more stringent approach. We restricted the list of genes to differentially regulated genes with high discriminatory power (Power > 0.80) within each cluster (Figure 2-4C). This approach indeed generated clear distinctions in global gene expression that was seen between individual cells assigned to each cluster. Collectively, our approach has established unique genetic biomarkers between hESC-derived HE and non-HE cells, as

well as demonstrating a subset of non-HE are capable of further transformation away from an endothelial cell lineage.

## DISCUSSION

In the present study, we utilized hESCs harboring a *RUNX1c*-tdTomato reporter to assess the phenotypic and transcriptional profiles of the earliest definitive hemato-endothelial cells. In conjunction with endothelial-cell specific immunophenotyping and *RUNX1c* expression, we identified hESC-derived HE that not only maintained vascular morphology in endothelial culture conditions, but also differentiated *RUNX1c*$^{+}$, non-adherent, hematopoietic progenitors when cultured in the presence of hematopoietic cytokines. Furthermore, through next generation sequencing of individual hemogenic endothelial cells, vascular endothelial cells lacking hematopoietic potential, and the earliest definitive hematopoietic progenitor cells, we determined that hESC-derived HE and HP are transcriptionally similar to each other, but distinct from a heterogeneous population of non-HE. We also identify several novel candidate genes that serve to distinguish HE from non-HE populations.

To date, there have been few reports fully characterizing the complete development of undifferentiated hESCs/hiPSCs through hemogenic endothelium to the generation of HSPCs. Many reports have relied on cell immunophenotyping alone, which has been useful in elucidating key differences between human endothelial and the first formed hematopoietic cells. For example, Nakajima-Takagi *et al.*[70] separated endothelial cells from the earliest hematopoietic progenitor cells (termed “pre-HPCs”) simply based upon

$CD34^+CD43^-$ and $CD34^+CD43^+CD45^{-/lo}$. With this strategy, they discovered *SOX17* was overexpressed in human hemogenic endothelium as compared to pre-HPCs and matured hematopoietic cells, and thus a key regulator of hematopoietic development. Indeed, we observed similar overexpression of *SOX17* in a majority of cells within our HE population as compared to the HP population. We now provide complementary data that *SOX17* is not expressed in endothelial cells lacking hematopoietic potential. Our finding parallels studies in the mouse model, in which knockout of *SOX17* abolished the definitive hematopoietic program (loss of T-lymphocyte potential), but did not alter expression levels of *EphrinB2 (*human homolog: *EFNB2*) or *Coup-TfII* (human homolog: *NR2F2*), genes that are associated with arterial and venous endothelium specification, respectively[69,71].

Choi *et al.*[157] and Raffi *et al.*[150] both used more specific hemato-endothelial phenotypes, relying on $CD31^+$, $CD34^+$, $CD117^+$, $CD144^+$, and $CD73^-$ to detect endothelial cells and $CD41a^+$, $CD43^+$, $CD235a^+$ to monitor hematopoietic development. While both studies provide convincing evidence for a precursor endothelial population that directly supports hematopoietic development, it is unclear as to which phase of hematopoiesis (primitive vs. definitive) these earliest cells arise from. Primitive hematopoiesis is thought to primarily originate from hemangioblasts, which are bi-potent cells able to differentiate only into embryonic vasculature cells or transient erythroid/myeloid cells. Hemangioblasts are almost identical in their endothelial surface antigen expression as hemogenic endothelium[79,181–184]. As such, our described system that is co-dependent on endothelial positive-selection ($CD31^+CD144^+CD73^-$) and *RUNX1c* expression provides more precise specification of the definitive hematopoietic program leading to a more resolved

understanding of the events preceding HSPC development. Indeed, a related approach has recently been verified in an elegant study by Ditadi, *et al*[95]. Here, human hESC-derived hemogenic endothelium restricted to an adherent $CD34^{+}CD73^{-}CD184^{-}$*RUNX1c*$^{+}$ population were able to generate *RUNX1c*$^{+}$ hematopoietic cells with T-lymphocyte potential. Furthermore, combinations of CD184 (CXCR4), CD73, and *RUNX1c* could be used as molecular labels in distinguishing the acquisition of either an arterial or venous phenotype from vascular endothelial progenitor cells. Moving forward, it is clear both cell surface and genetic identifiers must be used to adequately define and resolve specialized subsets from a heterogeneous collection of differentiating hemato-endothelial cells.

Our single-cell RNASeq experiments revealed several novel candidate markers that were specific to human hemogenic endothelium and definitive hematopoietic progenitor cells. *TIMP3*, *ESAM*, *RHOJ*, and *DLL4* were found to possess some of the highest discriminatory powers for distinguishing HE and HP from non-HE (Figure 2-4B). *TIMP3* (tissue inhibitor of metalloproteinase-3), while not previously implicated in developmental hematopoiesis, has previously been shown to play an important role in HSPC proliferation by recruiting quiescent hematopoietic stem cells into the cell cycle[185,186]. *ESAM* (endothelial cell selective adhesion molecule) has been identified (albeit in the mouse) as a reliable marker for long-term repopulating hematopoietic stem cells derived from the aorta-gonad-mesonephros region that also possessed lymphoid potential[187,188]. Moreover, *ESAM* expression is maintained throughout the transition of hematopoiesis to the bone marrow and its expression is increased during the aging process. Because *ESAM* was highly expressed in almost every HE and HP single cell we analyzed (Figure 2-3A), it represents

a potential candidate for hemogenic endothelial cell selection and/or overexpression studies to engineer hematopoietic progenitors from hESCs with hemato-lymphoid potential. *RHOJ* encodes a Rho GTPase that is normally restricted to vascular endothelial cells. *RHOJ* expression, as well as other key hemogenic endothelial proteins, such as VE-cadherin, endoglin, and vWF, are regulated upstream by *ERG*, which is further implicated in hESC differentiation into endothelial cells[178,189–191]. We observed overexpression of both *RHOJ* and *ERG* in our HE and HP populations. Interestingly, hyperactivation of *RhoJ* enhances endothelial cell focal adhesion disassembly and increases the mobility of endothelial cells[192]. Thus, a similar mechanism may be crucial during EHT to convert adherent endothelial cells into non-adherent and free-moving HSPCs. Lastly, EHT and definitive hematopoiesis have been hypothesized to be evolutionary Notch-dependent[30,95,193,194]. DLL4 is a downstream mediator of VEGF activity and induces the upregulation of Notch1 and its effector targets. DLL4 is highly enriched in the vascular niche and has recently been shown to support the production of partially engraftable $CD34^+$ cells derived from non-human primate induced pluripotent stem cells[93]. Consequently, enrichment of *DLL4* may serve as a useful method for identifying hemogenic endothelial cells derived from hESCs.

We also looked at other key transcriptional regulators of human EHT that have been recently reported from bulk cell sequencing. Dou *et al.*[68] provided insight that medial *HOXA* genes are silenced in hESC-derived hemato-endothelial cells, but were critical for fetal-liver HSPC expansion and maintenance. In corresponding fashion, we found no appreciable expression of any *HOXA* locus genes in our hESC-derived hemato-endothelial

cell populations, which is consistent with our prior analyses[77] (Supplemental Figure 2-8A). Interestingly, we observed significant increases in *HOXB* locus gene expression between hESC-derived HE/HP and non-HE populations, specifically in *HOXB3*, *HOXB5*, *HOXB6*, and to an extent, *HOXB7* (Supplemental Figure 2-8B). *HOXB5* has been recently described (albeit in mouse) to be expressed during EHT and defines HSCs with long-term engraftment potential[195]. As such, *HOXB* genes may be of higher biological importance in conferring hemogenic potential from hESC/hiPSC-derived hemogenic endothelium.

By assessing the transcriptional repertoire of individual cells, we also revealed heterogeneity in non-HE cells. Although all non-HE expressed traditional endothelial cell-specific surface antigens, a small subset of non-HE were heavily enriched with genes encoding extracellular matrix proteins (Cluster 4, Figure 2-4A). This genetic signature highly suggests transformation from an endothelial lineage to a mesenchymal or stromal cell lineage in a developmental process known as the endothelial-to-mesenchymal transition (EndMT). EndMT primarily is a TGF-β driven process that normally is required for intimal thickening and stabilization of vasculature during embryonic vasculogenesis[196]. Other groups have reported that hESC- and hiPSC-derived endothelial cells are highly susceptible to EndMT, particularly following long-term passaging and cell culture[196–198]. This, in part, may be due to a combination of defined factors within culture media and/or also the cellular origin of hiPSCs used. Our results suggest that a small degree of EndMT occurs even at the earliest development of hemato-endothelial cells from embryoid bodies (Figure 2-5). As such, it may be imperative to negatively select against these transitioning

cells to prevent the out-crowding of true vascular endothelial cells and/or hemogenic endothelial cells.

Lastly, it is an important distinction that we used a human platform to analyze the transcriptional profiles of single cells as they commit towards hemato-endothelial lineages at the earliest stage of hematopoiesis. Our findings share many commonalities to a related single-cell approach investigating mouse hemogenic endothelium[46]. Using a pan-*RUNX1* mouse reporter model and single-cell qRT-PCR, Swiers *et al.* demonstrated mouse hemogenic endothelium was also enriched for key endothelial and hematopoietic specific genes simultaneously, similar to what we observed with human HE. Here, they concluded hemogenic endothelium transitions away from an endothelial repertoire and towards a distinct hematopoietic repertoire through analysis of matured hematopoietic cell populations ($CD41^+$ and $CD45^+$). Our findings in which the very first developed human hematopoietic cells ($CD34^+CD43^+RUNX1c^+$)[199] are transcriptionally similar to hemogenic endothelium complements this working model of EHT. This also lends credence to pursuing future gain and/or loss of function studies using candidate genes described herein within hESCs to optimize the development of hemogenic endothelium. These studies would provide further mechanistic insight into the key molecular drivers regulating the development of multipotent and potentially engraftable human HSPCs.

**ACKONWLEDGEMENTS**

We thank Jerry Daniel and the University of Minnesota Genomic Center for technical assistance with the single-cell RNASeq. We thank Gene Yeo (UCSD) for helpful

discussion. This work was supported in part by the following National Institutes of Health grants: National Cancer Institute R01CA203348 (D.S.K.), National Institute of Diabetes and Digestive and Kidney Diseases F30DK107071 (M.G.A), National Institute of General Medicine Sciences T32GM113846 (M.G.A and D.S.K.) and T32GM008244 (M.G.A). Other support from the Regenerative Medicine Minnesota program (D.S.K.)

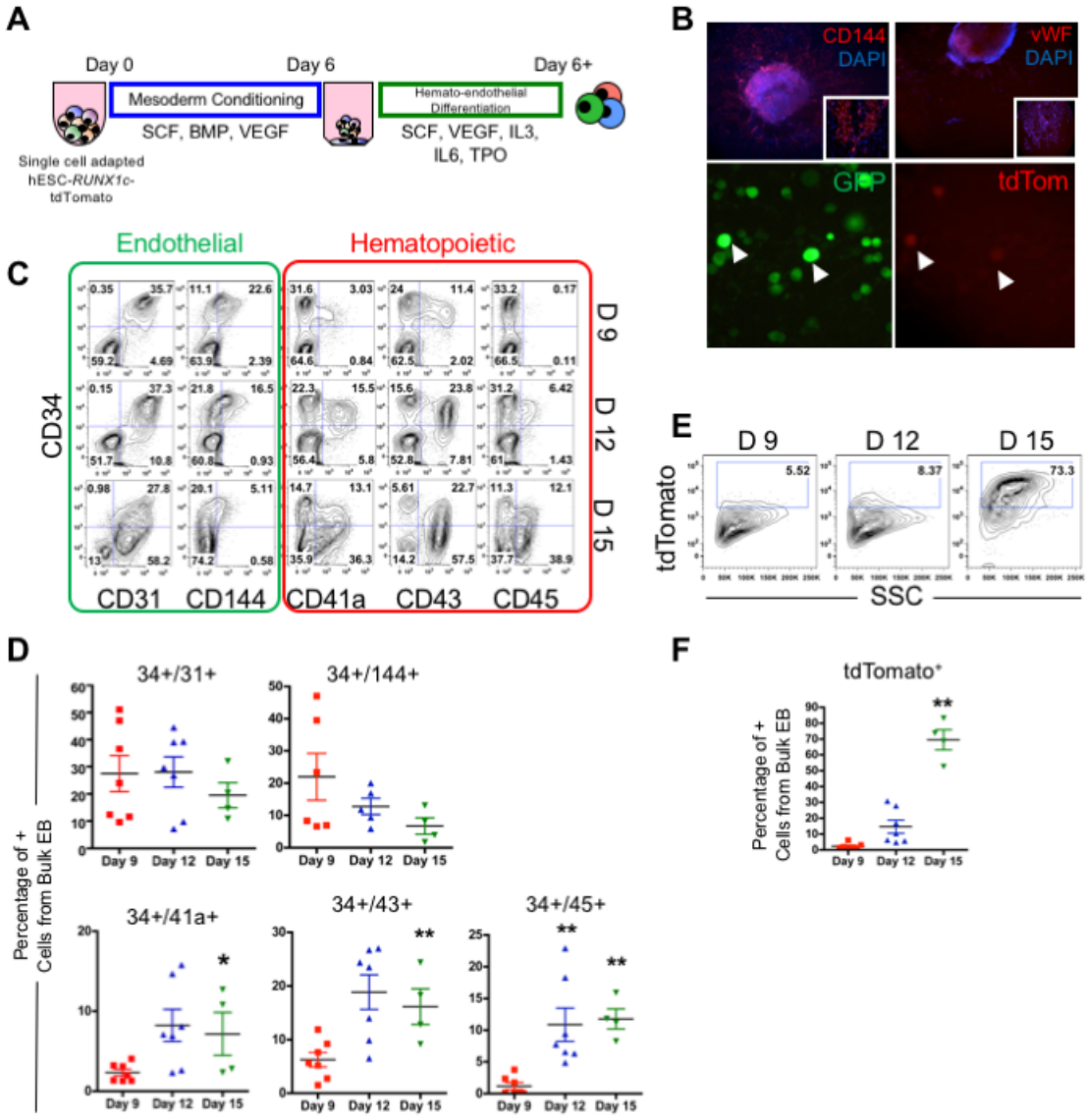


**Figure 2-1. hESC-*RUNX1c*-tdTomato cells can model the human endothelial-to-hematopoietic transition (EHT) *in vitro*.** (A) Schema of hemato-endothelial differentiation from hESC-*RUNX1c*-tdTomato cells as spin embryoid bodies (spin-EB). (B) Top; Representative immunofluorescent images of hESC-*RUNX1c*-tdTomato at Day 9 of differentiation for endothelial specific surface antigens CD144 and vWF (red). Magnification 4x and 10x (inset) are shown. Nuclei are counterstained with DAPI (blue).

Representative immunofluorescent images of hESC-*RUNX1c*-tdTomato at Day 12 of differentiation demonstrating development of non-adherent, dual constitutive $GFP^+$ (green) and $tdTomato^+$ (red) reporter hematopoietic cells from spin-EBs (bottom panels). Magnification 20x. (C) Representative flow cytometry plots of endothelial (CD31, CD144) and early hematopoietic surface antigens (CD41a, CD43, CD45) at Day 9 (D9), Day 12 (D12) and Day 15 (D 15) time points over the course of hESC-*RUNX1c*-tdTomato differentiation. (D) Quantification of flow cytometry as shown in panel C. *$p<0.05$, **$p<0.01$ as compared to Day 9 assessed by student's t-test. Each data point represents a distinct hESC-*RUNX1c*-tdTomato differentiation and errors bars represent SEM; n=4-7 (E) Representative flow cytometry plots of tdTomato (*RUNX1c*) expression at Day 9 (D9), Day 12 (D12) and Day 15 (D 15) time points over the course of hESC-*RUNX1c*-tdTomato differentiation. (F) Quantification of flow cytometry as shown in panel E. **$p<0.01$ as compared to Day 9 assessed by student's t-test, error bars represent SEM; n=4-7.

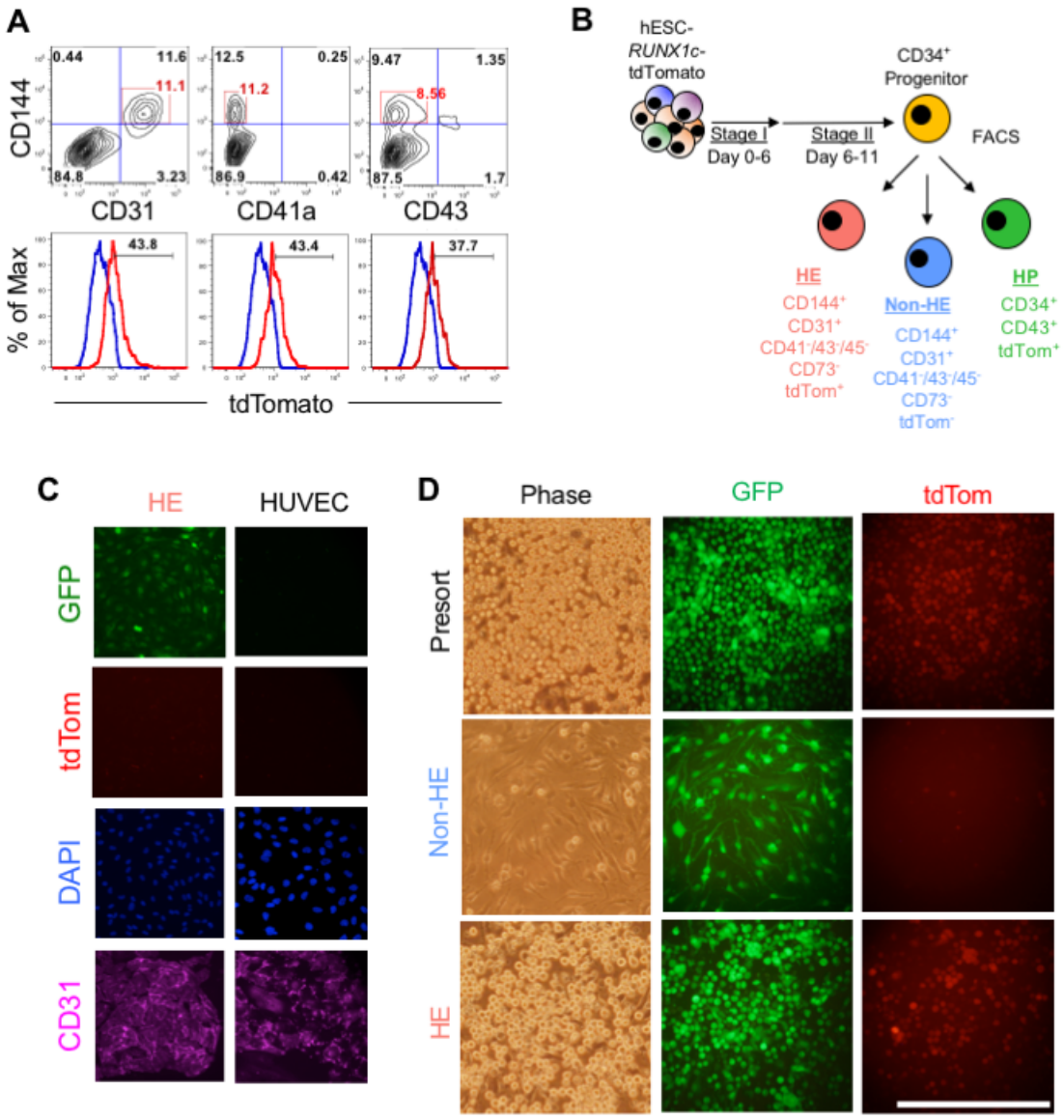


**Figure 2-2. Functional human hemogenic endothelium can be phenotypically identified and sorted from hESC-*RUNX1c*-tdTomato cells.** (A) Representative flow cytometry plots of differentiating hESC-*RUNX1c*-tdTomato cells at Day 11 expressing typical endothelial surface antigens ($CD144^{+}CD31^{+}$), but absent for early hematopoietic surface antigens ($CD144^{+}CD41a^{-}$, $CD144^{+}CD43^{-}$). Phenotypic endothelial cells were gated (top panel) and assessed for tdTomato expression (bottom panel). A fraction of endothelial

cells were tdTomato$^{dim}$ (red histogram) as compared to control hESCs lacking the GFP-*RUNX1c*-tdTomato reporter (blue histogram), consistent with the identification of hemogenic endothelium. n=2 independent differentiations. (B) Schema of FACS sorting hESC-*RUNX1c*-tdTomato cells into hemogenic endothelium (HE), endothelial cells that lack hematopoietic potential (non-HE), and early hematopoietic progenitor cells (HP). (C) Sorted HE cells seeded on fibronectin-coated wells with EGM-2 media for 5 days and subsequently immunofluorescently imaged for CD31 (left column). HE stained positive for CD31 (purple), GFP (green), and were tdTomato$^{dim}$ (red) while retaining a stereotypical cobblestone morphology of traditional endothelial cells. Untransfected human umbilical vein endothelial cells (HUVECs) are shown as an endogenous control (right column). (D) Presorted hESC-*RUNX1c*-tdTomato-derived adherent cells, sorted HE, and sorted non-HE were plated in Stage II hemato-endothelial differentiation media for two additional days to promote hematopoiesis. Both Presort and HE populations robustly generated non-adherent GFP$^{+}$tdTomato$^{+}$ hematopoietic progenitor cells, while non-HE did not adequately support hematopoietic development. Underlying non-HE cells further retain their endothelial morphology. Bar=100μm.

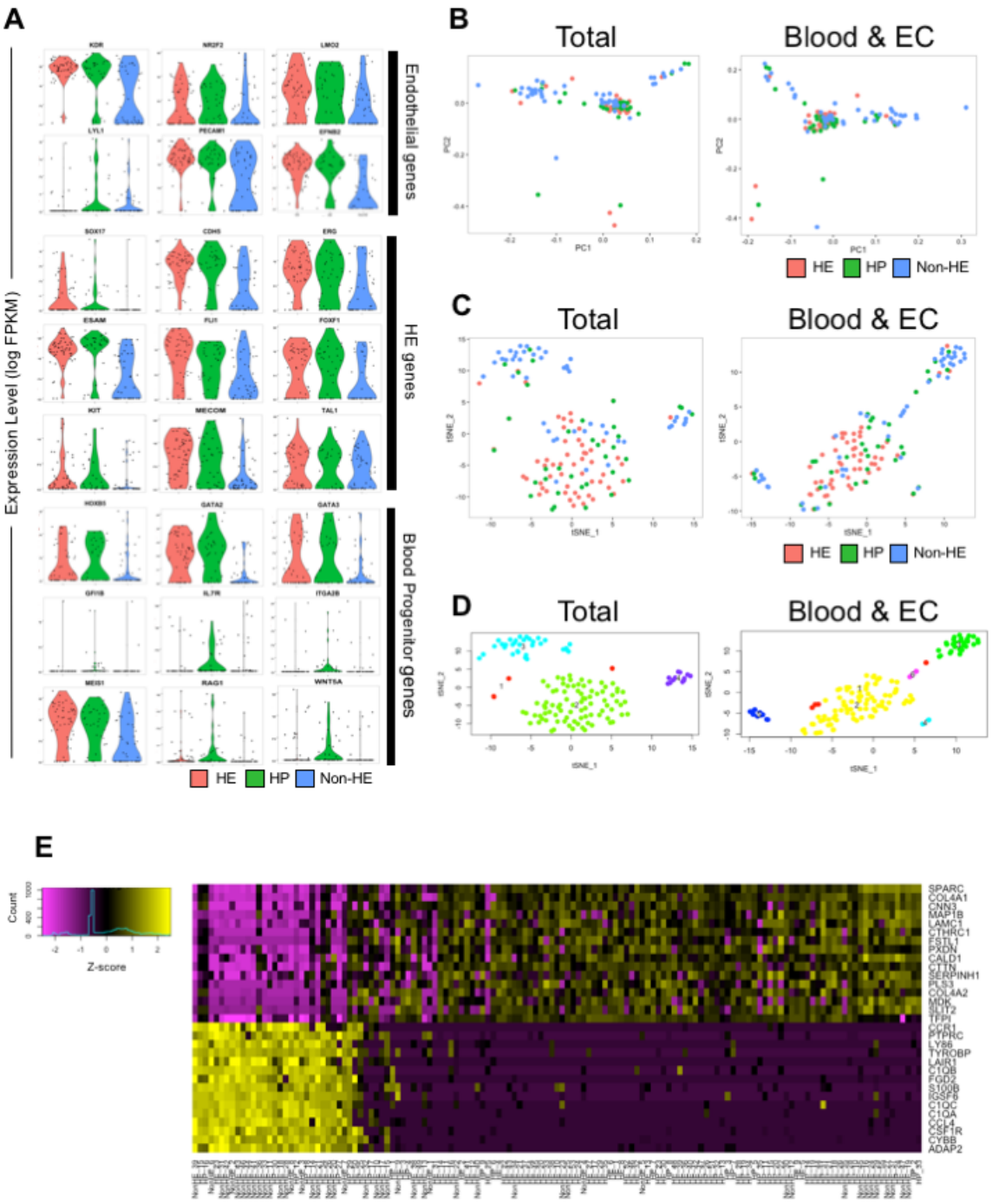


**Figure 2-3. Single-Cell RNASeq of hESC-*RUNX1c*-tdTomato hemato-endothelial cells reveals distinct transcriptional networks between HE and non-HE.** (A) Distribution of the fraction per kilobases per million (FPKM) reads mapped for

characteristic endothelial, hemogenic endothelium, and hematopoietic genes from HE, non-HE, and HP cells. Values along the vertical axis represents the log-transformed FPKM expression of each single cell sequenced, while the width of the violin indicates the frequency of cells at a particular FPKM level. (B) Principal component projections of the first and second statistically significant principal components for all 137 cells sequenced. PCA was performed using the entire mapped human genome sequence (Total; left panel) as well as a restricted gene list specific for known endothelial and hematopoietic genes (Blood & EC; right panel). Each data point represents the dimensionally reduced gene expression data for a single cell. (C) t-distributed stochastic neighbor embedding (t-SNE) plots of all 137 cells for Total (left) and Blood & EC (right) gene sets. (D) Statistically distinct clusters that originated from t-SNE dimensionality reduction shown in Panel C were computationally labelled and reclassified as belonging to a transcriptionally distinct population. Cluster 1 (red dots) are cells that failed to orient into one of the defined clusters (Cluster 2: green, Cluster 3: cyan, or Cluster 4: purple for the Total gene set; Cluster 2: yellow, Cluster 3: green, Cluster 4: cyan, or Cluster 5: blue for the Blood & EC gene set). (E) Heat map of Total gene expression defined within projected and statistically significant principal components (see Supplemental Figure 2-5A). Horizontal rows represent z-score expression of log-transformed FPKM values while vertical columns represent each single cell.

A

Cluster 2

| GENE | AVG DGE | POWER |
|---|---|---|
| TIMP3 | 2.06 | 0.91 |
| SHANK3 | 2.03 | 0.89 |
| ESAM | 2.20 | 0.88 |
| CDH5 | 2.07 | 0.87 |
| CEACAM1 | 2.21 | 0.85 |
| ADGRL4 | 2.11 | 0.85 |
| IGFBP5 | 2.04 | 0.85 |
| NOSTRIN | 2.40 | 0.84 |
| RHOJ | 2.27 | 0.84 |
| PCSK6 | 2.04 | 0.83 |
| ERG | 2.08 | 0.83 |
| WWTR1 | 2.06 | 0.83 |
| S100A16 | 2.74 | 0.83 |
| CLDN5 | 2.24 | 0.83 |
| UCP2 | -5.23 | 0.83 |
| TM4SF1 | 2.12 | 0.82 |
| SCHIP1 | 2.85 | 0.82 |
| DLL4 | 2.49 | 0.80 |
| CALCRL | 2.01 | 0.79 |
| NOTCH4 | 2.35 | 0.78 |
| IGDCC3 | 2.10 | 0.78 |
| HPGD | 2.52 | 0.77 |
| ECSCR | 2.03 | 0.77 |
| MIR503HG | 2.20 | 0.76 |
| GLIPR1 | -3.14 | 0.76 |
| MMP1 | 2.09 | 0.76 |
| PPAP2B | 2.13 | 0.76 |
| AFAP1L1 | 2.38 | 0.74 |
| PLEK | -4.56 | 0.74 |
| HAPLN1 | 2.03 | 0.74 |
| HEY1 | 2.47 | 0.74 |
| MECOM | 2.56 | 0.73 |
| TEK | 2.01 | 0.73 |
| BCL6B | 2.15 | 0.72 |
| MARCKSL1 | 2.10 | 0.72 |
| MMRN2 | 2.03 | 0.72 |
| EFNA1 | 3.29 | 0.71 |
| TYROBP | -4.78 | 0.71 |
| LST1 | -3.26 | 0.70 |
| IGSF6 | -3.71 | 0.70 |
| CSF1R | -4.81 | 0.70 |
| OSBPL10 | 2.04 | 0.70 |
| RASSF4 | -4.50 | 0.70 |
| CD34 | 2.27 | 0.69 |
| F13A1 | -5.06 | 0.69 |
| SMAD1 | 2.80 | 0.69 |
| PCAT19 | 3.17 | 0.69 |
| C1QB | -4.35 | 0.69 |
| IFI30 | -3.42 | 0.67 |
| ATP8B4 | -3.57 | 0.67 |
| ADAM9 | -2.15 | 0.67 |

Cluster 3

| GENE | AVG DGE | POWER |
|---|---|---|
| HCK | 4.29 | 0.99 |
| AIF1 | 3.93 | 0.99 |
| PTPRC | 3.56 | 0.97 |
| TYROBP | 3.78 | 0.97 |
| S100B | 4.36 | 0.96 |
| LAIR1 | 4.14 | 0.93 |
| CSF1R | 3.01 | 0.93 |
| IGSF6 | 3.71 | 0.93 |
| SPARC | -2.91 | 0.92 |
| DOCK8 | 2.68 | 0.92 |
| HCST | 3.03 | 0.92 |
| ATP8B4 | 2.63 | 0.91 |
| C1QC | 3.94 | 0.91 |
| COL4A1 | -2.53 | 0.91 |
| CYTH4 | 3.61 | 0.91 |
| FCGR2A | 3.27 | 0.90 |
| MS4A7 | 4.90 | 0.90 |
| PLEK | 3.04 | 0.90 |
| NCKAP1L | 2.65 | 0.90 |
| SPTBN1 | -2.11 | 0.89 |
| RNASE6 | 4.57 | 0.89 |
| CCL4 | 5.34 | 0.89 |
| LCP1 | 2.42 | 0.89 |
| UCP2 | 2.82 | 0.89 |
| TFPI | -2.26 | 0.89 |
| LY86 | 4.78 | 0.89 |
| ICAM2 | -2.74 | 0.88 |
| CYBB | 4.04 | 0.88 |
| C1QB | 4.54 | 0.88 |
| LST1 | 3.26 | 0.88 |
| ADAP2 | 3.49 | 0.87 |
| RASSF4 | 3.82 | 0.87 |
| C1QA | 4.99 | 0.87 |
| COL4A2 | -2.22 | 0.87 |
| CCL3 | 4.19 | 0.86 |
| IFI30 | 2.95 | 0.86 |
| F13A1 | 4.14 | 0.86 |
| CTSS | 3.52 | 0.86 |
| TIMP3 | -2.47 | 0.86 |
| TM4SF1 | -3.14 | 0.86 |
| LGALS9 | 2.43 | 0.85 |
| VSIG4 | 5.99 | 0.85 |
| FGD2 | 3.15 | 0.85 |
| SIGLEC14 | 2.76 | 0.85 |
| FLT1 | -2.15 | 0.85 |
| C3AR1 | 3.48 | 0.85 |
| NCF4 | 2.87 | 0.85 |
| SEMA6A | -2.27 | 0.84 |
| PXDN | -2.12 | 0.84 |
| SYK | 3.19 | 0.84 |
| MPEG1 | 2.81 | 0.84 |

Cluster 4

| GENE | AVG DGE | POWER |
|---|---|---|
| COL1A1 | 6.58 | 1.00 |
| COL1A2 | 4.63 | 1.00 |
| DCN | 6.09 | 1.00 |
| LUM | 4.87 | 1.00 |
| OLFML3 | 4.33 | 1.00 |
| COL3A1 | 3.50 | 0.99 |
| CRISPLD2 | 3.54 | 0.99 |
| FRZB | 3.37 | 0.98 |
| CCDC80 | 3.50 | 0.98 |
| VCAN | 3.55 | 0.98 |
| SNHG18 | 3.41 | 0.98 |
| LAMA2 | 2.20 | 0.98 |
| KRT8 | 4.15 | 0.97 |
| COL5A1 | 2.58 | 0.97 |
| PDGFRB | 2.14 | 0.97 |
| CTGF | 3.03 | 0.96 |
| MSRB3 | 2.82 | 0.96 |
| COL5A2 | 2.37 | 0.96 |
| FN1 | 2.19 | 0.96 |
| MEST | 2.84 | 0.95 |
| FKBP11 | 2.45 | 0.95 |
| THBS1 | 2.56 | 0.94 |
| CYR61 | 2.81 | 0.94 |
| ADAMTS1 | 2.60 | 0.93 |
| FBN1 | 2.06 | 0.93 |
| KRT18 | 3.28 | 0.93 |
| SEMA5A | 2.59 | 0.92 |
| TMEM45A | 2.17 | 0.92 |
| FCGRT | -2.40 | 0.91 |
| ANXA1 | 2.01 | 0.91 |
| GPC6 | 2.41 | 0.91 |
| MXRA8 | 2.84 | 0.90 |
| VTN | 4.52 | 0.90 |
| COL6A3 | 3.73 | 0.90 |
| PDZRN3 | 2.80 | 0.89 |
| C1S | 2.49 | 0.89 |
| LOX | 3.64 | 0.89 |
| ANTXR1 | 2.39 | 0.89 |
| RND3 | 2.80 | 0.89 |
| CTSD | -2.29 | 0.88 |
| KDELR3 | 2.19 | 0.88 |
| ELOVL2 | 2.37 | 0.88 |
| CREB3L1 | 2.38 | 0.88 |
| MMP2 | 2.75 | 0.87 |
| AXL | 2.01 | 0.87 |
| DAB2 | -2.36 | 0.87 |
| FCER1G | -5.19 | 0.87 |
| BMP4 | 3.56 | 0.87 |
| LAPTM5 | -2.99 | 0.86 |
| SOX6 | 2.15 | 0.86 |
| STAB1 | -2.91 | 0.86 |

B

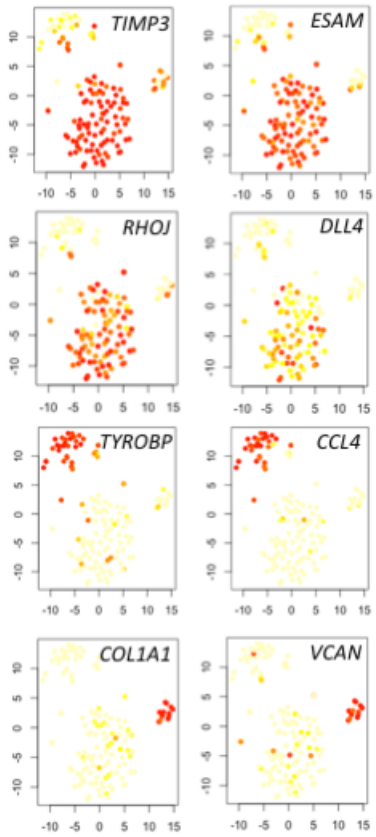


C

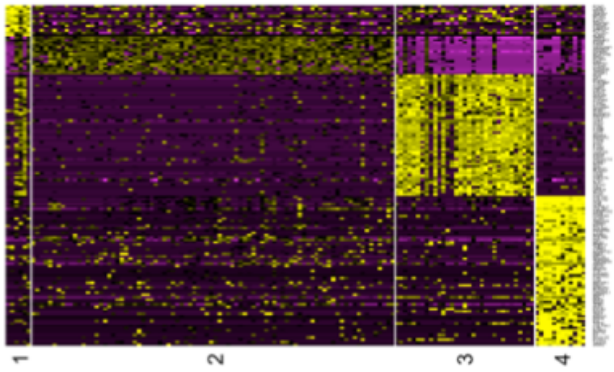


**Figure 2-4. hESC-*RUNX1c*-tdTomato-derived non-HE are heterogeneous and can be distinguished from HE and HP using defined gene signatures.** (A) Lists of the top 50 differentially expressed genes that distinguish cells assigned in Cluster 2, 3, and 4 as shown

in Figure 2-3D from the Total gene set. Gene screening was assessed by ROC analysis, with the average differential gene expression (Avg. DGE) and ROC classification power (0=random, 1=perfect correlation) for each gene listed; genes are ranked by their cluster distinguishing potential. (B) Gene expression superimposed onto Total t-SNE plots (Figure 2-3D) to reflect uniqueness to a cluster subset. Novel identifying biomarkers, such as *TIMP3* and *ESAM* possess high expression within cells of Cluster 2 (mainly HE/HP), while *TYROBP* and *CCL4* are uniquely expressed in Cluster 3 (non-HE), and ECM genes such as *COL1A1* and *VCAN* are expressed in a distinct subset of non-HE cells within Cluster 4. (C) Heat map of differentially regulated marker genes as defined by cell clustering in Panel A. Individual cells assigned to each cluster are plotted on the vertical axis.

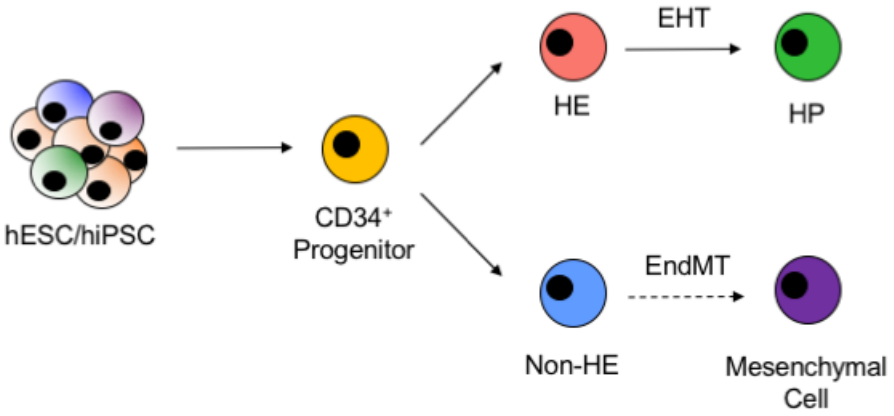


**Figure 2-5. Working model of human pluripotent stem cell EHT *in vitro*.** Undifferentiated hESCs/hiPSCs first develop towards mesodermal lineages and generate $CD34^+$ progenitor cells with dual hemato-endothelial potential. $CD34^+$ cells subsequently differentiate into endothelial cells that possess hematopoietic potential (HE) or endothelial cells that lack endothelial potential (non-HE). HE cells can then differentiate further into hematopoietic progenitor cells in a process known as EHT. A subset of non-HE can subsequently transform into other cells of mesenchymal lineages, such as a mesenchymal stem cell or fibroblast, in a process known as the endothelial-to-mesenchymal transition (EndMT).

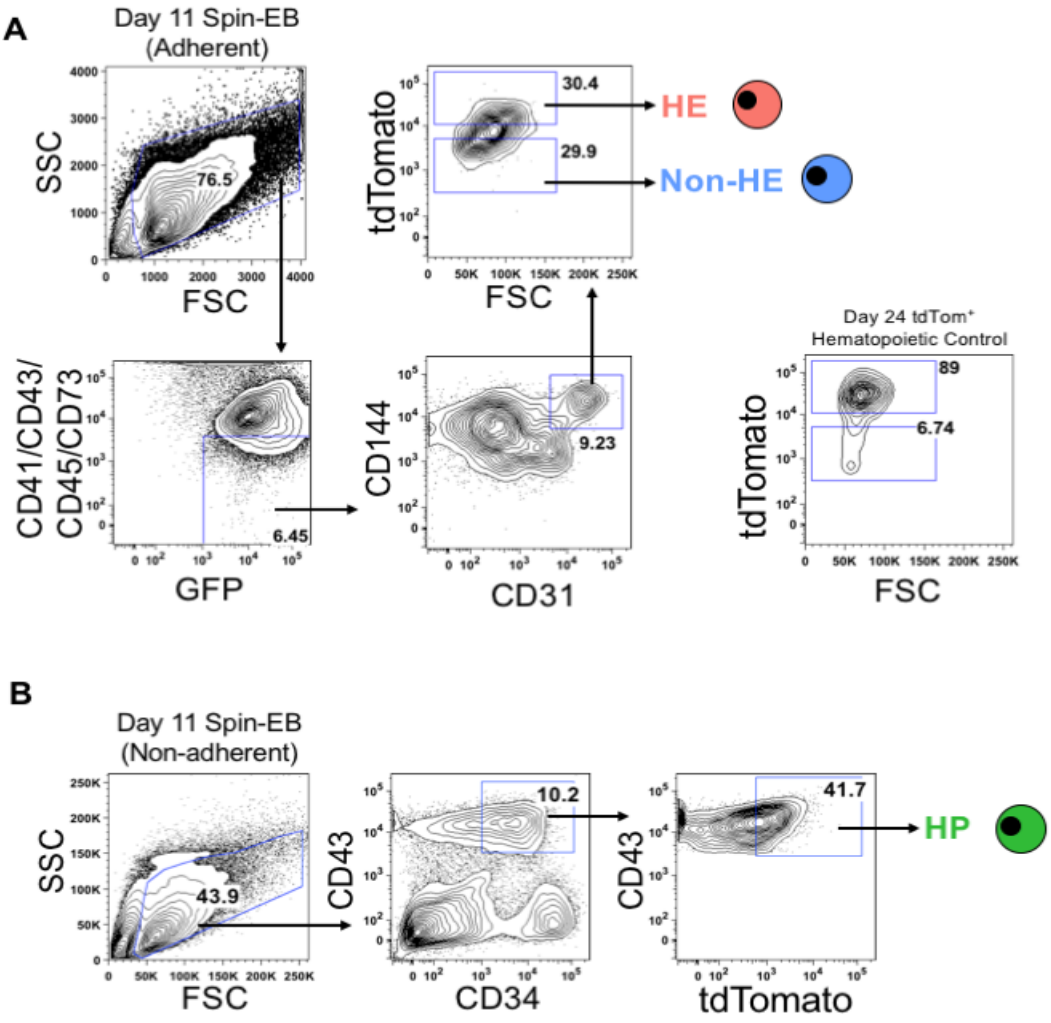


**Supplemental Figure 2-1. FACS sorting strategy of Day 11 hESC-*RUNX1c*-tdTomato-derived cells.** (A) Representative flow cytometry plots used to distinguish HE from non-HE within the adherent fraction of hESC-*RUNX1c*-tdTomato cells. Day 24 non-adherent hematopoietic cells also derived from hESC-*RUNX1c*-tdTomato cells in a parallel differentiation are also shown to establish positive gating controls of tdTomato expression. (B) Representative flow cytometry plots used to sort early hematopoietic progenitor cells from the non-adherent fraction of hESC-*RUNX1c*-tdTomato cells.

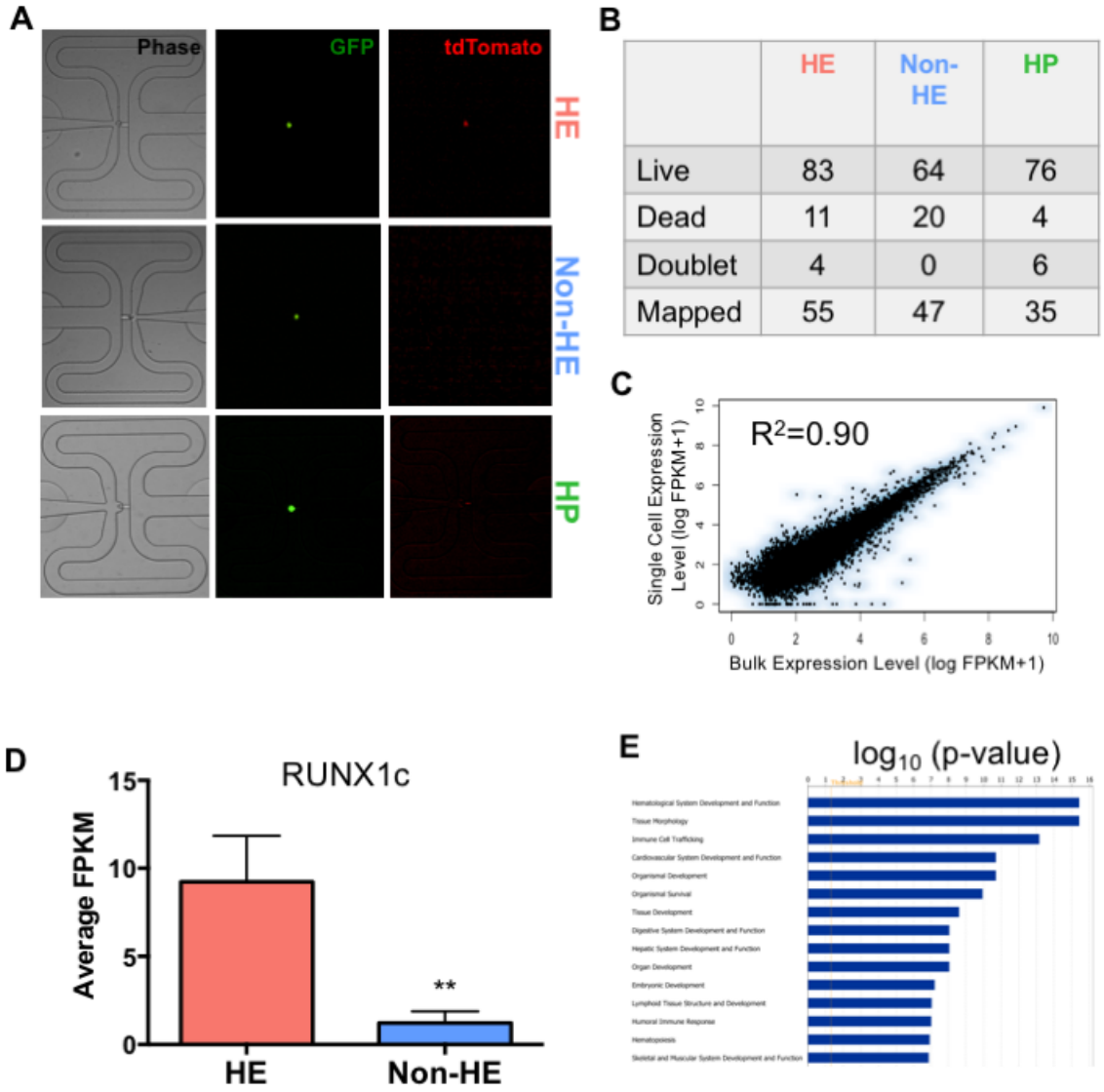


| | HE | Non-HE | HP |
|---|---|---|---|
| Live | 83 | 64 | 76 |
| Dead | 11 | 20 | 4 |
| Doublet | 4 | 0 | 6 |
| Mapped | 55 | 47 | 35 |

**Supplemental Figure 2-2. Fluidgm C1 Capture and quality control of single-cell RNASeq data.** (A) Representative images of 96-well microfluidic capture chambers, which served as the initial point of cell quality control. Within each fluidic capture point, cells were assessed for 1) singularity, 2) $GFP^{+}$ expression, and 3) absence of red-fluorescent ethidium homodimer-1 stain (dead stain). Furthermore, HE and HP sorted populations were validated for $tdTomato^{dim}$ expression, while non-HE were validated for $tdTomato^{-}$

expression. Cells that failed these quality control criteria were excluded from cDNA library preparation. (B) Statistics of Fluidigm C1 capture and HiSeq 2500 sequencing. A total of 55 HE, 47 non-HE, and 35 HP were considered validated for subsequent analyses. (C) Total gene expression across individual cells were plotted and compared to the gene expression of similarly collected bulk RNASeq sample controls. $R^2$=0.90. Each dot represents a single gene, while the blue cloud surrounding each gene reflects the variance across individual cells. (D) log-transformed FPKM values for the *RUNX1c* isoform averaged across all cells in HE and non-HE populations. **p<0.01 as compared to HE and assessed using student's t-test, error bars represent SEM. (E) Top 15 canonical pathways derived from the Ingenuity Pathway Analysis gene ontology algorithms for the HE and non-HE populations.

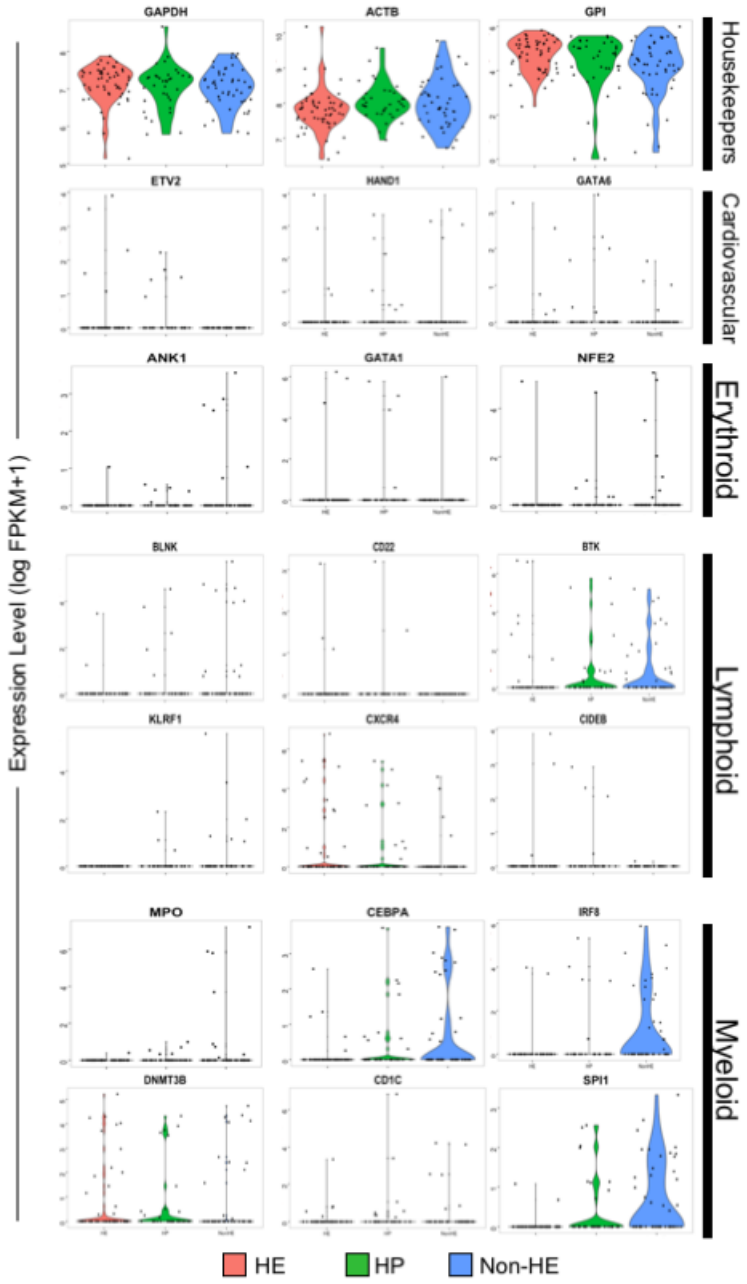


**Supplemental Figure 2-3. Supplemental violin plots of single-cell RNASeq gene expression.** Log-transformed FPKM values of key genes associated with cardiovascular development, erythroid, lymphoid, and myeloid cell phenotypes. Traditional housekeeper gene expression (*GAPDH*, *ACTB* and *GPI*) are also shown to demonstrate homogeneous expression and frequency across HE, non-HE, and HP populations.

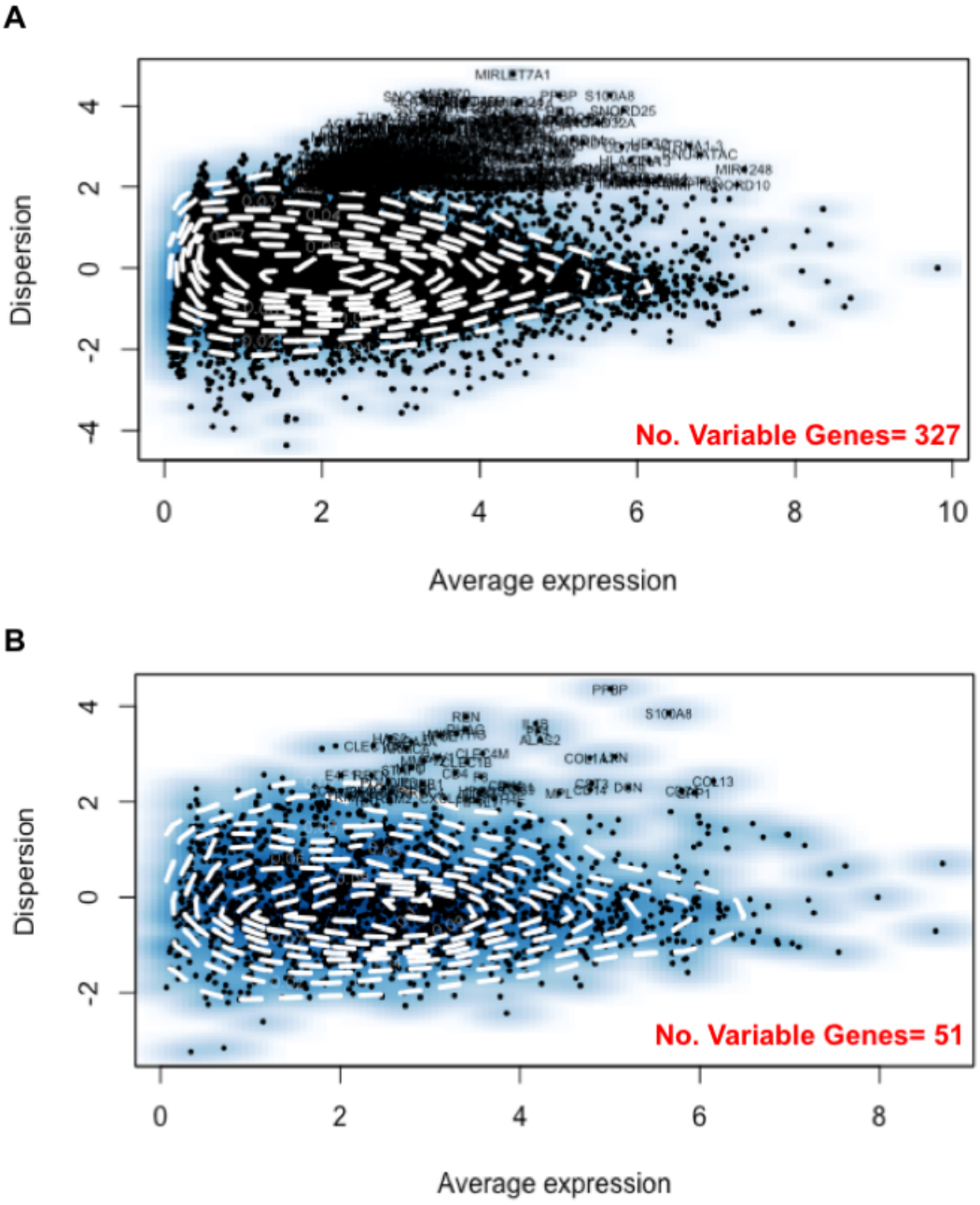


**Supplemental Figure 2-4. Dispersion plots reveal variable genes across individual cells**. (A) Dispersion (Variance of gene expression across single cells/average of gene expression) as a function of average gene expression (log (FPKM+1)) across all individual

for the total gene list and (B) blood and endothelial gene subset list. Black points with blue hues represent the mean expression of a gene, while dashed contours represent the density of single cells as obtained using Seurat's default density estimation settings. Genes of significant variability across sample populations are labeled with the gene symbol and number of variable genes is listed in the bottom right corner. These genes were included for initial PCA clustering algorithms.

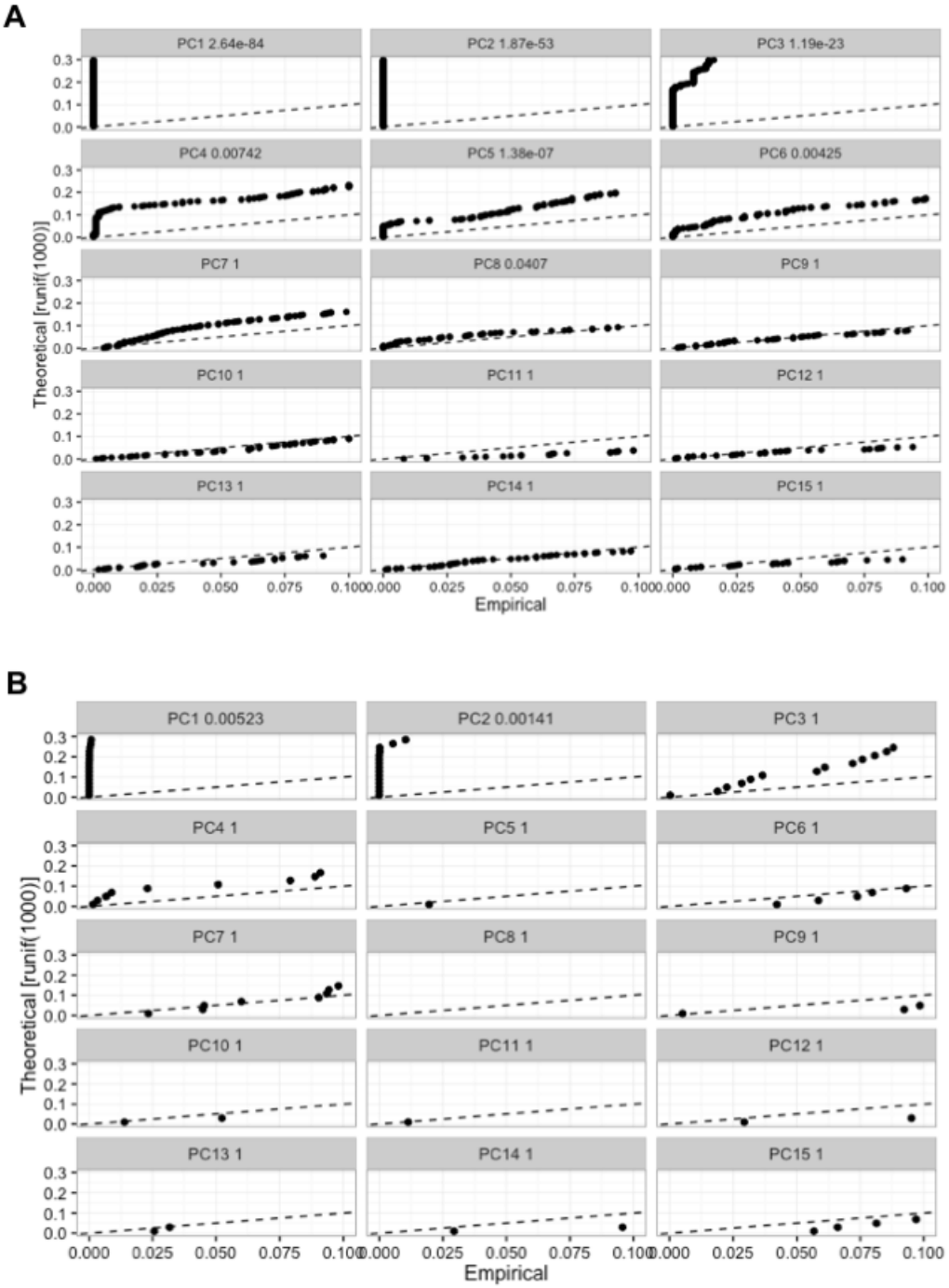


**Supplemental Figure 2-5. Significance level of principal components.** Output of Seurat p-value calculations of principal components as assessed from the (A) total gene list and (B) blood and endothelial gene restricted subset list. In brief, significance testing of

principal components is assessed by Jackstraw analysis[200]. Each subplot compares p-values of genes within the principal component via Jackstraw analysis (horizontal axis) as compared to a theoretical p-values from a random population sampling (vertical axis). Principal components with $p<0.05$ were subsequently used in t-SNE analysis and clustering classifications as described in Figure 2-3D.

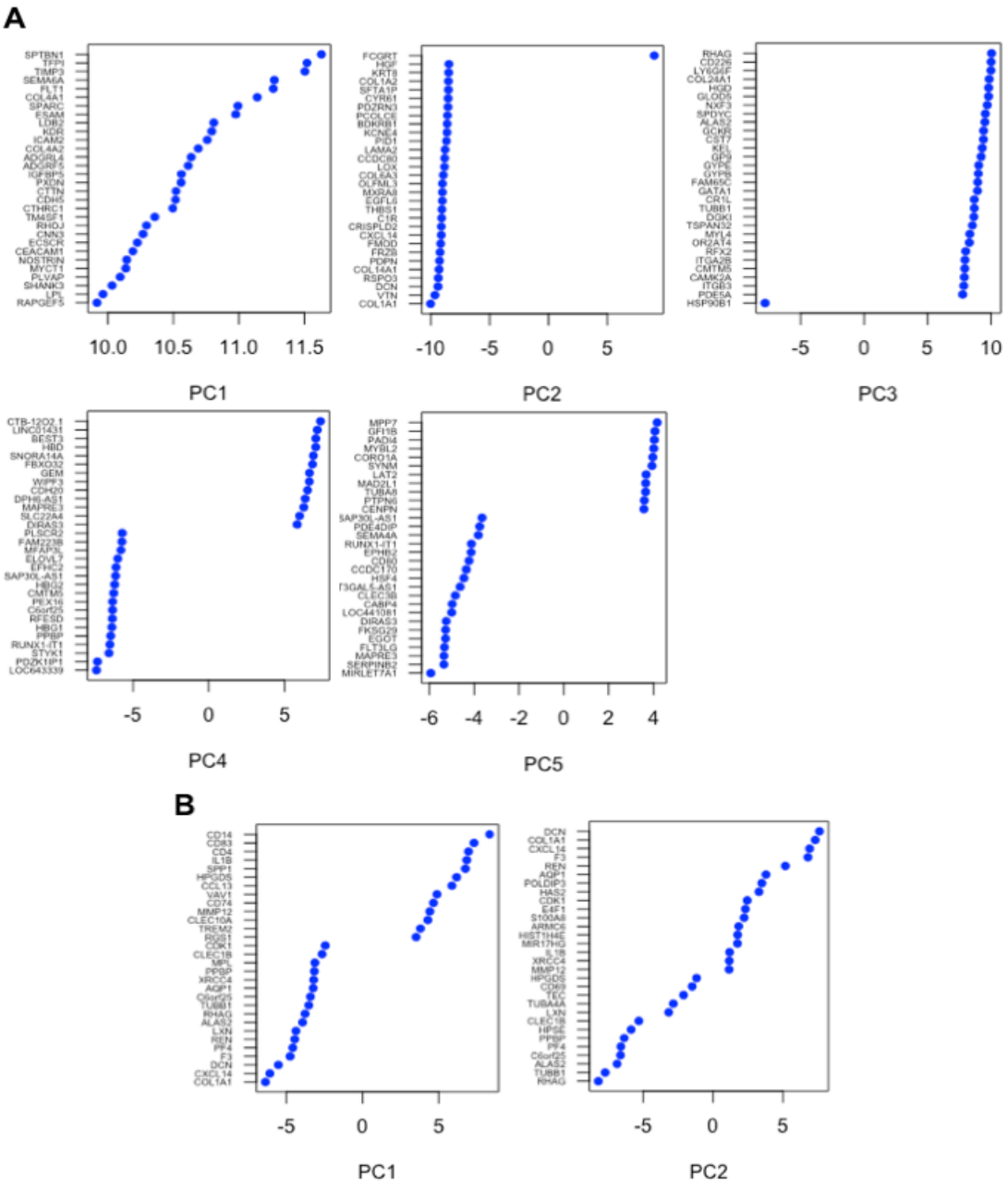


**Supplemental Figure 2-6. Gene identification from statistically significant principal components.** Visualization of principal component scores and gene symbol from each statistically significant principal component identified in Supplemental Figure 2-5 for (A) total gene list and (B) blood and endothelial gene restricted list subset.

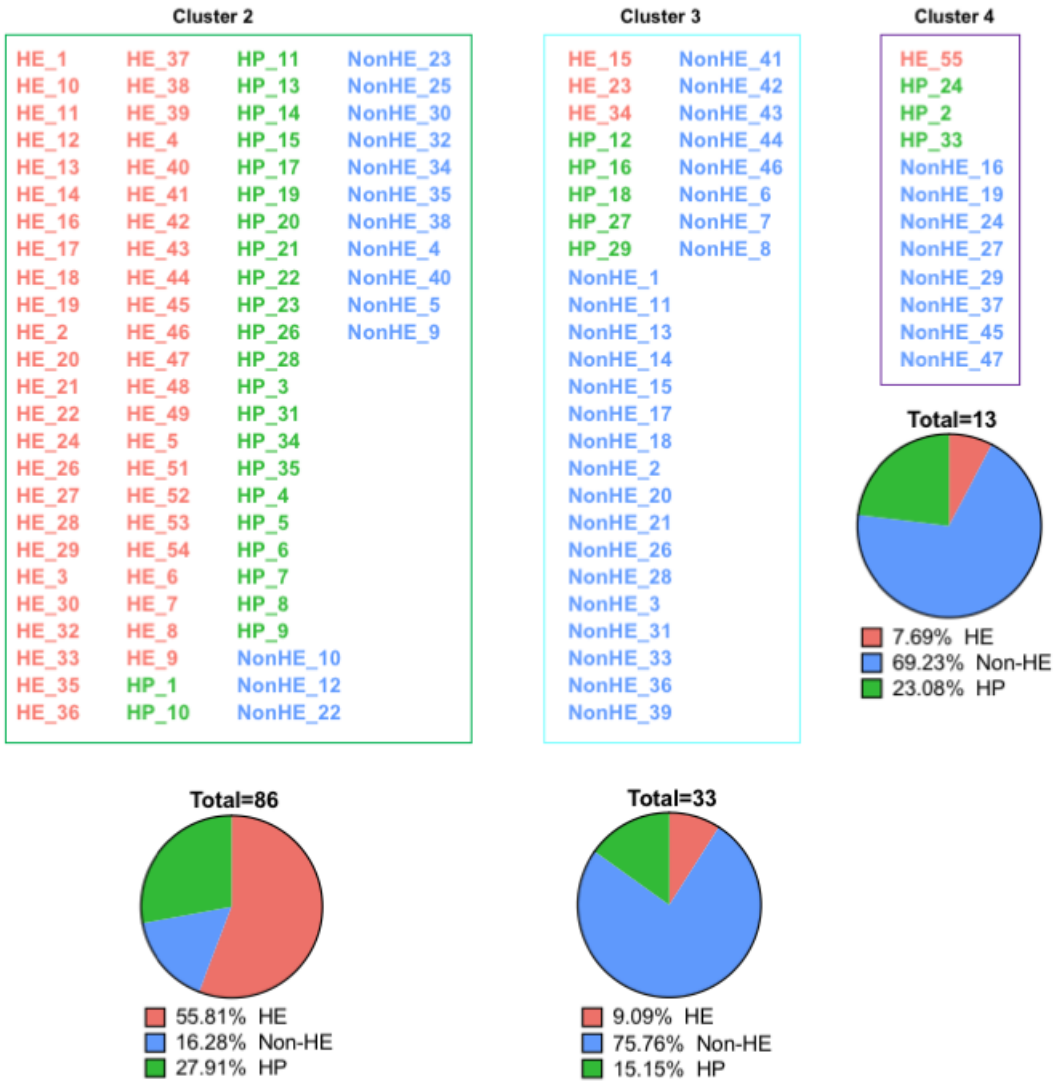


**Supplemental Figure 2-7. Cell identification of distinct clusters as determined by t-SNE analysis.** Cells assigned to cluster 2, 3, and 4 from the Total gene list t-SNE analysis are listed based on original single-cell sequencing classification. Cluster 2 comprises a majority of HE while Clusters 3 and 4 both comprise a majority of non-HE.

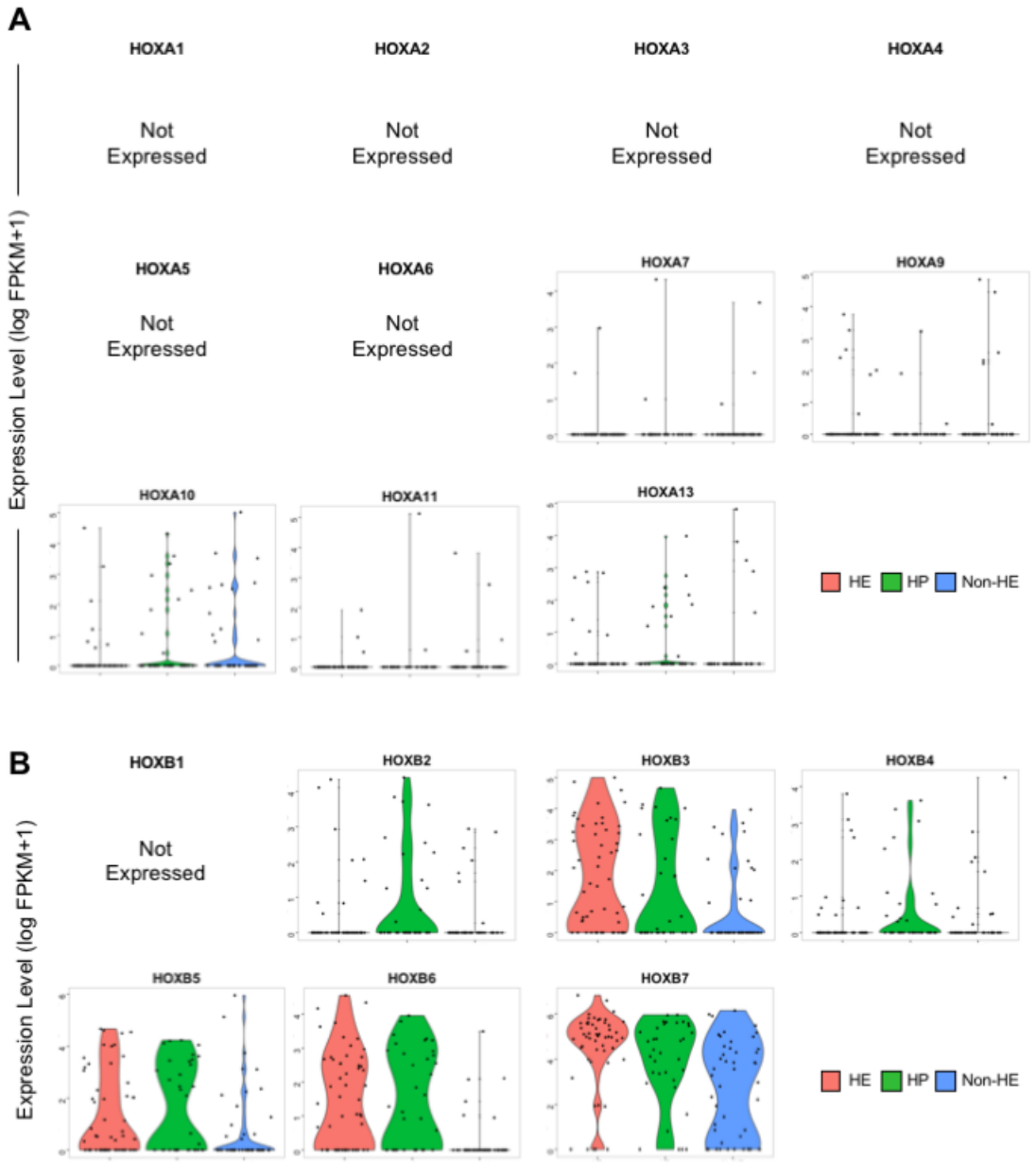


**Supplemental Figure 2-8. Violin plots of single-cell RNASeq expression of *HOXA* and *HOXB* locus genes.** A) Log-transformed FPKM gene expression values for *HOXA* locus genes. Genes that did not have any detectable level of expression are listed as "not-expressed." B) Log-transformed FPKM gene expression values for *HOXB* locus genes.

# CHAPTER 3

## *Aryl hydrocarbon receptor inhibition promotes hemato-lymphoid development from human pluripotent stem cells*

**ABSTRACT**

The aryl hydrocarbon receptor (AHR) plays an important physiological role in hematopoiesis. AHR is highly expressed in hematopoietic stem/progenitor cells (HSPCs) and inhibition of AHR results in a marked expansion of human umbilical cord blood-derived HSPCs following cytokine stimulation. It is unknown whether AHR also contributes earlier in human hematopoietic development. To model hematopoiesis, human embryonic stem cells (hESCs) were allowed to differentiate in defined conditions in the presence of the AHR antagonist StemReginin-1 (SR-1) or AHR agonist 2,3,7,8-tetrachlorodibenzo-*p*-dioxin (TCDD). We demonstrate a significant increase in $CD34^{+}CD31^{+}$ hemato-endothelial cells in SR-1 treated hESCs, as well as a two-fold expansion of $CD34^{+}CD45^{+}$ hematopoietic progenitor cells. Hematopoietic progenitor cells were also significantly increased by SR-1 as quantified by standard hematopoietic colony-forming assays. Using a CRISPR/Cas9 engineered hESC-*RUNX1c*-tdTomato reporter cell line with *AHR* deletion, we further demonstrate a marked enhancement of hematopoietic differentiation relative to wild-type hESCs. We also evaluated whether AHR antagonism could promote innate lymphoid cell differentiation from hESCs. SR-1 increased conventional natural killer (cNK) cell differentiation, whereas TCDD treatment blocked cNK development and supported Group 3 innate lymphoid cell (ILC3) differentiation. Collectively, these results demonstrate AHR regulates early human hemato-lymphoid cell development and may be targeted to enhance production of specific cell populations derived from human pluripotent stem cells.

## INTRODUCTION

Human pluripotent stem cells function as an important model system to elucidate basic genetic and cell signaling mediators of human hematopoietic development[201–203]. Previous studies demonstrate development of erythroid[155,156], myeloid[89,158,159,204], and lymphoid[78,160,161] cells from human embryonic stem cells (hESCs) and human induced pluripotent stem cells (hiPSCs). However, the molecular regulation of earlier human hematopoietic stem and progenitor cells (HSPCs) from pluripotent stem cells remains less well understood. Functional HSPCs develop during the definitive stage of hematopoiesis directly from specialized hemogenic endothelium in a process known as the endothelial-to-hematopoietic transition (EHT)[18,28]. Hemogenic endothelium capable of EHT has been identified from hESCs/hiPSCs and can thus be used as a platform to investigate the mechanistic cues supporting human HSPC development[78,157,205].

The aryl hydrocarbon receptor (AHR) is a member of the PAS (Per/Arnt/Sim) family of environment-sensing, basic helix-loop-helix transcriptional regulators that is well known for its ability to mitigate reactive oxygen species due to extracellular stressors. However, there is increasing evidence for an important physiological role of AHR in hematopoiesis[145]. AHR mRNA and protein are enriched in both murine and human HSPCs, with a significant reduction in expression at the onset of HSPC proliferation[130,206]. *Ahr* knock-out mice yield an increased number of bone-marrow derived $Lin^{-}Sca^{+}Kit^{+}$ HSPCs that are hyperproliferative and have an increased propensity for leukemogenesis[143]. This finding has been extended to human HSPCs through directed small molecule targeting of AHR in $CD34^{+}$ umbilical cord blood (UCB). Treatment with StemReginin-1 (SR-1), a

potent human-specific antagonist of AHR, substantially increases the proportion of engraftable UCB $CD34^+$ cells while also sustaining hematopoietic multipotency[207]. This strategy has recently been used in clinical trials that demonstrate dramatic HSPC expansion and an improved time to neutrophil engraftment following transplantation with SR-1 expanded UCB[142].

While these results confirm the integral role of AHR in the maintenance of HSPCs, there are a paucity of studies investigating what function, if any, AHR has in the initial differentiation of hematopoietic cells from mesodermal and endothelial progenitor cells. Here, we utilize hESCs differentiated in chemically-defined conditions to test the hypothesis that AHR regulates early human hematopoietic development at the stage of EHT. We demonstrate inhibition of AHR using SR-1 or deletion of *AHR* using CRISPR/Cas9 leads to increased hemato-endothelial and functional hematopoietic progenitor cell differentiation. Additionally, we provide novel evidence that AHR inhibition also improves development of conventional natural killer (cNK) cells from hESCs, while AHR hyperactivation supports Group 3 innate lymphoid cell (ILC3) differentiation. Collectively, these studies demonstrate AHR inhibition enhances both early human HSPC and lymphoid development, and this strategy may be useful to improve the quantity and homogeneity of clinically useful hematopoietic cell populations derived from human pluripotent stem cells.

## METHODS

### Hemato-endothelial differentiation of hESCs

Single-cell adapted hESCs (H9) were maintained on irradiated mouse embryonic fibroblasts (MEF) in ES growth media, as previously described[77]. hESCs were allowed to differentiate as spin-embryoid bodies (EBs) as previously described (Figure 3-1A)[77,170]. In brief, hESCs were plated at 3,000 cells/100 μL in a round-bottom 96-well plate using serum-free BPEL media supplemented with 20 ng/mL BMP4, 40 ng/mL SCF, and 20 ng/mL VEGF (all R&D Systems, Minneapolis, MN). Cells were centrifuged to form embryoid bodies (defined as Day 0) and were incubated for 6 additional days (defined as Day 6) to promote mesoderm induction. To differentiate early endothelial and hematopoietic progenitor cells, Day 6 EBs were transferred to pre-gelatinized 24-well plates (approx. 8-16 EBs/well) with BEL media supplemented with 40 ng/mL SCF, 40 ng/mL VEGF, 30 mg/mL thrombopoietin (all R&D Systems), 30 ng/mL IL-3, and 30 ng/mL IL-6 (both PeproTech, Rocky Hill, NJ). To modulate AHR activity, EBs were treated at Day 6+0 with DMSO, 1 μM SR-1 (Cellagen Technologies, San Diego, CA), or 10 nM 2,3,7,8-tetrachlorodibenzo-*p*-dioxin (TCDD) (Sigma-Aldrich, St. Louis, MO). Media was exchanged every 3 days with small molecule and cytokine supplementation. At indicated time points, non-adherent cell fractions were collected and saved while the remaining adherent fractions were treated with 0.05% trypsin containing 2% chicken serum. Adherent cells were combined with the non-adherent fractions for analysis, unless otherwise stated.

**Innate lymphoid cell (cNK cell and ILC3) differentiation from spin-EBs**

Spin-EBs were generated as described above[122,160,161]. Following 11 days of mesoderm conditioning (Day 11), spin-EBs were collected and analyzed by flow cytometry to assess hematopoietic progenitor cell potential (see flow cytometry methods for antibodies used) (Figure 4A). Spin-EBs yielding >30% $CD34^{+}CD45^{+}$ cells were transferred onto 24-well plates coated with irradiated OP9-DL1 cells[208,209] (now defined as Day 11+0). EBs and OP9-DL1 were co-cultured in NK differentiation media (NKDM) supplemented initially with SCF, IL-15, IL-7, Flt3-L (all R&D Systems), and IL-3 (PeproTech) for one week; DMSO, SR-1, or TCDD were also added at Day 11+0. Every week, a one-half media change with NKDM supplemented with SCF, IL-15, IL-7, Flt3-L, and drugs was performed. hESCs were differentiated for four additional weeks (Day 11+28) and non-adherent cells were harvested for analysis.

**Hematopoietic colony-forming unit (CFU) assay**

Day 6+5 spin-EB non-adherent fractions were resuspended in IMDM. 50,000 cells were seeded in 2 mL of H4436 Methocult (StemCell Technologies, Vancouver, CAN) and plated directly in 35 mm culture dishes (Greiner, Monroe, NC). Plates were incubated for 14 days and subsequently counted and phenotypically scored using standard criteria[89].

**CRISPR-Cas9 gene editing and hESC transfection**

gRNA against *AHR* exon 1 (5'-TCAGATTGTCCCTGGAGGTC-3') driven by U6 promoter was subcloned into a pCR4-TOPO vector (ThermoFisher Scientific). Single-cell cell adapted H9 *RUNX1c*-tdTomato reporter cell lines previously produced by our group[77]

were transfected with 1 μg plasmid DNA, 1 μg Cas9 mRNA (TriLink Biotechnologies, San Diego, CA), and mCherry fluorescent protein mRNA using the Neon Transfection System (ThermoFisher Scientific) set at 1100V, 20ms, 1 pulse. Post-transfection, cells were resuspended in MEF conditioned media without antibiotics supplemented with 5 μM Y-27632 and seeded onto Matrigel-coated 6 well plates. 96-hour post-transfection, individual mCherry$^{+}$ colonies were picked onto fresh MEFs for clonal expansion. Genomic DNA was isolated using the DNeasy Blood and Tissue Kit (Qiagen) and *AHR* PCR products were generated with high fidelity AccuPrime *Taq* DNA Polymerase (ThermoFisher Scientific). PCR products were purified and subcloned into a pCR-TOPO4 vector for sequencing. Cloned products were transformed into One Shot TOP10 competent cells (ThermoFisher Scientific) and were colony sequenced via rolling circle amplification (Sequetech, Mountain View, CA) using M13R primers. On- and off-target effects were assessed using a Surveyor mutation detection kit (IDT Technologies, Coralville, IA) and the following AHR-specific primers: F: 5'- AGGCAGCTCACCTGTACT-3'; R: 5': CATCTCGCCTTACCAAACTCTAC-3'. Only clones that displayed AHR specific cleavage products and had *AHR* Exon 1 specific deletions as determined by sequencing were chosen for experiments.

**Flow Cytometry**

The following additional antibodies were used (all anti-human): LFA-1 (CD11a/CD18)-APC-R700 (BD Biosciences), CD31-APC (eBioscience), CD33-APC (BD Biosciences), CD34-PECy7 (BD Biosciences), CD34-APC (BD Biosciences), CD41a-

APC (BD Biosciences), CD43-APC (BD Biosciences), CD45-APC (BD Biosciences), CD56-PECy7 (BD Biosciences), CD56-BV421 (BD Biosciences), CD94-PerCP-Cy5.5 (BD Biosciences), CD117-PECy7 (BD Biosciences), CD117-APC (eBiosciences), CD144-APC (eBioscience). Samples were analyzed on either an LSRFortessa or LSRII flow cytometer (BD Biosciences). Gating was set relative to isotype controls of identical fluorophores. Data from flow cytometry was analyzed using FlowJo software (Treestar, Ashland, OR).

**FACS sorting and CD34$^+$ cell expansion**

Non-adherent cells from Day 6+5 spin EBs were washed, filtered, and stained with anti-human CD45-PECy7 (eBioscience) and CD34-APC (BD Biosciences) in FACS Buffer (DPBS + 2% FBS and 0.1% sodium azide) for 30 minutes at 4°C. Dead cells were counterstained with Sytox Blue (ThermoFisher Scientific) immediately prior to sorting. Live CD34$^+$CD45$^+$ populations were sorted using a FACSAria II (BD Biosciences). Human UCB CD34$^+$ cells (ClinImmune Lab, Denver, CO) were sorted using MACS separation columns and CD34$^+$ microbead kit (Miltenyi Biotec). Immediately post-sort, cells were cultured with Flt-3L, SCF, TPO, and IL-6 (all 100 nM) as described elsewhere[141] and supplemented with DMSO, SR-1, or TCDD. Cells were counted every 3 days and assessed for CD34 expression by flow cytometry. Total CD34$^+$CD45$^+$ cell count was determined by multiplying the absolute cell count by the percentage of CD34$^+$CD45$^+$ cells remaining.

**Cell cycle analysis and proliferation studies**

Spin EBs were differentiated into hemato-endothelial cells with non-adherent cells harvested on Day 6+5. Cells were cultured in a 24-well plate and harvested after 1 week for flow cytometry analysis. Cells were co-stained with anti-human CD34-PECy7 to monitor proliferation of HSPCs. For cell cycle analysis, Day 6+5 non-adherent cells derived from EBs were harvest and monitored for S-phase using the Click-iT EdU Alex Fluor 647 flow cytometry assay kit per manufacturer instructions. Prior to flow cytometry, cells were counterstained with 50 μg/mL propidium iodide supplemented with 100 μg/mL RNAse A (New England BioLabs, Ipswich, MA).

**RNA isolation and quantitative real-time PCR (qRT-PCR) analysis**

Non-adherent cell fractions were harvested as previously described in the main text. Total RNA was harvested using the Qiashredder tissue homogenizer kit (Qiagen, Valencia, CA) with RNAeasy Mini Kit. RNA concentration and purity was assessed using a NanoDrop 2000 (ThermoFisher Scientific) spectrophotometer and subsequently revere transcribed with a SensiFAST cDNA Synthesis Kit (Bioline, Taunton, MA). qPCR was performed using the All-in-One qPCR Mix (GeneCopoeia, Rockville, MD) and cDNA was used at 50 ng/uL per reaction for qRT-PCR using gene specific human primer pairs (Supplementary Table 1). qPCR reactions were run on an StepOnePlus Real-Time PCR System thermocycler (ThermoFisher Scientific) in either technical duplicate or triplicate. Ct values were normalized to a GAPDH housekeeper for each sample. Data were then normalized relative to controls using the 2^-(ΔΔCt) method.

**Immunoblotting**

Undifferentiated hESCs were harvested and lysed in lysis buffer (10mM HEPES pH 7.4, 150 mM KCl, 0.1% NP40, 5mM $MgCl_2$ supplemented with EDTA-free protease inhibitor tablet (Roche, Branchburg, NJ)) overnight at 4°C. Protein concentration was determined by bicinchoninic acid (BCA) assay, per manufacturer protocol (ThermoFisher Scientific). 50 μg of protein lysate was added to 6x SDS loading buffer (250mM Tris, 2% SDS, 20% glycerol, 0.05% bromphenol blue), loaded onto a 4-20% Mini-PROTEAN TGX Gel (BioRad, Hercules, CA), and electrophoresed at 120V for 1 hour. Protein was then transferred to a nitrocellulose membrane in transfer buffer (25x Tris-Glycine transfer buffer with 5x 100% methanol) overnight at 30V. Membranes were blocked with 5% milk for 1 hr at room temperature and subsequently incubated with the following primary antibodies overnight at 4°C in blocking buffer (all human): mouse monoclonal anti-AHR (ab2769; Abcam, Cambridge, MA), rabbit polyclonal anti-AHRR (ab108518; Abcam), rabbit polyclonal anti-CYP1B1 (ab137562; Abcam), or rabbit monoclonal anti-actin (Sigma-Aldrich, St. Louis, MO). Membranes were washed three times with PBST and incubated with either anti-rabbit or anti-mouse IgG HRP-link secondary antibody (Cell Signaling Technologies, Danvers, MA). Bands were visualized on film using SuperSignal West Dura Extended Duration Substrate (ThermoFisher Scientific) and standard film processor at various exposure times.

**CD107a Degranulation Assay**

To examine NK cell activity, as previously described[126,210–212], hESC-derived NK cells were harvested, washed, and plated at 100,000 cells per well of a V-bottomed 96-well plate co-cultured with K562 at a 2:1 effector-to-target ratio. NK cell only and NK+K562 wells were incubated with anti-CD107a-AF700 (BD Biosciences, San Jose, CA) for 1 hour. Following incubation, 1:1500 Golgi Stop and 1:1000 Golgi Plug mix (BD Biosciences) was added and cells were incubated for 4 hours. Cells were washed with PBS and counterstained with Near-IR Live/Dead Fixable Dye (ThermoFisher Scientific). Cells were washed again and co-stained with the following antibodies (all anti-human): CD3-PE-Texas Red (eBioscience, San Diego, CA), CD14 PE-Texas Red (eBioscience), CD19-PE-Texas Red (eBioscience), and CD56-PE (Beckman Coulter, Indianapolis, IN) for 30 minutes at 4°C. Cells were then transferred to FACS tubes and analyzed.

**Fluorescent Activated Cell Sorting (FACS) of NKP, cNK, and ILC3 derived from hESCs**

To assess the effects of AHR modification on NK cell and ILC specification, non-adherent hematopoietic cells derived from hESCs on Day 11+28 cultured in NKDM supplemented with DMSO, SR-1, or TCDD were harvested as single-cell suspensions. Cells were washed with DPBS, filtered, and stained with the following antibodies (all anti-human): CD56-BV421, CD94-PerCP-Cy5.5, CD117-PECy7, and LFA-1 (CD11a/CD18)-APC-R700 in sterile FACS Buffer (DPBS + 2% FBS and 0.1% sodium azide) for 30 minutes at 4°C. Cells were washed with FACS buffer and cells were counterstained with Sytox Blue (ThermoFisher Scientific) immediately prior to sorting. Live NKP, cNK, and

ILC3 populations were sorted directly into FACS tubes containing NKDM basal media using a FACSAria II (BD Biosciences) cell sorter. Cells were immediately centrifuged, washed once with PBS, and processed from total RNA isolation as described above.

**Statistical Analyses**

Differences between groups were compared either with student's t-test or one-way/two-way ANOVA using Prism 6 (GraphPad Software, San Diego, CA). Results were considered statistically significant at p-values $< 0.05$.

**RESULTS**

**Small molecule antagonism of AHR enhances early hemato-endothelial differentiation from hESCs**

To establish whether AHR mediates development of the earliest human hematopoietic cells, we differentiated hESCs using a two-stage defined culture system, as previously described (Figure 3-1A)[77,213]. We first assessed whether endogenous *AHR* was expressed in undifferentiated hESCs and hESCs differentiating into hemato-endothelial cells using qRT-PCR. *AHR* expression was increased 4.30±1.24 fold in the differentiated cell population at Day 6+3 relative to undifferentiated hESCs and became significantly increased at Day 6+5 (7.33±1.24 fold, $p<0.01$) (Supplemental Figure 3-1A). We also observed a corresponding increase in the expression of two downstream effector targets of AHR signaling (*CYP1A1* and *CYP1B1*). These data indicate that endogenous *AHR* activity is upregulated at the onset of hemato-endothelial differentiation from hESCs, suggesting

that AHR is implicated in early hematopoiesis. We next treated hESCs with SR-1 or TCDD to modulate AHR signaling, or DMSO vehicle control. Following 4 days of culture, hESCs treated with 1 μM SR-1 had reduced expression of *CYP1A1* and *CYP1B1*, whereas hESCs treated with TCDD yielded a significantly increased expression of *CYP1A1* and *CYP1B1* as compared to DMSO normalized controls. We also confirmed that there were no significant cytotoxic effects on hESCs due to the presence of SR-1 or TCDD (Supplemental Figure 3-1C). Together, SR-1 and TCDD can effectively be used as agents to selectively regulate AHR-mediated activity in hESCs.

We next investigated differentiating hemato-endothelial cells when exposed to SR-1 or TCDD. As early as Day 6+3, there was a marked increase in the total percentage of $CD34^+CD144^+$ (1.71±0.22 fold, $p<0.05$) and $CD34^+CD31^+$ (1.58±0.28 fold) cells that have dual hemato-endothelial cell developmental potential in SR-1 treated hESCs as compared to DMSO controls[214–216] (Figure 3-1B & 3-1C). As differentiation continued to Day 6+6, there were also notable increases in the total percentage of both $CD34^+CD31^+$ (1.62±0.12 fold, $p<0.05$) hemato-endothelial cells and budding $CD34^+CD43^+$ (1.36±0.12 fold) hematopoietic progenitor cells[70,77,199,204] when SR-1 treatment was applied. At Day 6+9, there was a significant increase in development of $CD34^+CD45^+$ hematopoietic progenitor cells[77,93,217] (1.40±0.11, $p<0.05$) in the SR-1 treated cells. We also observed development of more terminally differentiated hematopoietic phenotypes ($CD34^-CD43^+$ and $CD34^-CD45^+$) when hESCs were treated with TCDD. This effect was most pronounced at the Day 6+9 time point, where there was a reduction in the total percent of $CD34^+CD144^+$ (0.33±0.13), $CD34^+CD31^+$ (0.49±0.06, $p<0.05$), $CD34^+CD43^+$(0.67±0.09, $p<0.05$), and

$CD34^+CD45^+$ (0.44±0.06, $p<0.05$) progenitor cells with an increase in the total percent of $CD34^-$ hematopoietic cells. Taken together, these data demonstrate that AHR inhibition with SR-1 promotes early hemato-endothelial cell development, whereas AHR hyperactivation with TCDD accelerates differentiation towards more terminally differentiated hematopoietic lineages.

**Increased AHR-mediated production of hESC-derived hemato-endothelial cells is not due to increased proliferation of $CD34^+$ cells**

Since we observed that SR-1 treatment increased the total percentage of $CD34^+$ cells derived from hESCs, we next questioned whether this was caused by increased proliferation and/or cycling of developed $CD34^+$ cells. We sorted Day 6+5 $CD34^+CD45^+$ hematopoietic progenitor cells and expanded them over the course of 15 days in expansion media supplemented with SR-1, TCDD, or DMSO. In parallel, we sorted $CD34^+CD45^+$ human UCB as a positive control. The absolute number of nucleated cells derived from UCB and treated with either DMSO, SR-1, and TCDD expanded at a significantly greater rate than their counterparts derived from Day 6+5 hESCs beginning by Day 9 of culture (Supplemental Figure 3-2A). By Day 15, there was a significant increase in the absolute number of nucleated cells in the UCB SR-1 group ($14.2\pm1.0 \times 10^6$, $p<0.05$) relative to both DMSO ($9.00\pm0.71 \times 10^6$) and TCDD ($7.14\pm0.46 \times 10^6$) groups. However, we did not find a similar expansion of Day 6+5 hESC derived total cells as UCB-derived $CD34^+$ cells between treatment groups at any time point. We further characterized the differentiating cells for development of $CD34^+CD45^+$ cells and calculated the total number of these cells

remaining over time. Again, by Day 15, there were significant increases in the number of $CD34^+CD45^+$ cells in the UCB SR-1 group ($5.62\pm0.40 \times 10^6$, $p<0.05$) as compared to DMSO ($1.69\pm0.13 \times 10^6$) and TCDD ($0.15\pm0.01 \times 10^6$) treated UCB. As expected from the previous differentiation studies directly from spin-EBs, TCDD treatment of both UCB and hESC-derived $CD34^+CD45^+$ accelerated the differentiation to terminally differentiated $CD34^-$ hematopoietic cells as compared to DMSO, while SR-1 slowed this progression and retained hematopoietic cells in a progenitor state (Supplemental Figure 3-2B). These data suggest hESC-derived hemato-endothelial progenitor cells do not proliferate in response to SR-1 as do UCB $CD34^+$ cells, but rather are enhanced through differentiation pathways.

**AHR-modulation in hESC-derived hemato-endothelial cells alters cell cycle progression**

We next evaluated whether increased hemato-endothelial phenotype was due to alterations in cell cycle progression when SR-1 was applied. We analyzed hESC-derived, non-adherent hematopoietic progenitor cells treated with either DMSO, SR-1, or TCDD at Day 6+5 to assess for the percentage of cells in $G_0/G_1$ ($EdU^-PI^{low}$), S-phase ($EdU^+PI^+$), and $G_2/M$ ($EdU^-PI^{hi}$) (Supplemental Figure 3-3A). SR-1 treated hematopoietic progenitor cells had a significant increase for $G_0/G_1$ phase ($43.7\%\pm1.82$, $p<0.05$) rather than S-phase ($38.2\%\pm1.00$, $p<0.01$) as compared to DMSO treated controls ($39.6\%\pm0.35$ and $44.6\%\pm0.48$, respectively) (Supplemental Figure 3-3B). Conversely, TCDD treated hematopoietic progenitor cells were significantly enriched for S-phase ($38.2\%\pm1.03$, $p<0.001$) rather than $G_0/G_1$ phase ($25.8\pm0.34$, $p<0.01$) as compared to the same controls.

Collectively, these data demonstrate AHR regulates hemato-endothelial and hematopoietic progenitor cell phenotype via cell cycle modification.

**AHR inhibition leads to functional hematopoietic progenitor cells and increased expression of key hematopoietic genes**

We next examined whether SR-1 supported the production of functional hematopoietic progenitor cells by standard methylcellulose-based colony forming unit (CFU) assays. SR-1 conditioning led to a marked increase in hematopoietic progenitor cell development compared to DMSO-treated controls (245.67±64.4 colonies vs. 60.3±1.20 colonies, respectively, $p<0.05$), while the TCDD treated cells were significantly decreased (28.3±2.67 colonies, $p<0.05$) (Figure 3-2A).

We further assessed key transcriptional regulators of human hematopoiesis that may be modulated by AHR expression within developing hemato-endothelial cells. We again analyzed the non-adherent hematopoietic fractions of differentiating hESC-derived cells treated with DMSO, SR-1, and TCDD and performed qRT-PCR probing for AHR-related genes (*AHR, CYP1B1*), megakaryotic-erythropoietic genes[218] (*GATA1* and *GATA2*), a myelopoiesis regulator (*PU.1*)[218], and a definitive hematopoiesis specific gene (*CMYB*)[40,205,219]. We found SR-1 treatment increased the expression of *GATA1* (2.58±0.40 fold) and *GATA2* (6.85±0.74 fold, $p<0.05$) as early as Day 6+3 (Figure 3-2B). The mean *GATA2*:*GATA1* at Day 6+3 was 2.67, and this positive ratio is in accord with the elevated *GATA2* endogenous gene progression relative to *GATA1* throughout early erythropoiesis[220,221]. TCDD treatment decreased the expression of *GATA1* at Day 6+3

(0.31±0.08 fold, $p<0.05$) as compared to DMSO controls and induced a reduction in *GATA2* later at Day 6+6 (0.37±0.13 fold, $p<0.05$). There was a similar induction of *PU.1* with SR-1 treatment and reciprocal expression in TCDD treated hematopoietic cells at each time point. The increased fold-change of *GATA1*/*GATA2* and *PU.1* expression supports the enhanced production of CFU-E and CFU-M in SR-1 treated hematopoietic progenitor cells (Figure 3-2A). Moreover, SR-1 treatment also mediated a significant increase of *CMYB* at all time points. Collectively, these results further demonstrate AHR inhibition leads to enhanced activation of a functional and multilineage hematopoietic transcriptional program from hESCs.

### *AHR* knockout in hESCs promotes early hematopoietic differentiation

We next investigated whether genetic deletion of *AHR* in hESCs would similarly mediate or even further enhance hemato-endothelial and hematopoietic progenitor cell production. To do this, we utilized CRIPSR/Cas9 to develop stable and clonally-derived hESCs cell lines with a deletion in *AHR*, preventing expression. Specifically, we utilized hESCs previously modified with a *RUNX1c*-tdTomato reporting cassette generated in our lab that demonstrates faithful measurement of early hemato-endothelial cells[77]. As previously described, these cells allowed us to observe EHT and isolate early human hematopoietic cells as they emerge from adherent endothelial cells. These cells now allow us to dually evaluate the effect of *AHR* gene modification on the induction of EHT[77,205]. We clonally expanded hESCs transfected with a gRNA target complementary to *AHR* exon 1 and probed for modification using primers flanking the exon 1 sequence (Figure 3-3A).

We identified clones that yielded a 718bp amplicon (wild-type, WT), a 718bp amplicon with an additional 571bp amplicon indicative of partial exon 1 deletion (*AHR*$^{+/-}$), and only the 571bp amplicon (*AHR*$^{-/-}$) (Figure 3-3B). We confirmed functional loss of AHR protein with significant attenuation of the AHR-downstream targets aryl hydrocarbon receptor repressor (AHRR) and CYP1B1 in AHR$^{-/-}$-hESC-*RUNX1c*-tdTomato cells, as compared to K562 and NK92 positive controls, and wild-type hESC-*RUNX1c*-tdTomato cells (Figure 3-3C). We additionally validated the on-target specificity of the gRNA by probing the AHR amplicons generated from the genomic DNA of each clone with Surveyor endonuclease as well as with direct sequencing (data not shown). These data confirmed we successfully generated heterozygous and homozygous deletions of *AHR* within hESCs.

We next differentiated WT-, *AHR*$^{+/-}$-, and *AHR*$^{-/-}$-*RUNX1c*-tdTomato hESCs as in previous studies. At Day 6+3, there was approximately a 2-fold increase in development of hemato-endothelial cells (CD34$^{+}$CD31$^{+}$ and CD34$^{+}$CD144$^{+}$) as compared to WT- and *AHR*$^{+/-}$-hESCs at Day 6+3 (Figure 3-3D, quantified in Supplemental Figure 3-4A). We also found that *AHR*$^{-/-}$-*RUNX1c*-tdTomato hESCs produced more than a 2-fold increase in CD34$^{+}$CD43$^{+}$ and CD34$^{+}$CD45$^{+}$ hematopoietic progenitor cells at both Day 6+3 and Day 6+6 time points. Importantly, the total percentage of CD34$^{+}$ was not compromised as hematopoietic progenitor cells further differentiated into mature hematopoietic cells (CD34$^{-}$CD33$^{+}$, CD34$^{-}$CD41a$^{+}$, CD34$^{-}$CD43$^{+}$, CD34$^{-}$CD45$^{+}$). By Day 6+9, a majority of the *AHR*$^{-/-}$-hESC-derived cells continued to differentiate into matured hematopoietic lineages at a greater rate than WT- and *AHR*$^{+/-}$-hESCs, as indicated by an increased total percentage of CD34$^{-}$CD45$^{+}$ cells.

Using the *RUNX1c*-tdTomato reporter, we also demonstrated an increased commitment towards *RUNX1c*$^{+}$ cell development in *AHR*$^{-/-}$-*RUNX1c*-tdTomato hESCs as compared to WT- and *AHR*$^{+/-}$-*RUNX1c*-tdTomato hESCs. Specifically, there was a 5-fold expansion in the total percentage of tdTomato$^{+}$ hematopoietic progenitor cells at both Day 6+3 and Day 6+6 in *AHR*$^{-/-}$-*RUNX1c*-tdTomato hESCs compared to WT- and *AHR*$^{+/-}$-*RUNX1c*-tdTomato hESCs (Figure 3-3E, quantified in Supplemental Figure 3-4B). We also further confirmed increased development of functional hematopoietic progenitor cells derived from *AHR*$^{-/-}$-*RUNX1c*-tdTomato hESCs compared to the controls using hematopoietic colony-forming unit assays. There was a significant increase in the total number of colonies formed in the *AHR*$^{-/-}$-hESCs (188.67±11.29 colonies, $p<0.05$) as compared to *AHR*$^{+/-}$-hESCs (54.0±2.08 colonies) and WT-hESCs (50.33±4.91 colonies) (Figure 3-3F). Collectively, these data suggest that genetic deletion of *AHR* in hESCs can robustly support functional hemato-endothelial differentiation.

**AHR inhibition enhances cNK cell differentiation from hESCs while AHR hyperactivation supports ILC3 cell phenotype**

Recent studies also demonstrate an important role of AHR to mediate development and function of both innate and adaptive immune cells[129,222]. Since AHR attenuation supports the differentiation of CD34$^{+}$CD45$^{+}$ hematopoietic progenitor cells (Figures 3-1B, 3-3D), we assessed whether NK cell differentiation could also be enhanced from hESCs using defined conditions and a small molecule approach. Here, we used our previously described system for NK cell development from hESCs as a model for

lymphopoiesis[122,160,161] (Figure 3-4A). By Day 11, spin-EBs produced a high percentage of $CD34^{+}CD45^{+}$ hematopoietic progenitor cells (range: 38.5%-65.0% for n=3 separate studies) (Figure 3-4B). At Days 11+21 (11 days in hematopoietic differentiation conditions, then 21 days in NK cell differentiation conditions) and Day 11+28, SR-1 treated hESC-derived hematopoietic cells demonstrated increased development of NK cells compared to DMSO treated controls, while TCDD treated hESC-derived hematopoietic cells had fewer phenotypic NK cells (Figures 3-4B & 3-4C). In addition to surface antigen acquisition, we also assessed lymphoid-specific gene expression in the hematopoietic cells produced in each treatment group. As compared to the DMSO treated control group, SR-1 treated hESC-derived hematopoietic cells expressed a significantly higher amount of *ID2* (2.49±0.003 fold, $p<0.01$), *TBX21/TBET* (3.44±0.55 fold, $p<0.05$), and *EOMES* (5.12±0.52 fold, $p<0.05$), transcriptional factors that mediate increased NK cell lineage commitment (Figure 3-4D). While we also observed a significant increase in *TBX21/TBET* (1.56±0.07 fold, $p<0.05$) and *EOMES* (1.84±0.11 fold, $p<0.05$) in the TCDD treated hESC-derived hematopoietic cells, the fold-induction was significantly lower than those of the SR-1 treated group. We further assessed the functionality of differentiated NK cells by assessing CD107a degranulation when stimulated with K562 target cells. SR-1 treated hESC-derived hematopoietic cells were comparable to DMSO treated controls in CD107a expression (58.1±0.67% vs. 47.2±2.76%), while TCDD treated hESC-derived hematopoietic cells expressed less CD107a (36.8±2.1%) (Figure 3-4E & 3-4F). Collectively, these data support SR-1 treatment of differentiating hESCs enhances the production of functional NK cells.

We further defined the identity of developing lymphoid phenotypes regulated by AHR activity by evaluating natural killer progenitor cells (NKP), conventional NK cells (cNK), and developmentally related innate lymphoid group 3 cells (ILC3)[100,106,118]. At Day 11+28, hESC-derived hematopoietic cells treated with DMSO control produced cNK ($CD94^+CD117^-CD56^+LFA1^+$) and ILC3 ($CD94^-CD117^+CD56^+LFA1^-$) cells, but with a majority of the differentiated cells restricted to the NKP ($CD94^+CD117^+$) gate (Figures 3-5A & 3-5B). Treatment with SR-1 significantly shifted hESC-derived hematopoietic cells away from NKPs (16.13±0.58% vs. 32.0±2.98%, $p<0.01$) and toward cNK cells (37.0±2.92% vs. 16.5±1,77%, $p<0.001$) compared to DMSO, with a significant reduction in the $CD94^-CD117^+$ population (Figure 3-5D). Treatment with TCDD also significantly shifted hESC-derived hematopoietic cells away from an NKPs, but conversely led to reciprocal increase in $CD94^-CD117^+$ cells (28.5±4.42% vs. 13.1±1.34%, $p<0.01$). When $CD94^-CD117^+$ cells were subgated to distinguish the presence of ILC3s, a significantly larger percentage TCDD treated hESC-derived hematopoietic cells were absent for LFA1, as compared to DMSO treated controls (69.4±4.57% vs. 48.8±4.81%, $p<0.05$) (Figure 3-5E). We have previously shown that LFA1 expression is a unique and distinguishing marker between ILC3 ($LFA1^-$) and cNK ($LFA1^+$)[106]. We next sorted populations of cNK, NKP, and ILC3 and performed qRT-PCR to assess for both NK and ILC3 specific gene expression (Supplemental Figure 3-5A). As expected, hESC-derived phenotypic ILC3 cells had a classical ILC3 gene signature, specifically *RORc*, *IL1-R1*, and *IL-22*. Additionally, ILC3 sorted populations were virtually deficient for *GATA3*, a critical transcriptional regulator of Group 2 ILCs[223], and were decreased for *TBX21*/*TBET*

expression (Supplemental Figure 3-5B). These data further support that AHR inhibition promotes the differentiation of NK progenitor cells into mature cNK cells. Furthermore, for the first time, we demonstrate AHR hyperactivation promotes development of an ILC3 phenotype from hESCs.

## DISCUSSION

Human pluripotent stem cells provide an important starting point to better define key molecular and genetic drivers of human hemato-endothelial development. Here, we established that AHR antagonism using the chemical inhibitor SR-1, as well as *AHR* gene deletion using the CRIPSR/Cas9 system, enhances human EHT and hematopoietic progenitor cell development. In corresponding fashion, AHR hyperactivation using TCDD suppresses development of hematopoietic progenitor cells with multilineage potential and accelerates their differentiation into more matured hematopoietic lineages (Figure 3-6).

To our knowledge, no other study has reported on the ability of AHR inhibition to promote early human hemato-endothelial differentiation. Gori *et al.* assessed the effect of AHR inhibition using short-term SR-1 treatment in a non-human primate iPSC model of hematopoiesis[224]. While these studies showed an increase in phenotypic $CD34^+CD45^+$ cells, there were no differences in the kinetics or quantity of $CD34^+$ or $CD34^+CD31^+$ cells. SR-1 treated non-human primate iPSCs also did not enhance the total number of CFUs, unlike our findings using hESCs. These differences may be due to differences in culture conditions and/or possible species-specific differences. Indeed, AHR ligand selectivity, and AHR interaction with co-activator motifs all substantially differ between non-human

and primary human cells[225–227]. Our finding that AHR modulation can alter hematopoietic progenitor cell cycling are further corroborated by studies demonstrating AHR hyperactivation using FICZ in hiPSCs leads to increased EdU incorporation, which is similar to our result using TCDD[130]. Our model provides complementary data in which hESC-derived hematopoietic progenitor cells treated with SR-1 are reciprocally enriched in a $G_0/G_1$ state, presumably to support hematopoietic differentiation and progenitor cell maturation[228–230].

Interestingly, we also determined *AHR* gene deletion enhances development of early hematopoietic progenitor cells that are committing towards definitive hematopoietic lineages. We, and others, have reported the *RUNX1c* isoform is correlated with emerging definitive HSPCs from aorta-gonad-mesonephros region endothelial cells[40,77]. Using our previously developed *RUNX1c*-tdTomato reporter system to model EHT, we found hESCs harboring *AHR* gene deletion enhanced the differentiation of *RUNX1c*$^+$ hematopoietic cells. We also observed an induction of a multilineage transcriptional program, including typical genes expressed during definitive hematopoiesis. One hypothesis for this effect is that AHR may function as a modulator of β-catenin/Wnt signaling. Exogenous activation of Wnt through GSK-3 inhibition has been recently shown to support a definitive hematopoietic phenotype from human pluripotent stem cells[79]. Interestingly, AHR and Wnt signaling have known associations both in normal embryological and disease pathogenesis. β-catenin gene expression (*CTNNB1*) is known to be overexpressed in *Ahr*$^{-/-}$ mice, causing the development of intestinal tumors[134,231]. Another study also demonstrated *Ahr*$^{-/-}$ mice had increased expression of genes regulated by β-catenin/Wnt signaling, specifically

within hematopoietic stem cells[232]. These *Ahr*$^{-/-}$ mice demonstrated splenomegaly, anemia, leukocytosis, and HSC accumulation outside the bone marrow. Together, these studies all implicate AHR as a potent regulator of definitive hematopoiesis.

In addition to increased development of hemato-endothelial cells, we also found differentiation of lymphoid cells (NK cells) was increased by treatment of hESCs with SR-1. These findings are complementary to prior studies that observed SR-1 treatment not only enhanced several transcription factors that are indispensable for NK cell differentiation, such as *ID2, GATA3,* and *EOMES*, but also promoted an increased absolute number of NK cells derived from mobilized peripheral blood CD34$^{+}$ hematopoietic progenitor cells[233]. Our hESC-derived NK cells in the presence of SR-1 were functional, in that they comparably degranulated (CD107a) relative to controls when stimulated with K562 targets. We further emphasize the role of AHR in hemato-lymphoid development by demonstrating AHR antagonism accelerates differentiation of NK progenitor cells into cNK phenotypes. This study illustrates that SR-1 can be added into currently defined differentiation protocols to enhance the efficiency and homogeneity of hESC-derived NK cells suitable to human clinical trials.

Finally, to our knowledge, this is the first report demonstrating that ILC3s can be derived from human pluripotent stem cells. hESC-derived ILC3, like those located in secondary lymphoid tissue and peripheral blood, require AHR to drive their development[106,119,234]. Several studies have highlighted the critical immunomodulatory role ILC3 play in the gut mucosa, specifically in the production of IL-22 that is required for intestinal

homeostasis[235]. It remains unclear whether they can be harnessed for clinical application, such as the attenuation of acute graft-vs-host disease post-hematopoietic stem cell transplantation[236]. hESCs, particularly in conjunction with a CRISPR/Cas9 gene editing system as we present, can be used as a powerful platform to better understand the development of a range of human ILCs, as well as to better analyze their effector phenotypes and therapeutic potential.

**ACKONWLEDGEMENTS**

We thank Anna Kim (University of Minnesota LLSURP summer student) for technical assistance and Dejene Tufa for ILC antibody panel. This work was supported in part by the following National Institutes of Health grants: National Cancer Institute R01CA203348 (D.S.K.), National Institute of Diabetes and Digestive and Kidney Diseases F30DK107071 (M.G.A), National Institute of Allergy and Immunology R01AI100879 (M.R.V), National Institute of General Medicine Sciences T32GM113846 (M.G.A and D.S.K.) and T32GM008244 (M.G.A). Other support from the Regenerative Medicine Minnesota program (D.S.K.)

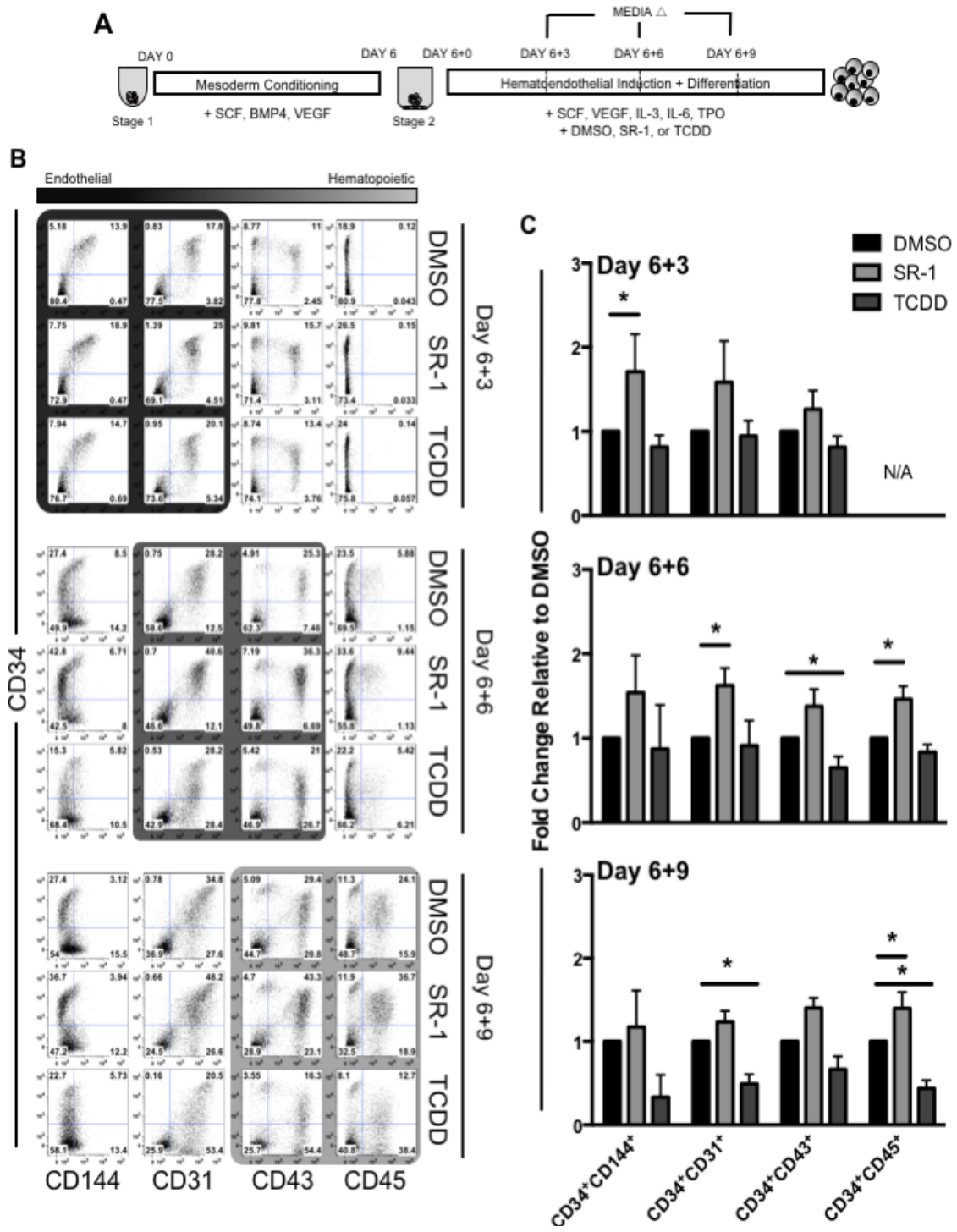


**Figure 3-1. Small molecule antagonism of AHR enhances early hemato-endothelial development from hESCs. A**) Schema of hESC differentiation into early hemato-

endothelial cells as spin-embryoid bodies (spin-EBs). hESCs are made into spin-EBs at Day 0 and conditioned into mesoderm lineages for 6 days using defined cytokines (Stage 1). At Day 6, spin-EBs are transferred into hemato-endothelial culture media (Stage 2) to promote endothelial and hematopoietic cell differentiation. For these studies, cells are treated with either 1 μM SR-1, 10nM TCDD, or DMSO vehicle control beginning at Day 6+0 with media exchanges and/or harvesting performed at Day 6+3, Day 6+6, and Day 6+9. **B**) Representative flow cytometry plots of one hESCs differentiation. Both adherent and non-adherent cell fractions are harvested at Day 6+3, Day 6+6, and Day 6+9 and assessed for endothelial cell ($CD34^+CD31^+$, $CD34^+CD144^+$) and hematopoietic progenitor cell ($CD34^+CD43^+$, $CD34^+CD45^+$) phenotype. **C**) Fold change of the total percentage of each hemato-endothelial phenotype for SR-1 and TCDD treated hESCs normalized to matched DMSO treated controls. n=4-6, error bars represent SEM, *$p<0.05$ as compared to DMSO treated controls by student's t-test. N/A: Not applicable due to absence appreciable of $CD34^+CD45^+$ populations at Day 6+3 time point.

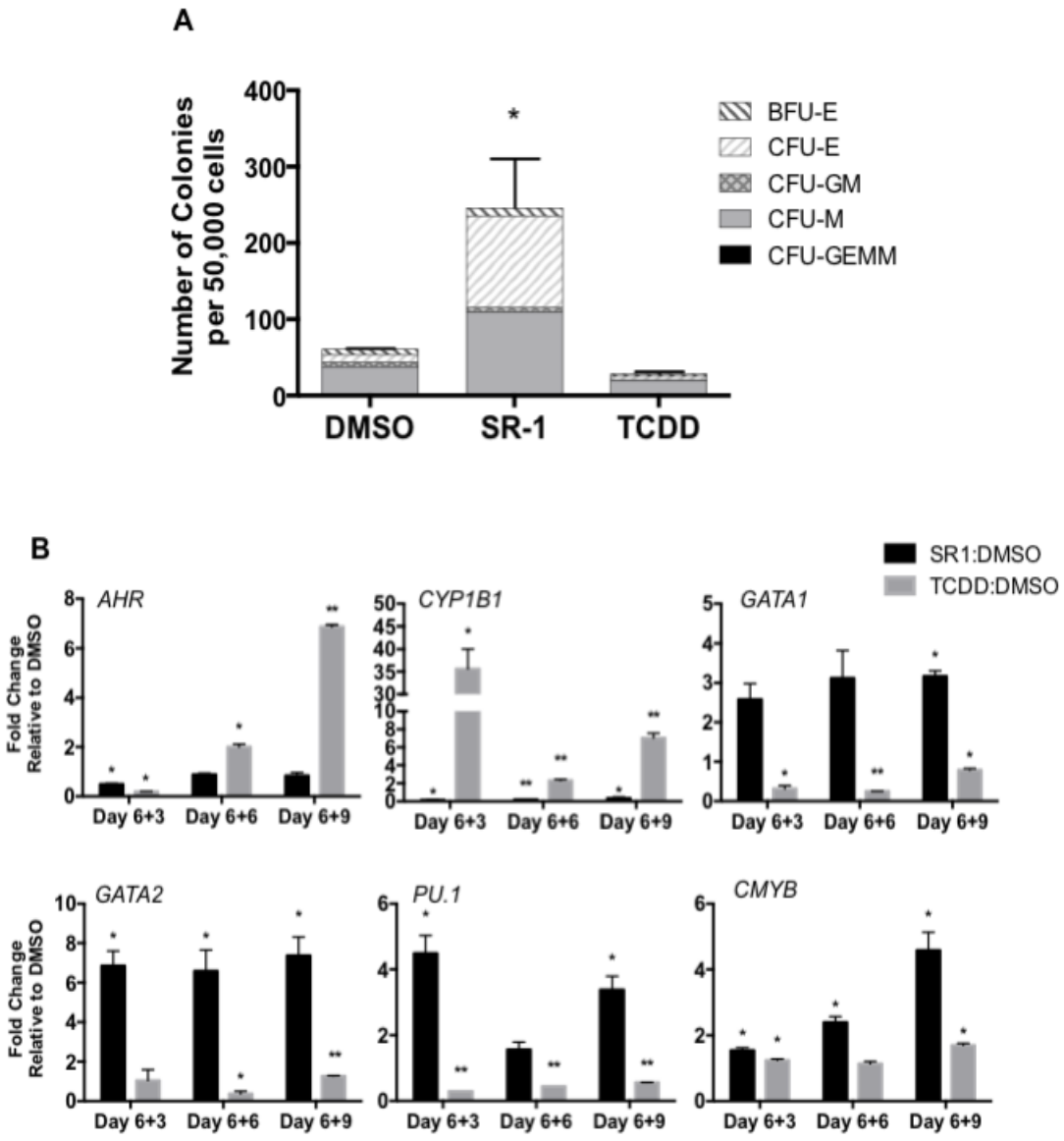


**Figure 3-2. SR-1 treated hESCs demonstrate increased multilineage hematopoietic development. A**) Non-adherent hematopoietic progenitor cells derived from hESCs differentiated in the presence of SR-1, TCDD, or DMSO controls were harvested at Day 6+5 and seeded at 50,000 cells/dish in a standard methylcellulose colony-forming unit assay (CFU). Colonies were counted for each treatment group following 2 weeks of culture and scored for the following morphological subsets: BFU-E: burst-forming unit-erythroid;

CFU-E: colony-forming unit-erythroid; CFU-GM: colony-forming unit-granulocyte, macrophage, CFU-M: colony-forming unit-macrophage; CFU-GEMM: colony-forming unit-granulocyte, erythroid, macrophage, megakaryocyte. n=3, error bars represent SEM of the total number of colonies/50,000 cells seeded, *$p<0.05$ as assessed with one-way ANOVA + Tukey-Kramer multiple comparisons post-hoc test. **B**) Non-adherent hematopoietic progenitor cells derived from hESCs differentiated in the presence of SR-1, TCDD, or DMSO controls were harvested at Day 6+3, Day 6+6, and Day 6+9 time points and probed for gene expression by quantitative real-time PCR (qRT-PCR). For each gene, $C_t$ values were normalized to *GAPDH* at each time point and data is presented as relative fold-change to DMSO treated controls. n=3, error bars represent SEM, *$p<0.05$, **$p<0.01$ using student's t-test.

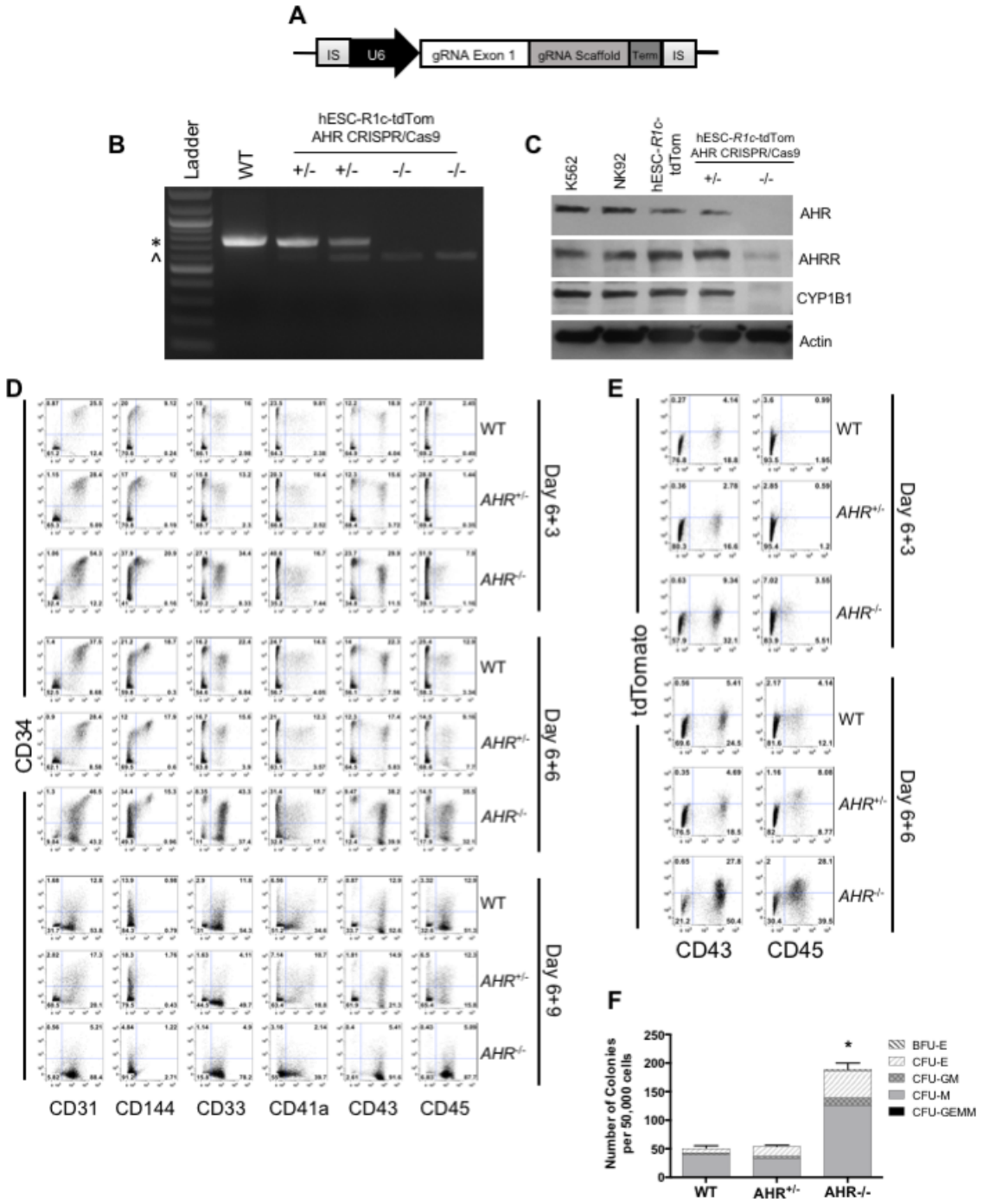


**Figure 3-3. CRISPR/Cas9 engineered hESCs with *AHR* deletion demonstrate increased early hemato-endothelial cell development. A**) gRNA cassette design

targeting *AHR*. IS: insertion sequence; U6: Promoter, gRNA Exon 1: 22-nt gRNA specific to *AHR* exon 1, Term: termination sequence. **B**) Gel electrophoresis of PCR products produced from clonally-derived hESC-*RUNx1c*-tdTomato cells nucleofected with *AHR* gRNA cassette. Genomic DNA was harvested and primers flanking the *AHR* exon 1 locus were used to generate a PCR product with predicted full-length of 718 bp. WT: Negatively selected nucleofected hESC-*RUNX1c*-tdTomato hESCs; +/-: Individual clones with *AHR* heterozygous deletion ($AHR^{+/-}$); -/-: Individual clones with *AHR* homozygous deletion ($AHR^{-/-}$); *: 718bp amplicon, ^: 571bp amplicon. **C**) Immunoblot of protein lysate harvested from K562 cells (positive control), NK92 natural killer cells (positive control), wild-type hESC-*RUNX1c*-tdTomato (hESC-*R1c*-tdTom), heterozygous *AHR* deleted hESC-*RUNX1c*-tdTomato (+/-), and homozygous *AHR* deleted hESC-*RUNX1c*-tdTomato (-/-). AHRR: aryl hydrocarbon receptor repressor. **D**) Representative flow cytometry plots at Day 6+3, Day 6+6, and Day 6+9 from one differentiation of wild-type hESC-*RUNX1c*-tdTomato (WT), heterozygous *AHR* hESC-*RUNX1c*-tdTomato deletion ($AHR^{+/-}$), and homozygous *AHR* hESC-*RUNX1c*-tdTomato deletion ($AHR^{-/-}$). Both adherent and non-adherent cell fractions are harvested at Day 6+3, Day 6+6, and Day 6+9 and assessed for endothelial (CD31, CD144), and hematopoietic (CD33, CD41a, CD43, CD45) phenotype. **E**) Representative flow cytometry plots at Day 6+3 and Day 6+6 from one differentiation assessing for *RUNX1c* expression based on tdTomato fluorescent reporter protein. **F**) Non-adherent hematopoietic progenitor cells derived from WT hESC-*RUNX1c*-tdTomato, $AHR^{+/-}$ hESC-*RUNX1c*-tdTomato, or $AHR^{-/-}$ hESC-*RUNX1c*-tdTomato were harvested at Day 6+5 and seeded at 50,000 cells/dish in a standard methylcellulose colony-forming unit

assay (CFU). Colonies were counted for each treatment group following 2 weeks of culture and scored for the following morphological subsets, as previously described. n=3, error bars represent SEM of the total number of colonies/50,000 cells seeded, *$p<0.05$ as assessed with one-way ANOVA + Tukey-Kramer multiple comparisons post-hoc test.

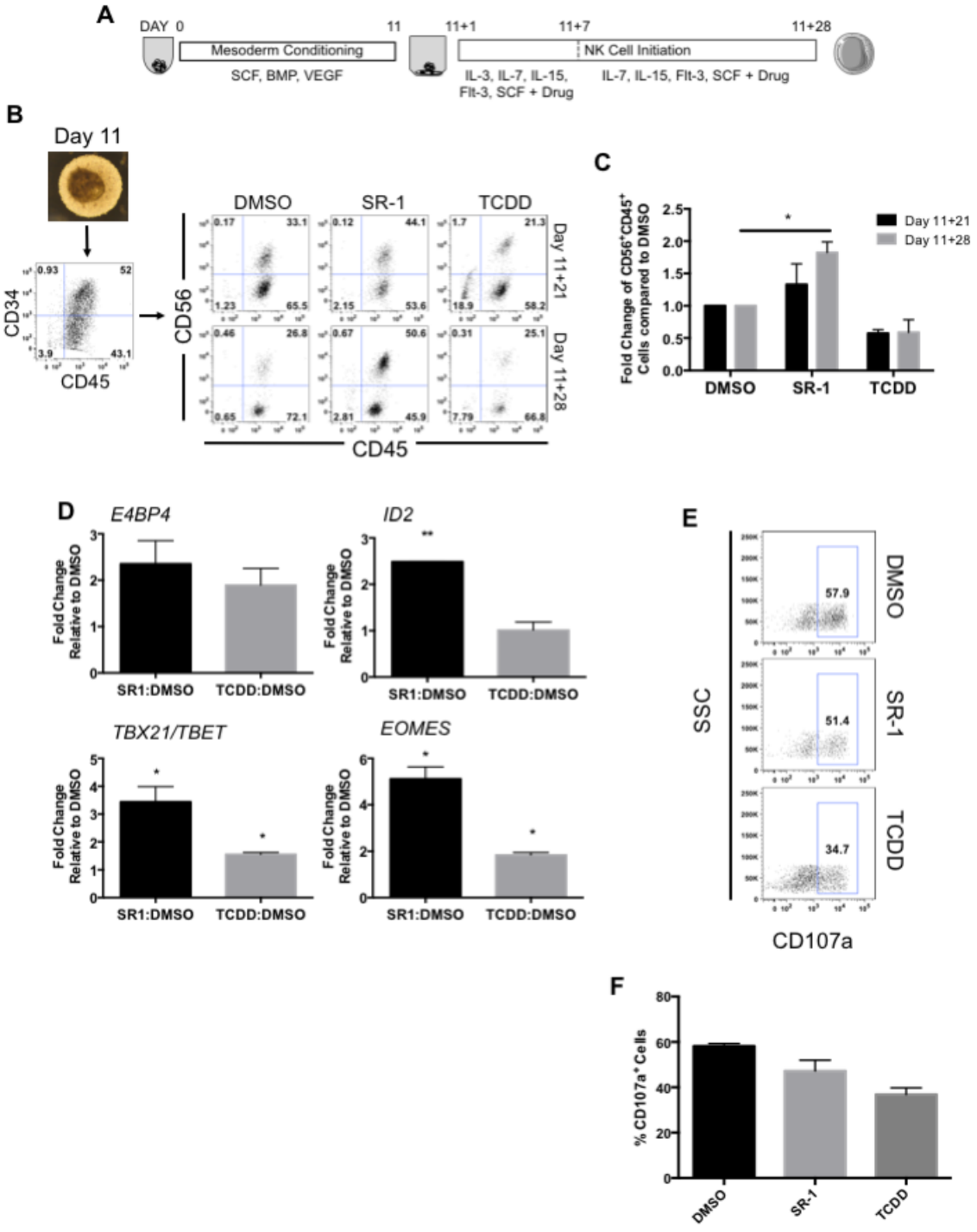


**Figure 3-4. hESCs differentiated in the presence of SR-1 promotes the development of functional natural killer (NK) cells. A**) Schema of hESC differentiation into lymphoid

cells as spin-embryoid bodies (spin-EBs). hESCs are made into spin-EBs at Day 0 and cultured in Stage 1 conditions with defined cytokines to promote mesoderm development for 11 days. At Day 11, spin-EBs are transferred onto OP9-DL1 in the presence of NK cell differentiation media (NKDM) to promote lymphoid differentiation. Cells are treated beginning at Day 11+0 with either 1 μM SR-1, 10nM TCDD, or DMSO vehicle control with media exchanges and/or harvesting performed every week for up to 4 weeks. **B**) At Day 11, differentiated spin-EBs (photo) are phenotyped for $CD34^{+}CD45^{+}$ expression and transferred to OP9-DL1 stroma in NKDM. Non-adherent hematopoietic cells cultured either in the presence of DMSO, SR-1, or TCDD were assessed for developing NK cell immunophenotype based on $CD56^{+}CD45^{+}$ expression at Days 11+21, and 11+28; representative flow cytometry plots from one differentiation are shown. **C**) Quantification of fold-change in total percentage of $CD56^{+}CD45^{+}$ cells at both Day 11+21 and Day 11+28 when treated with DMSO, SR-1, or TCDD. SR-1 and TCDD treatments for each differentiation are normalized to DMSO controls. n=3 independent differentiation experiments, error bars represent SEM, *$p<0.05$ as assessed with two-way ANOVA + Tukey-Kramer multiple comparisons post-hoc test. **D)** Non-adherent hematopoietic progenitor cells derived from hESCs differentiated in the presence of SR-1, TCDD, or DMSO controls were harvested at Day 11+28 and probed for gene expression by quantitative real-time PCR (qRT-PCR). For each gene, $C_t$ values were normalized to *GAPDH* at each time point and data is presented as relative fold-change to DMSO treated controls. n=3, error bars represent SEM, *$p<0.05$, #$p<0.01$ using student's t-test. **E**) Non-adherent hematopoietic progenitor cells derived from hESCs differentiated in the presence

of SR-1, TCDD, or DMSO controls were harvested at Day 11+28 and assessed for CD107a expression following 4 hours of co-culture with K562 target cells at 2:1 effector:target ratio. SSC: side scatter. Representative flow cytometry plots are shown from one experiment. **F)** Quantification of percentage of $CD107a^{+}$ cells when treated with DMSO, SR-1, or TCDD at Day 11+28, n=2-3 replicates.

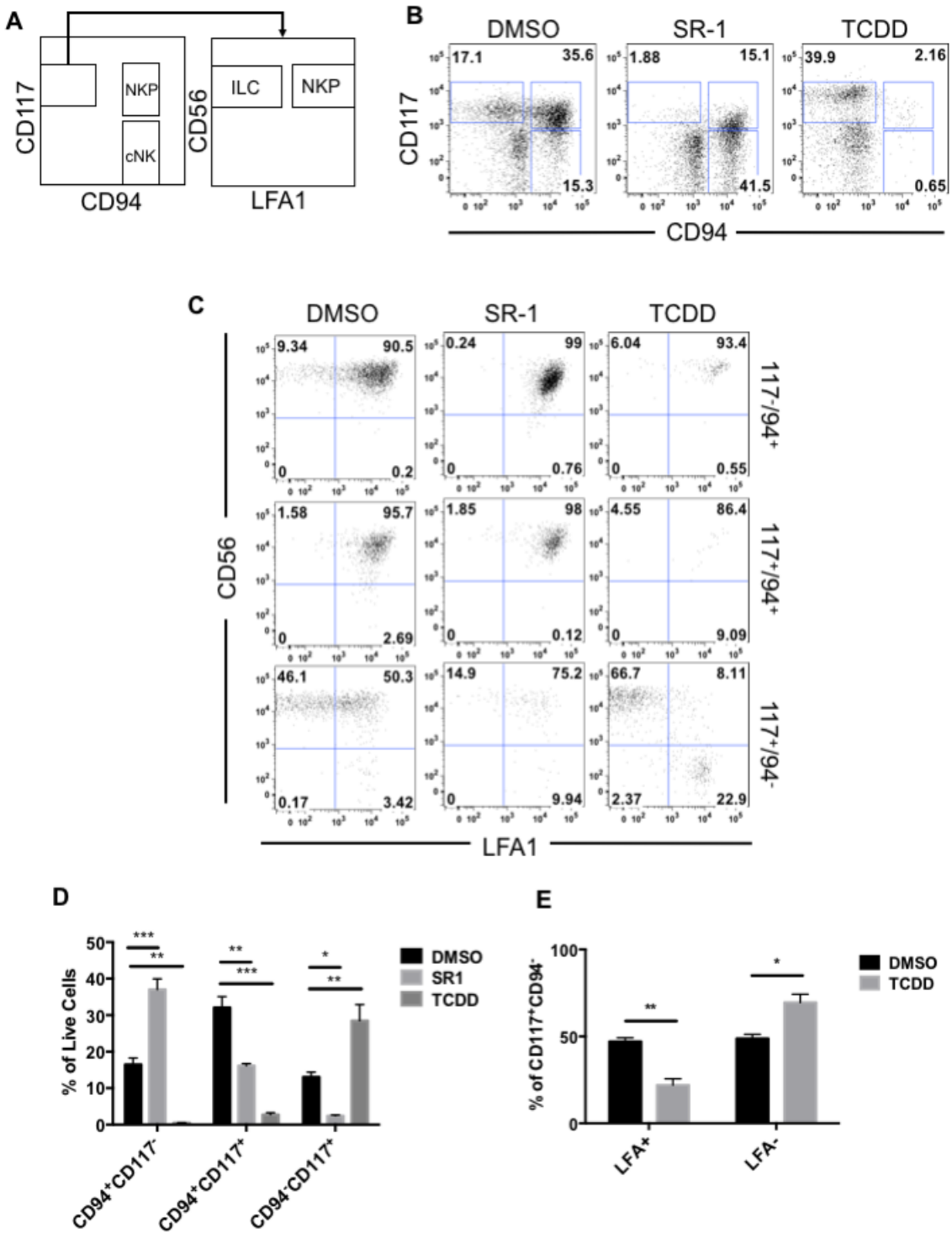


**Figure 3-5. hESCs differentiated in the presence of SR-1 skews development towards conventional NK cells (cNK) while TCDD supports of the development of an innate**

**lymphoid cell (ILC) phenotype. A**) Gating scheme for identifying cNK ($CD94^{-}CD117^{+}$), NK progenitor cells (NKP, $CD94^{+}CD117^{-}$ and $CD94^{+}CD117^{-}LFA1^{+}$), and ILC ($CD94^{-}CD117^{+}LFA1^{-}$) phenotypes. **B**) Representative flow cytometry profile of non-adherent hematopoietic cells differentiated from hESCs in the presence of DMSO, SR-1, or TCDD at Day 11+28. **C**) cNK, NKP, and NKP/ILC subpopulations from Day 11+28 DMSO, SR-1, and TCDD differentiated hESCs assessed for CD56 and LFA (CD11a/CD18) surface antigen expression. Representative flow cytometry plots are shown, n=3. **D**) Total percentage of cNK, NKP, and NKP/ILCs present in the non-adherent fraction of differentiating hESCs in the presence of DMSO, SR-1, or TCDD at Day 11+28. n=3, error bars represent SEM, *p<0.05, **p<0.01, ***p<0.001 as compared to DMSO treated controls and assessed by two-way ANOVA + Tukey-Kramer multiple comparisons post-hoc test. **E**) $CD94^{-}CD117^{+}$ subpopulations were further quantified for expression of $LFA^{+}$ (NKP) and $LFA^{-}$ (ILC) by flow cytometry. n=3, error bars represent SEM, *p<0.05, **p<0.01 as compared to DMSO treated controls and assessed by two-way ANOVA + Tukey-Kramer multiple comparisons post-hoc test.

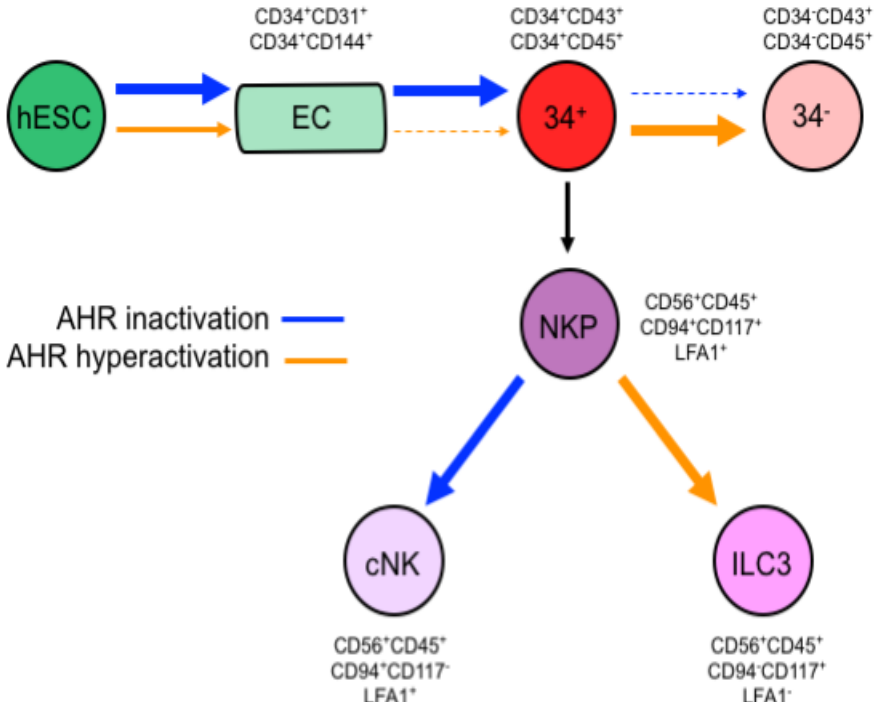


**Figure 3-6. Model of AHR activity in human developmental hematopoiesis.** AHR inhibition mediated by SR-1 (blue arrow) enhances the differentiation of both endothelial cells (ECs) and $CD34^+$ hematopoietic progenitor cells. AHR hyperactivation mediated by TCDD (orange arrow) reciprocally acts to attenuate both EC and $CD34^+$ hematopoietic progenitor cells. Once $CD34^+$ have been differentiated, AHR inhibition deters further differentiation into $CD34^-$ terminally matured hematopoietic cells, while AHR hyperactivation supports this process. Upon production of natural killer progenitor (NKP) cells, AHR inhibition promotes conventional NK cell differentiation (cNK), while AHR hyperactivation promotes Group 3 ILC (ILC3) differentiation.

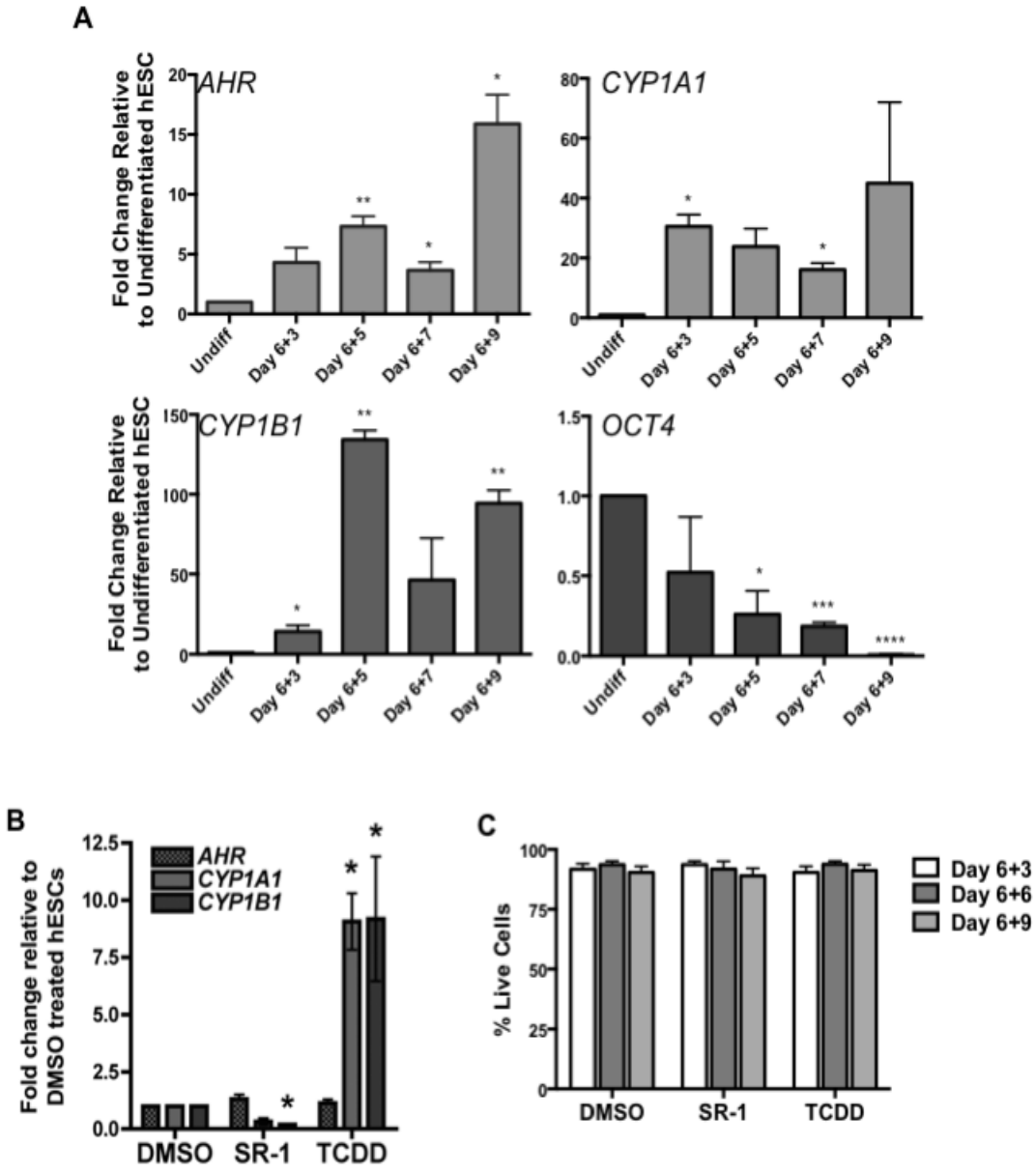


**Supplemental Figure 3-1. AHR is implicated in normal human hematopoiesis and can be targeted by small molecules in hESCs. A**) Non-adherent hematopoietic progenitor cells derived from hESCs were harvested at Day 6+3, Day 6+5, Day 6+7, and Day 6+9 time points and probed for gene expression by quantitative real-time PCR (qPCR). For each gene, $C_t$ values were normalized to *GAPDH* at each time point and data is presented

as relative fold-change as compared to undifferentiated hESCs. Differentiation was confirmed by a significant reduction of *OCT4*, a marker of pluripotency. n=3, error bars represent SEM, *p<0.05, **p<0.01, ***p<0.001, **** p<0.0001 using student's t-test. **B**) Undifferentiated hESCs were cultured in the presence of 1 μM SR-1, 10nM TCDD, or DMSO vehicle control for 96 hours and probed for gene expression by qPCR. For each gene, $C_t$ values were normalized to *GAPDH* at each time point and data is presented as relative fold-change as compared to DMSO treated hESCs. n=3, error bars represent SEM, *p<0.05 assessed by two-way ANOVA + Tukey-Kramer multiple comparisons post-hoc test. **C**) Both adherent and non-adherent cell fractions treated with either DMSO, SR-1, or TCDD were harvested at Day 6+3, Day 6+6, and Day 6+9 and probed for viability with Sytox Blue Live/Dead Stain. Total percentage of viable cells for each group and time point are plotted. n=3.

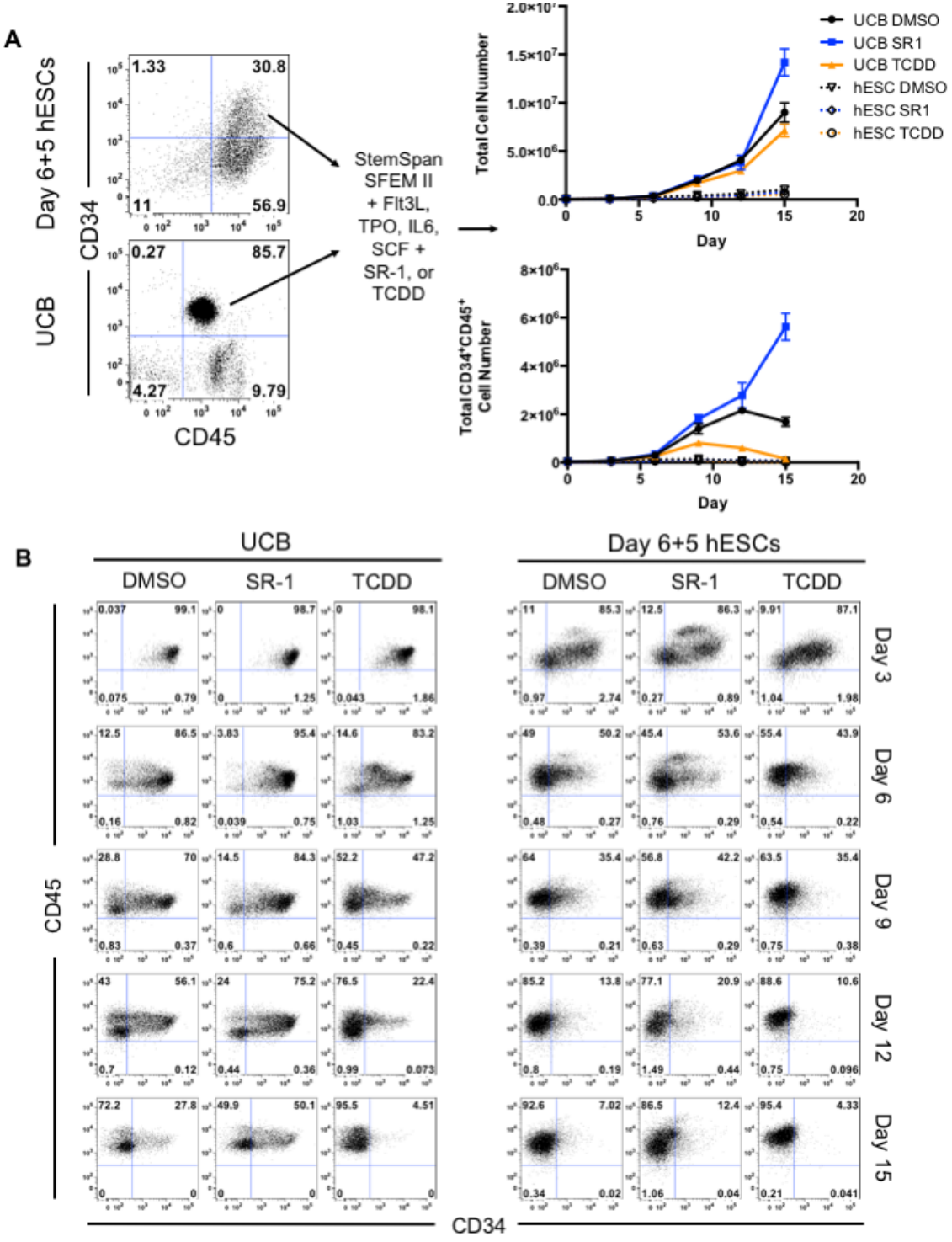


**Supplemental Figure 3-2. AHR antagonism in early human hematopoietic progenitors derived from hESCs does not cause cell expansion. A**) Left: Human

umbilical cord blood (UCB) and non-adherent Day 6+5 hematopoietic cells derived from hESCs were sorted for $CD34^{+}CD45^{+}$ and further cultured in StemSpan SFEM II expansion media for 15 additional days either in the presence of DMSO, SR-1, or TCDD. Every 3 days, both the total cell number (Top right) and the total $CD34^{+}CD45^{+}$ cell number (bottom right) as assessed by flow cytometry was determined for each group. n=3 independent experiments. **B**) Representative flow cytometry plots throughout the time course assessing for total percentage of $CD34^{+}CD45^{+}$ phenotypes.

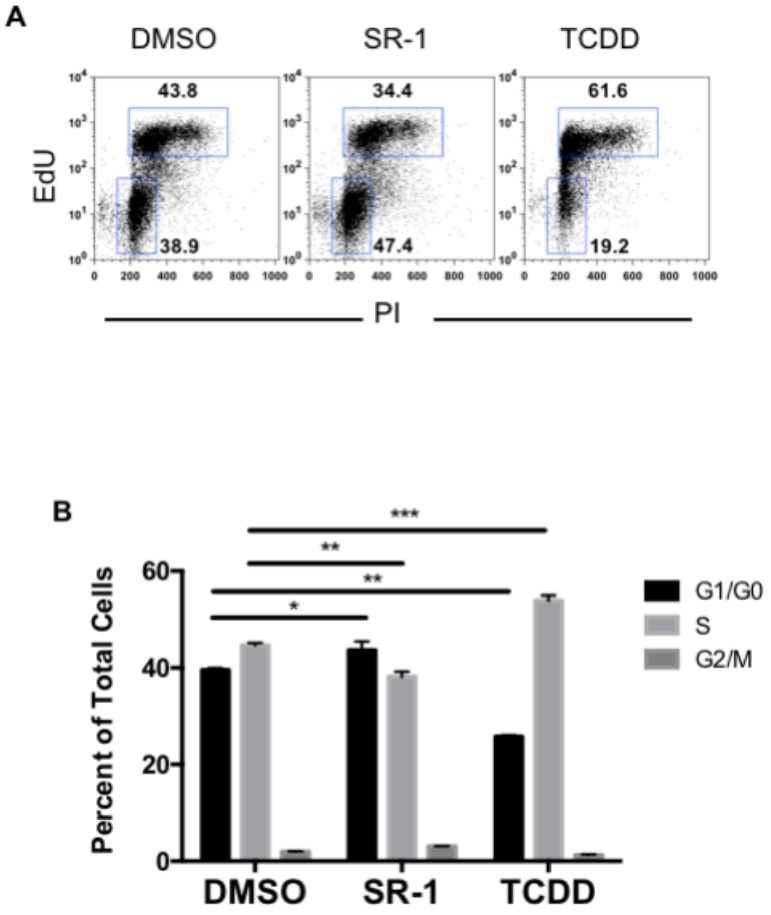


**Supplemental Figure 3-3. AHR regulates cell cycle progression during hematopoietic cell development from hESCs. A)** Non-adherent hematopoietic progenitor cells derived from hESCs were cultured in the presence of DMSO, SR-1, and TCDD until Day 6+5. Cell cycle phase was assessed using flow cytometry to determine the total percentage of $G_0/G_1$ ($EdU^-PI^{lo}$), S-phase ($EdU^+PI^+$), or $G_2/M$ ($EdU^-PI^{hi}$). Representative flow cytometry plots are shown. **B**) Quantification of cell cycle analysis, n=3, *p<0.05, **p<0.01, ***p<0.001 as assessed by two-way ANOVA + Tukey-Kramer multiple comparisons post-hoc test.

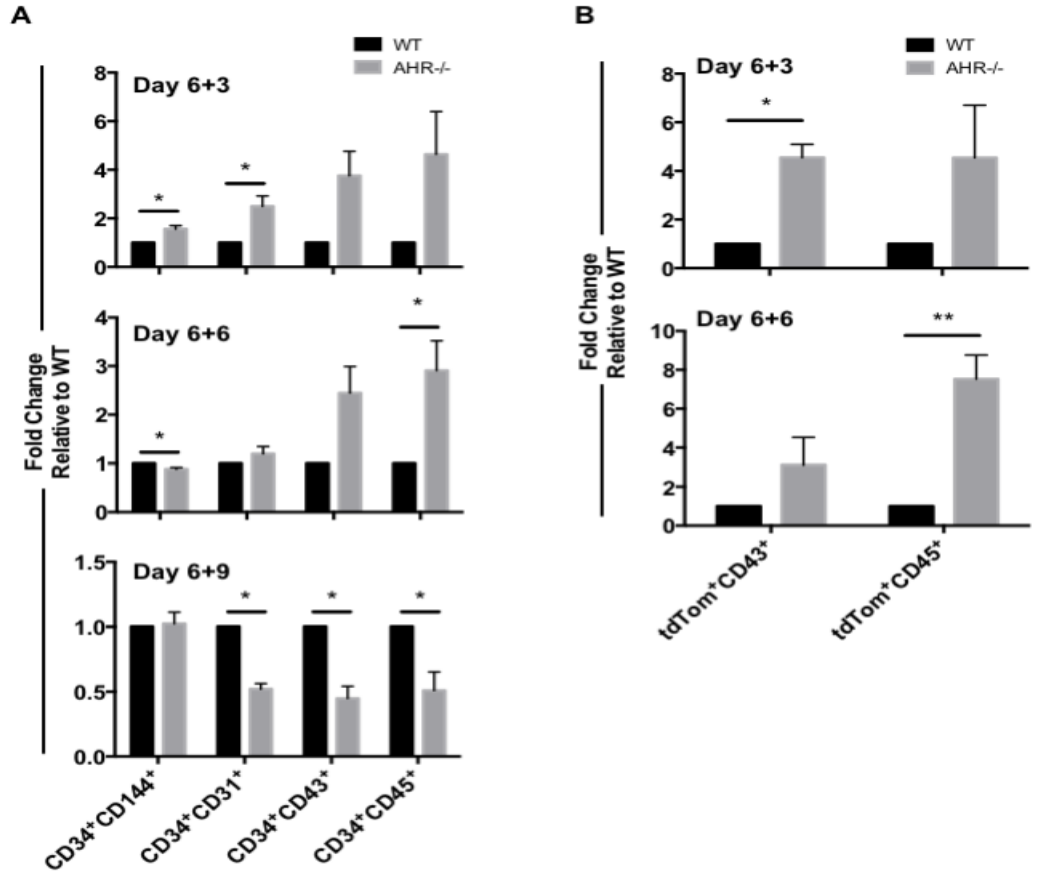


**Supplemental Figure 3-4. CRISPR/Cas9 engineered hESCs with *AHR* deletion demonstrate increased early hemato-endothelial cell development.** A) Quantification from flow cytometry profiles at Day 6+3, Day 6+6, and Day 6+9 of $CD34^+CD144^+$ and $CD34^+CD31^+$ endothelial cells and $CD34^+CD43^+$ and $CD34^+CD45^+$ early hematopoietic progenitor cells differentiated from wild-type hESC-*RUNX1c*-tdTomato (WT) or $AHR^{-/-}$ hESC-*RUNX1c*-tdTomato ($AHR^{-/-}$). Total percentage of each cell population was normalized to WT and plotted as fold-change relative to WT. n=3 representative differentiations, *$p<0.05$ using student's t-test. B) Quantification from flow cytometry profiles at Day 6+3 and Day 6+6 of $tdTom^+CD43^+$ and $tdTom^+CD45^+$ cells derived from WT or $AHR^{-/-}$ hESCs. n=3 representative differentiations, *$p<0.05$ using student's t-test.

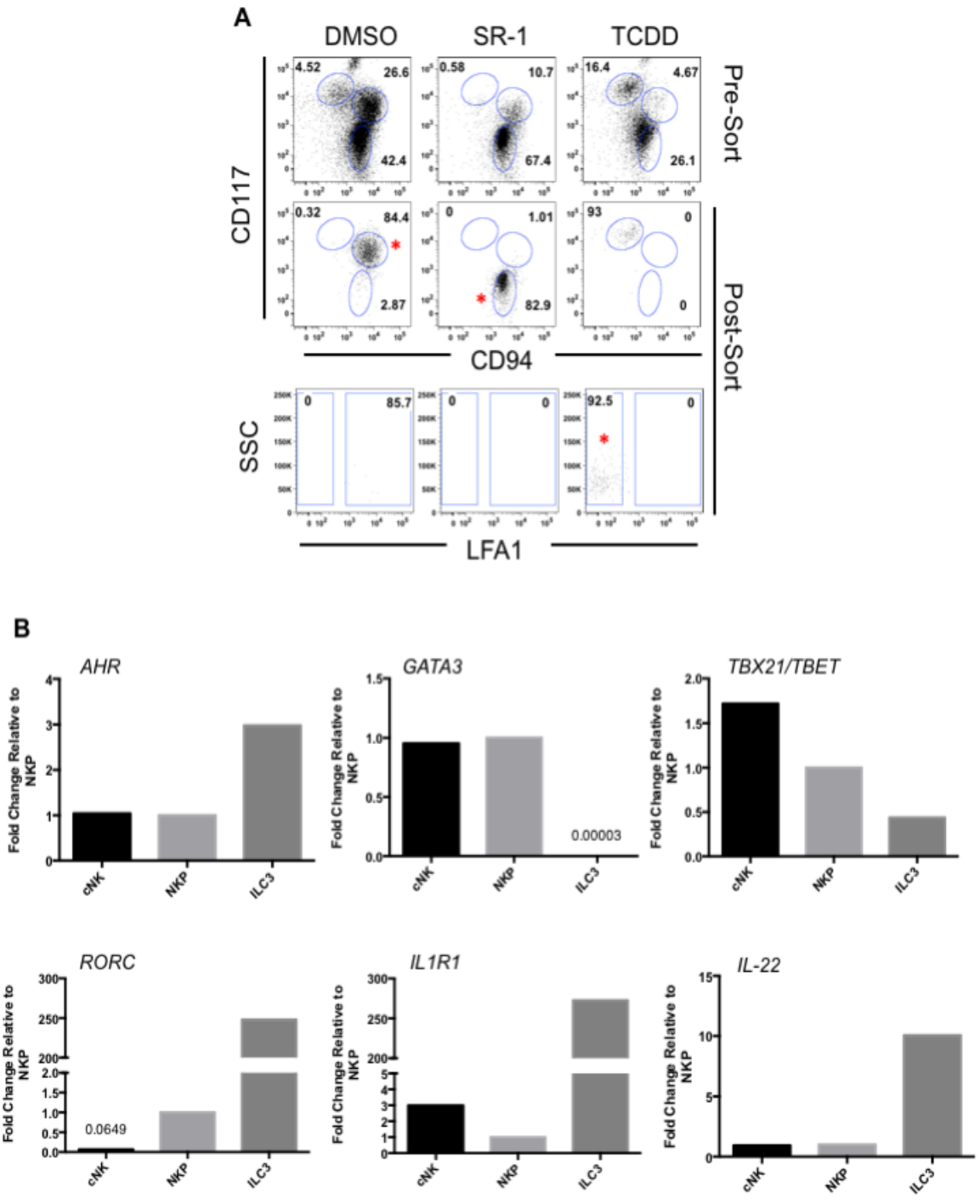


**Supplemental Figure 3-5. AHR hyperactivation in hESC-derived hematopoietic cells increase Group 3 ILC development. A)** Day 11+28 hESC-derived non-adherent

hematopoietic cells were treated with SR-1 to enrich for $CD94^{+}CD117^{-}$ (cNK), TCDD to enrich for $CD94^{-}CD117^{+}LFA1^{-}$ (ILC), and DMSO to enrich for $CD94^{+}CD117^{+}$ (NKP). Each phenotype was FACS sorted and RNA was harvested to assess for gene expression. *: Sorted population. **B**) qRT-PCR analysis of genes associated with cNK and ILC3 development. Data are represented as fold-change in gene expression relative to NKP sorted cells. n=2, means of duplicate experiments are shown.

**Supplemental Table 3-1. Oligonucleotide primers used for qRT-PCR.**

| Gene | Primer Sequence | Amplicon Size (bp) | Tm (°C) |
|---|---|---|---|
| *AHR* | F: 5'-CTTAGGCTCAGCGTCAGTTAC-3'<br>R: 5'-CGTTTCTTTCAGTAGGGGAGGAT-3' | 79 | 60<br>61 |
| *CYP1A1* | F: 5'-TCGGCCACGGAGTTTCTTC-3'<br>R: 5'-GGTCAGCATGTGCCCAATCA-3' | 141 | 62<br>63 |
| *CYP1B1* | F: 5'-AAGTTCTTGAGGCACTGCGAA-3'<br>R: 5'-GGCCGGTACGTTCTCCAAAT-3' | 142 | 63<br>63 |
| *OCT4* | F: 5'-GCAGCTCGGAAGGCAGAT-3'<br>R: 5'-TGGATTTTAAAAGCGAGAAGACTTG-3' | 135 | 62<br>62 |
| *CMYB* | F: 5'-GTCACAAATTGACTGTTACAACACCAT-3'<br>R: 5'-TTCTACTAGATGAGAGGGTGTCTGAGG-3' | 212 | 59<br>60 |
| *GATA1* | F: 5'-GGGATCACACTGAGCTTGC-3'<br>R: 5'-ACCCCTGATTCTGGTGTGG-3' | 176 | 64<br>65 |
| *GATA2* | F: 5'-GCGTCTCCAGCCTCATCTT-3'<br>R: 5'-GGAAGAGTCCGCTGCTGTAG-3' | 226 | 61<br>60 |
| *PU.1* | F: 5'-CACAGCGAGTTCGAGAGCTT-3'<br>R: 5'-GATGGGTACTGGAGGCACAT-3' | 194 | 61<br>61 |
| *E4BP4* | F: 5'-GCAGAGCCGATGGAATTAG-3'<br>R: 5'-ATCAGTTTCCGACGTTCTCA-3' | 222 | 56<br>57 |
| *EOMES* | F: 5'-TCAGATTGTCCCTGGAGGTC-3'<br>R: 5'-AGTTTGTTGGTCCCAGGTTG-3' | 207 | 58<br>58 |
| *ID2* | F: 5'-CGGATATCAGCATCCTGTCC-3'<br>R: 5'-TCATGAACACCGCTTATTCAG-3' | 100 | 58<br>56 |
| *T-BET* | F: 5'-GATGTTTGTGGACGTGGTCTTG-3'<br>R: 5'-CTTTCCACACTGCACCCACTT-3' | 76 | 60<br>61 |
| *GATA3* | F: 5'-GCCCCTCATTAAGCCCAAG-3'<br>R: 5'-TTGTGGTGGTCTGACAGTTCG-3' | 80 | 58<br>60 |
| *RORγt* | F: 5'- GCCAAGGCTCAGTCATGAGAA-3'<br>R: 5'-TTGTCCCCACAGATTTTGCA-3' | 61 | 60<br>58 |
| *IL1R1* | F: 5': CCTGCTATGATTTTCTCCCAATAAa-3'<br>R: 5'- AACACAAAAATATCACAGTCAGAGGTAGAC-3' | 115 | 57<br>62 |
| *IL22* | F: 5'- GCTTGACAAGTCCAACTTCCA-3'<br>R: 5'- GCTCACTCATACTGACTCCGTG-3' | 140 | 59<br>60 |
| *GAPDH* | F: 5'-CCACTCCTCCACCTTTGAC-3'<br>R: 5'-ACCCTGTTGCTGTAGCCA-3 | 102 | 58<br>58 |

# CHAPTER 4

## *Conclusions and Future Directions*

This thesis research has identified novel genetic and molecular mechanisms that influence hemato-endothelial specification from human pluripotent stem cells. In Chapter 2, we established a cell identification scheme to distinguish human hemogenic endothelial cells from vascular endothelial cells that lacked hematopoietic potential. We employed cutting-edge technological tools to perform RNA-sequencing of single cells from hESC-derived hemogenic endothelium, non-hemogenic endothelium, and the earliest definitive hematopoietic progenitor cells to reveal distinct transcriptional signatures between each population. We identified many known transcriptional regulators of hemogenic endothelium (such as *GATA2*, *FLI1*, and *SOX17*) that were enriched in hESC-derived hemogenic endothelium and established additional candidates that may be integral to the mechanism of EHT (i.e. *ESAM*, *TIMP3, RHOJ, DLL4*). We further demonstrated that hESC-derived vascular endothelial cells without hematopoietic potential are heterogeneous and that a small subset can further transform into mesenchymal phenotypes. These studies provide novel data for expanding upon the current processes underlying human EHT and vasculogenesis.

In Chapter 3, we determined AHR is implicated in the earliest events of human hematopoietic development. First, we found AHR inhibition enhanced the number of functional hematopoietic progenitor cells derived from hESCs, while AHR hyperactivation accelerated hematopoietic maturation. *AHR* inhibition and gene deletion enhanced the expression of key EHT genes, suggesting that AHR, in part, may contribute to hemogenic endothelial cell fate. Interestingly, many individual hESC-derived hemogenic endothelial cells expressed *AHR* and *AHR*-related downstream effector targets as compared to vascular

endothelial cells without hemogenic potential (Appendix 1). This supports a potentially novel role of the AHR pathway at the level of EHT. We also discovered that AHR functions as a molecular switch in human hemato-lymphoid specification. Here, we found AHR antagonism supported conventional NK cell (cNK) differentiation while AHR hyperactivation robustly produced phenotypic ILC3s. Taken together, these data provide a framework for improved NK cell differentiation from hESCs and also a platform to better assess the developmental biology and functionality of human ILC subsets.

Although here we demonstrate methods to improve EHT and lymphoid lineage commitment using a human system, the challenge of generating *long-term, engraftable* HSPCs from hESC/hiPSCs remains. Previous studies from our lab demonstrate that although we can select and purify hESC-derived *RUNX1c*$^{+}$ hematopoietic cells, these cells fail to contain long-term culture initiating cells (LTC-ICs)[77]. These assays are considered by many in the field as an *in vitro* surrogate to *in vivo* transplantation[237,238]. Other groups who have overexpressed important human EHT genes (i.e. *GATA2*, *SOX17*, *HOXA9*) to generate a hemogenic endothelium phenotype have at best shown improved time to engraftment, but fail at secondary transplantation[67,69]. Recently, expression of medial *HOXA* genes was found to be critical in mediating human EHT, however, even with overexpression in hESC-derived HSPCs, still failed to confer long-term engraftment[68,239]. Therefore, intrinsic cell modification alone is probably insufficient to support hESC/hiPSC-derived HSPCs. Instead, complementary differentiation techniques that additionally aim to recapitulate the embryological hematopoietic niche will need to be employed in future studies.

While hematopoietic stem cell transplantation using hESC/hiPSC-derived HSPCs is not currently possible, transient therapies using hiPSC-derived terminal hematopoietic products are quickly approaching clinical feasibility. hiPSC-derived erythroid cells for blood transfusion is an attractive initial option, in theory, because erythroid cells are easily differentiated in the presence of erythropoietin and are immunologically inert due to lack of MHC molecules. However, *ex vivo* expansion of enough erythroid cells suitable for a single unit of blood is currently not possible. It is also economically inefficient to scale hiPSC/hESC culture for erythogenesis (in fact, since 1 unit of donated blood has on average ~2 $x10^{12}$ erythroid cells, it is conservatively estimated a single unit of hiPSC-derived erythroid cells would cost $8,330)[240,241]. Similar limitations exist for hiPSC-derived platelets (megakaryocytes)[242,243].

hESC/hiPSC-derived NK cells are most primed for clinical translation, as they can be cultured and expanded to large numbers suitable for treating a single patient[126]. Of particular interest is that undifferentiated hESC/hiPSC can be modified with chimeric antigen receptors (CARs) and can be "personalized" to target essentially any foreign or tumor-presenting antigen of interest[122,244,245]. NK cells with surface CAR presentation can then be directly differentiated from these gene-modified hiPSCs using previously developed xenogenic-free and chemically-defined methods. Our data that demonstrates AHR inhibition of differentiating hESCs using StemRegnin-1 (a small molecule previously used in clinical trials[142]) skews hemato-lymphoid development towards cNK could be used advantageously to optimize hESC/hiPSC-derived NK cell production. Furthermore, we demonstrate that gene editing can effectively be accomplished in undifferentiated hESCs

using the CRISPR/Cas9 endonuclease system. We found this method to be highly efficient for hESC gene modification with high specificity to the *AHR* endogenous gene locus and without off-target effects. Such an approach could similarly be employed to engineer clinical quality hiPSCs and/or hiPSC-CAR-NK cells using a patient's autologous cells in a highly efficient manner (Figure 4-1). Together, these strategies can be used to make hiPSC-based personalized medicine an even closer reality.

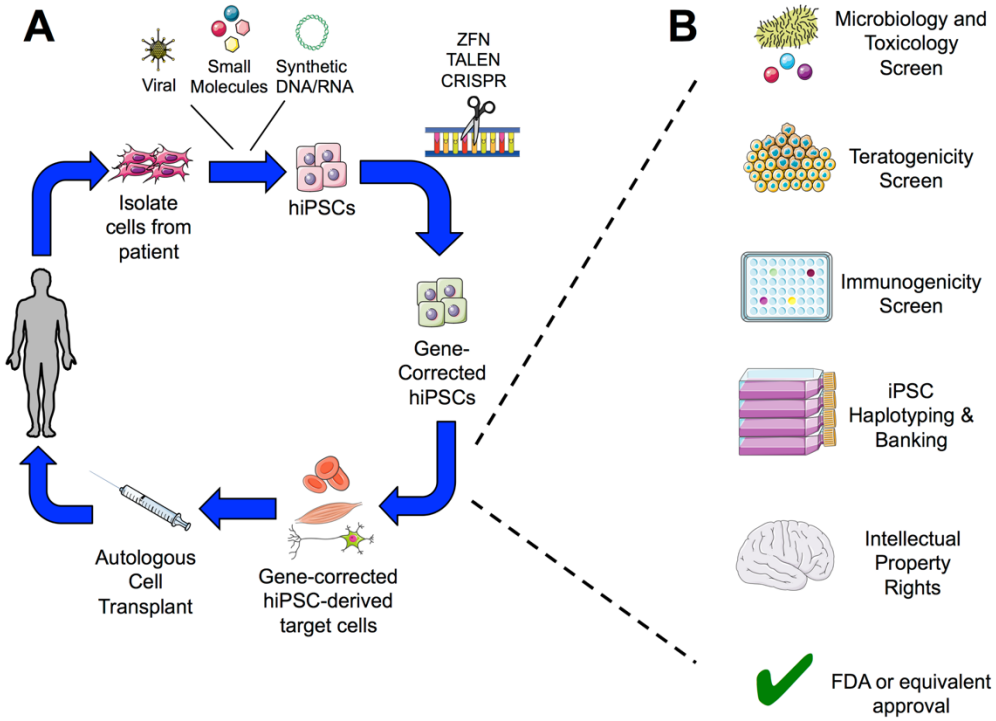


**Figure 4-1. Clinical strategy for wide-scale hiPSC-based gene and cell therapy.** A) Dermal fibroblasts and/or peripheral mononuclear blood cells are harvested from a patient with defined genetic disease. hiPSCs are engineered from autologous cells via reprogramming with defined factors. Pathological mutations can be corrected through zinc-finger nucleases (ZFN), TAL effector nucleases (TALEN), or clustered regulatory interspaced short palindromic repeat (CRISPR)/CRISPR-associated (Cas) gene-editing technologies. Gene-corrected hiPSCs can then be differentiated into the desired cell and/or tissue products prior to autologous transplantation via direct injection or seeding on a biocompatible scaffold. B) Prior to autologous cell transplantation, gene-corrected hiPSC-derived cell products must first pass several safety checkpoints, such as viral, toxicology, and tumorigenicity screens, lack of teratoma expansion, and lack immune response to the

transplanted cells. Cells would also be immunophenotyped and banked for future patient use based on human leukocyte antigen (HLA) expression at this time. Furthermore, logistical hurdles such as obtaining intellectual property rights for product commercialization and regulatory agency approval must be in place prior to clinical trial.

## REFERENCES


1. Doulatov S, Notta F, Laurenti E, Dick JE. Hematopoiesis: a human perspective. *Cell Stem Cell*. 2012;10(2):120–36.
2. Palis J, Yoder MC. Yolk-sac hematopoiesis: The first blood cells of mouse and man. *Exp. Hematol.* 2001;29(8):927–936.
3. Palis J. Primitive and definitive erythropoiesis in mammals. *Front. Physiol.* 2014;5 JAN(January):1–9.
4. Orkin SH, Zon LI. Hematopoiesis: An Evolving Paradigm for Stem Cell Biology. *Cell*. 2008;132(4):631–644.
5. Rowe RG, Mandelbaum J, Zon LI, Daley GQ. Engineering Hematopoietic Stem Cells: Lessons from Development. *Cell Stem Cell*. 2016;18(6):707–720.
6. Müller AM, Medvinsky A, Strouboulis J, Grosveld F, Dzierzak E. Development of hematopoietic stem cell activity in the mouse embryo. *Immunity*. 1994;1(4):291–301.
7. Medvinsky A, Dzierzak E. Definitive hematopoiesis is autonomously initiated by the AGM region. *Cell*. 1996;86(6):897–906.
8. de Bruijn MF, Speck NA, Peeters MC, Dzierzak E. Definitive hematopoietic stem cells first develop within the major arterial regions of the mouse embryo. *EMBO J.* 2000;19(11):2465–74.
9. Pereira CF, Chang B, Gomes A, et al. Hematopoietic Reprogramming In Vitro Informs In Vivo Identification of Hemogenic Precursors to Definitive Hematopoietic Stem Cells. *Dev. Cell*. 2016;36(5):525–539.
10. Ottersbach K, Dzierzak E. The murine placenta contains hematopoietic stem cells within the vascular labyrinth region. *Dev. Cell*. 2005;8(3):377–387.
11. Gekas C, Dieterlen-Lievre F, Orkin SH, Mikkola HKA. The placenta is a niche for hematopoietic stem cells. *Dev. Cell*. 2005;8(3):365–375.
12. Zovein AC, Turlo KA, Ponec RM, et al. Vascular remodeling of the vitelline artery initiates extravascular emergence of hematopoietic clusters. *Blood*. 2010;116(18):3435–3444.
13. Yokomizo T, Ng CEL, Osato M, Dzierzak E. Three-dimensional imaging of whole midgestation murine embryos shows an intravascular localization for all hematopoietic clusters. *Blood*. 2011;117(23):6132–6134.
14. Amanda D. Yzaguirre NAS. Extravascular endothelial and hematopoietic islands form through multiple pathways in midgestation mouse embryos. *Reliab. Eng. Syst. Saf.* 2016;415(1):111–121.
15. Yokomizo T, Dzierzak E. Three-dimensional cartography of hematopoietic clusters in the vasculature of whole mouse embryos. *Development*. 2010;137(21):3651–3661.
16. Li Z, Vink CS, Mariani S, Dzierzak E. Localization and characterization of hematopoietic cells in the mouse embryonic head. *Exp. Hematol.* 2015;43(9):S76.
17. Kissa K, Herbomel P. Blood stem cells emerge from aortic endothelium by a novel type of cell transition. *Nature*. 2010;464(7285):112–5.
18. Bertrand JY, Chi NC, Santoso B, et al. Haematopoietic stem cells derive directly

from aortic endothelium during development. *Nature*. 2010;464(7285):108–11.
19. Lam EYN, Hall CJ, Crosier PS, Crosier KE, Flores MV. Live imaging of Runx1 expression in the dorsal aorta tracks the emergence of blood progenitors from endothelial cells Enid. *Blood*. 2016;116(6):909–915.
20. Adamo L, Naveiras O, Wenzel PL, et al. Biomechanical forces promote embryonic haematopoiesis. *Nature*. 2009;459(7250):1131–5.
21. North TE, Goessling W, Peeters M, et al. Hematopoietic Stem Cell Development Is Dependent on Blood Flow. *Cell*. 2009;137(4):736–748.
22. Wang L, Zhang P, Wei Y, et al. A blood flow-dependent klf2a-NO signaling cascade is required for stabilization of hematopoietic stem cell programming in zebrafish embryos. *Blood*. 2011;118(15):4102–4110.
23. Diaz MF, Li N, Lee HJ, et al. Biomechanical forces promote blood development through prostaglandin E2 and the cAMP-PKA signaling axis. *J. Exp. Med.* 2015;212(5):665–680.
24. Lux CT, Yoshimoto M, Mcgrath K, et al. All primitive and definitive hematopoietic progenitor cells emerging before E10 in the mouse embryo are products of the yolk sac. *Blood*. 2008;111(7):3435–3438.
25. Dzierzak E, Speck NA. Of lineage and legacy: the development of mammalian hematopoietic stem cells. *Nat Immunol*. 2008;9(2):129–136.
26. Zhong TP, Childs S, Leu JP, Fishman MC. Gridlock signalling pathway fashions the first embryonic artery. *Nature*. 2001;414(6860):216–220.
27. Lawson ND, Scheer N, Pham VN, et al. Notch signaling is required for arterial-venous differentiation during embryonic vascular development. *Development*. 2001;128(19):3675–3683.
28. Zape JP, Zovein AC. Hemogenic endothelium: origins, regulation, and implications for vascular biology. *Semin. Cell Dev. Biol.* 2011;22(9):1036–47.
29. Walker L, Carlson a, Tan-Pertel HT, Weinmaster G, Gasson J. The notch receptor and its ligands are selectively expressed during hematopoietic development in the mouse. *Stem Cells*. 2001;19(6):543–52.
30. Kumano K, Chiba S, Kunisato A, et al. Notch1 but not Notch2 is essential for generating hematopoietic stem cells from endothelial cells. *Immunity*. 2003;18(5):699–711.
31. Vercauteren SM, Sutherland HJ. Constitutively active Notch4 promotes early human hematopoietic progenitor cell maintenance while inhibiting differentiation and causes lymphoid abnormalities in vivo. *Blood*. 2004;104(8):2315–2322.
32. Kanz D, Konantz M, Alghisi E, North TE, Lengerke C. Endothelial-to-hematopoietic transition: Notch-ing vessels into blood. *Ann. N. Y. Acad. Sci.* 2016;1370:97–108.
33. Burns CE, Traver D, Mayhall E, Shepard JL, Zon LI. Hematopoietic stem cell fate is established by the Notch – Runx pathway. *Genes Dev.* 2005;19:2331–2342.
34. Nakagawa M, Ichikawa M, Kumano K, et al. AML1/Runx1 rescues Notch1-null mutation-induced deficiency of para-aortic splanchnopleural hematopoiesis. *Blood*. 2006;108(10):3329–3334.
35. Ichikawa M, Asai T, Chiba S, Kurokawa M, Ogawa S. Runx1/AML-1 ranks as a

master regulator of adult hematopoiesis. *Cell Cycle*. 2004;3(6):722–724.
36. Ng CEL, Yokomizo T, Yamashita N, et al. A Runx1 intronic enhancer marks hemogenic endothelial cells and hematopoietic stem cells. *Stem Cells*. 2010;28(10):1869–1881.
37. Chen MJ, Yokomizo T, Zeigler B, Dzierzak E, Speck A. Runx1 is required for the endothelial to hematopoietic cell transition but not thereafter. *Nature*. 2009;457(7231):887–891.
38. Sroczynska P, Lancrin C, Kouskoff V, Lacaud G. The differential activities of Runx1 promoters define milestones during embryonic hematopoiesis. *Blood*. 2009;114(26):5279–5289.
39. Tanaka Y, Joshi A, Wilson NK, et al. The transcriptional programme controlled by Runx1 during early embryonic blood development. *Dev. Biol.* 2012;366(2):404–419.
40. Challen GA, Goodell MA. Runx1 isoforms show differential expression patterns during hematopoietic development but have similar functional effects in adult hematopoietic stem cells. *Exp. Hematol.* 2010;38(5):403–416.
41. North T, Gu TL, Stacy T, et al. Cbfa2 is required for the formation of intra-aortic hematopoietic clusters. *Development*. 1999;126(11):2563–75.
42. Lacaud G, Kouskoff V, Trumble A, Schwantz S, Keller G. Haploinsufficiency of Runx1 results in the acceleration of mesodermal development and hemangioblast specification upon in vitro differentiation of ES cells. *Blood*. 2004;103(3):886–889.
43. Wang Q, Stacy T, Binder M, et al. Disruption of the Cbfa2 gene causes necrosis and hemorrhaging in the central nervous system and blocks definitive hematopoiesis. *Proc. Natl. Acad. Sci. U. S. A.* 1996;93(8):3444–9.
44. Cai Z, de Bruijn M, Ma X, et al. Haploinsufficiency of AML1 affects the temporal and spatial generation of hematopoietic stem cells in the mouse embryo. *Immunity*. 2000;13(4):423–431.
45. Tober J, Yzaguirre AD, Piwarzyk E, Speck N a. Distinct temporal requirements for Runx1 in hematopoietic progenitors and stem cells. *Development*. 2013;140(18):3765–76.
46. Swiers G, Baumann C, O'Rourke J, et al. Early dynamic fate changes in haemogenic endothelium characterized at the single-cell level. *Nat. Commun.* 2013;4:2924.
47. Bee T, Ashley ELK, Bickley SRB, et al. The mouse Runx1 +23 hematopoietic stem cell enhancer confers hematopoietic specificity to both Runx1 promoters. *Blood*. 2009;113(21):5121–5214.
48. Bee T, Swiers G, Muroi S, et al. Nonredundant roles for Runx1 alternative promoters reflect their activity at discrete stages of developmental hematopoiesis. *Blood*. 2010;115(15):3042–3051.
49. Bee T, Liddiard K, Swiers G, et al. Alternative Runx1 promoter usage in mouse developmental hematopoiesis. *Blood Cells, Mol. Dis.* 2009;43(1):35–42.
50. Tober J, Maijenburg MW, Speck NA. Taking the Leap: Runx1 in the Formation of Blood from Endothelium. Elsevier Inc.; 2016.

51. Tsai FY, Keller G, Kuo FC, et al. An early haematopoietic defect in mice lacking the transcription factor GATA-2. *Nature*. 1994;371(6494):221–226.
52. de Pater E, Kaimakis P, Vink CS, et al. Gata2 is required for HSC generation and survival. *J. Exp. Med.* 2013;210(13):2843–50.
53. Ling K-W, Ottersbach K, van Hamburg JP, et al. GATA-2 plays two functionally distinct roles during the ontogeny of hematopoietic stem cells. *J. Exp. Med.* 2004;200(7):871–882.
54. Gao X, Johnson KD, Chang Y-I, et al. Gata2 cis-element is required for hematopoietic stem cell generation in the mammalian embryo. *J. Exp. Med.* 2013;210(13):2833–42.
55. Butko E, Distel M, Pouget C, et al. Gata2b is a restricted early regulator of hemogenic endothelium in the zebrafish embryo. *Development*. 2015;142(6):1050–61.
56. Liu F, Walmsley M, Rodaway A, Patient R. Fli1 Acts at the Top of the Transcriptional Network Driving Blood and Endothelial Development. *Curr. Biol.* 2008;18(16):1234–1240.
57. Pimanda JE, Ottersbach K, Knezevic K, et al. Gata2, Fli1, and Scl form a recursively wired gene-regulatory circuit during early hematopoietic development. *Proc Natl Acad Sci U S A*. 2007;104(45):17692–17697.
58. Brown LA, Rodaway ARF, Schilling TF, et al. Insights into early vasculogenesis revealed by expression of the ETS-domain transcription factor Fli-1 in wild-type and mutant zebrafish embryos. *Mech. Dev.* 2000;90(2):237–252.
59. Spyropoulos DD, Pharr PN, Lavenburg KR, et al. Hemorrhage, impaired hematopoiesis, and lethality in mouse embryos carrying a targeted disruption of the Fli1 transcription factor. *Mol. Cell. Biol.* 2000;20(15):5643–5652.
60. Porcher C, Swat W, Rockwell K, et al. The T cell leukemia oncoprotein SCL/tal-1 is essential for development of all hematopoietic lineages. *Cell*. 1996;86(1):47–57.
61. Visvader JE. development Unsuspected role for the T-cell leukemia protein SCL / tal-1 in vascular development. *Genes Dev.* 1998;12:473–479.
62. Robb L, Elwood NJ, Elefanty a G, et al. The scl gene product is required for the generation of all hematopoietic lineages in the adult mouse. *EMBO J.* 1996;15(16):4123–4129.
63. Lancrin C, Sroczynska P, Stephenson C, et al. The haemangioblast generates haematopoietic cells through a haemogenic endothelium stage. *Nature*. 2009;457(7231):892–5.
64. Iacovino M, Chong D, Szatmari I, et al. HoxA3 is an apical regulator of haemogenic endothelium. *Nat. Cell Biol.* 2011;13(1):72–8.
65. Kyba M, Perlingeiro RCR, Daley GQ. HoxB4 confers definitive lymphoid-myeloid engraftment potential on embryonic stem cell and yolk sac hematopoietic progenitors. *Cell*. 2002;109(1):29–37.
66. Wang L, Menendez P, Shojaei F, et al. Generation of hematopoietic repopulating cells from human embryonic stem cells independent of ectopic HOXB4 expression. *J. Exp. Med.* 2005;201(10):1603–14.
67. Ramos-Mejia V, Navarro-Montero O, Ayllon V, et al. HOXA9 promotes

hematopoietic commitment of human embryonic stem cells. *Blood*. 2014;124(20):3065–3075.
68. Dou DR, Calvanese V, Sierra MI, et al. Medial HOXA genes demarcate haematopoietic stem cell fate during human development. *Nat. Cell Biol.* 2016;18(6.):
69. Clarke RL, Yzaguirre AD, Yashiro-Ohtani Y, et al. The expression of Sox17 identifies and regulates haemogenic endothelium. *Nat. Cell Biol.* 2013;15(5):502–10.
70. Nakajima-Takagi Y, Osawa M, Oshima M, et al. Role of SOX17 in hematopoietic development from human embryonic stem cells. *Blood*. 2013;121(3):447–58.
71. Clarke RL, Robitaille AM, Moon RT, Keller G. A quantitative proteomic analysis of hemogenic endothelium reveals differential regulation of hematopoiesis by SOX17. *Stem Cell Reports*. 2015;5(2):291–304.
72. Serrano AG, Gandillet A, Pearson S, Lacaud G, Kouskoff V. Contrasting effects of Sox17- and Sox18-sustained expression at the onset of blood specification. *Blood*. 2010;115(19):3895–3898.
73. Corrigan PM, Dobbin E, Freeburn RW, Wheadon H. Patterns of Wnt/Fzd/LRP gene expression during embryonic hematopoiesis. *Stem Cells Dev.* 2009;18(5):759–772.
74. Reya T, Duncan AW, Ailles L, et al. A role for Wnt signalling in self-renewal of haematopoietic stem cells. *Nature*. 2003;423(6938):409–414.
75. Murdoch B, Chadwick K, Martin M, et al. Wnt-5A augments repopulating capacity and primitive hematopoietic development of human blood stem cells in vivo. *Proc. Natl. Acad. Sci. U. S. A.* 2003;100:3422–3427.
76. Luis TC, Weerkamp F, Naber BAE, et al. Wnt3a deficiency irreversibly impairs hematopoietic stem cell self-renewal and leads to defects in progenitor cell differentiation. *Blood*. 2009;113(3):546–554.
77. Ferrell PI, Xi J, Ma C, Adlakha M, Kaufman DS. The RUNX1 +24 enhancer and P1 promoter identify a unique subpopulation of hematopoietic progenitor cells derived from human pluripotent stem cells. *Stem Cells*. 2015;33(4):1130–41.
78. Kennedy M, Awong G, Sturgeon CM, et al. T Lymphocyte Potential Marks the Emergence of Definitive Hematopoietic Progenitors in Human Pluripotent Stem Cell Differentiation Cultures. *Cell Rep.* 2012;2(6):1722–1735.
79. Sturgeon CM, Ditadi A, Awong G, Kennedy M, Keller G. Wnt signaling controls the specification of definitive and primitive hematopoiesis from human pluripotent stem cells. *Nat. Biotechnol.* 2014;32(6):554–61.
80. Gupta S, Zhu H, Zon LI, Evans T. BMP signaling restricts hemato-vascular development from lateral mesoderm during somitogenesis. *Development*. 2006;133(11):2177–2187.
81. Maeno M, Mead PE, Kelley C, et al. The role of BMP-4 and GATA-2 in the induction and differentiation of hematopoietic mesoderm in Xenopus laevis. *Blood*. 1996;88(6):1965–1972.
82. Shin M, Nagai H, Sheng G. Notch mediates Wnt and BMP signals in the early separation of smooth muscle progenitors and blood/endothelial common

progenitors. *Development*. 2009;136(4):595–603.
83. Mestas J, Hughes CCW. Of mice and not men: differences between mouse and human immunology. *J. Immunol.* 2004;172(5):2731–2738.
84. Doeing DC, Borowicz JL, Crockett ET. Gender dimorphism in differential peripheral blood leukocyte counts in mice using cardiac, tail, foot, and saphenous vein puncture methods. *BMC Clin. Pathol.* 2003;3(1):3.
85. Beer PA, Eaves CJ. Modeling Normal and Disordered Human Hematopoiesis. *Trends in Cancer*. 2016;1(3):199–210.
86. Sitnicka E, Buza-vidas N, Larsson S, et al. Human CD34? hematopoietic stem cells capable of multilineage engrafting NOD/SCID mice express flt3: distinct flt3 and c-kit expression and response patterns on mouse and candidate human hematopoietic stem cells. *Blood*. 2003;102(3):881–886.
87. Parekh C, Crooks GM. Critical differences in hematopoiesis and lymphoid development between humans and mice. *J. Clin. Immunol.* 2013;33(4):711–715.
88. Rongvaux A, Takizawa H, Strowig T, et al. Human Hemato-Lymphoid System Mice: Current Use and Future Potential for Medicine. *Annu. Rev. Immunol.* 2013;31(1):635–674.
89. Kaufman DS, Hanson ET, Lewis RL, Auerbach R, Thomson J a. Hematopoietic colony-forming cells derived from human embryonic stem cells. *Proc. Natl. Acad. Sci. U. S. A.* 2001;98(19):10716–21.
90. Vodyanik M, Bork J, Thomson J, Slukvin I. Human embryonic stem cell – derived CD34 ♀ cells : efficient production in the coculture with OP9 stromal cells and analysis of lymphohematopoietic potential. *Blood*. 2005;105(2):617–626.
91. Choi K-D, Yu J, Smuga-Otto K, et al. Hematopoietic and endothelial differentiation of human induced pluripotent stem cells. *Stem Cells*. 2009;27(3):559–67.
92. Timmermans F, Velghe I, Vanwalleghem L, et al. Generation of T cells from human embryonic stem cell-derived hematopoietic zones. *J. Immunol.* 2009;182(11):6879–6888.
93. Gori JL, Butler JM, Chan YY, et al. Vascular niche promotes hematopoietic multipotent progenitor formation from pluripotent stem cells. *J. Clin. Invest.* 2015;125(3):1243–1254.
94. Nostro MC, Cheng X, Keller GM, Gadue P. Wnt, Activin, and BMP Signaling Regulate Distinct Stages in the Developmental Pathway from Embryonic Stem Cells to Blood. *Cell Stem Cell*. 2008;2(1):60–71.
95. Ditadi A, Sturgeon CM, Tober J, et al. Human definitive haemogenic endothelium and arterial vascular endothelium represent distinct lineages. *Nat. Cell Biol.* 2015;17(5):580–91.
96. Patel D, Webber BR, Dunmire SK, et al. Enhanced lymphocyte generation from T-iPSC by coordinated manipulation of Wnt and TGF-beta signaling. *Int. Soc. Stem Cell Res. Annu. Meet.* 2016;574.
97. Suzuki N, Yamazaki S, Yamaguchi T, et al. Generation of engraftable hematopoietic stem cells from induced pluripotent stem cells by way of teratoma formation. *Mol. Ther.* 2013;21(7):1424–31.

98. Amabile G, Welner RS, Nombela-arrieta C, et al. In vivo generation of transplantable human hematopoietic cells from induced pluripotent stem cells. 2013;121(8):1–3.
99. Artis D, Spits H. The biology of innate lymphoid cells. *Nature*. 2015;517(7534):293–301.
100. Hazenberg MD, Spits H. Review Article Human innate lymphoid cells. *Blood*. 2014;124(5):700–710.
101. Eberl G, Colonna M, Di Santo JP, McKenzie ANJ. Innate lymphoid cells: A new paradigm in immunology. *Science (80-. ).* 2015;348(6237):aaa6566.
102. Klose CSN, Flach M, Mohle L, et al. Differentiation of type 1 ILCs from a common progenitor to all helper-like innate lymphoid cell lineages. *Cell*. 2014;157(2):340–356.
103. Fuchs A, Vermi W, Lee JS, et al. Intraepithelial type 1 innate lymphoid cells are a unique subset of IL-12 and IL-15-responsive IFNg-producing cells. *Immunity*. 2013;38(4):769–781.
104. Hoorweg K, Peters CP, Cornelissen F, et al. Functional differences between human NKp44- and NKp44+ RORC+ innate lymphoid cells. *Front. Immunol.* 2012;3(APR.):
105. Cella M, Fuchs A, Vermi W, et al. A human natural killer cell subset provides an innate source of IL-22 for mucosal immunity. *Nature*. 2008;457(7230):722–725.
106. Ahn Y, Blazar BR, Miller JS, Verneris MR. Lineage relationships of human interleukin-22-producing CD56+ RORgt+ innate lymphoid cells and conventional natural killer cells. *Blood*. 2013;121(12):2234–2243.
107. Spits H, Cupedo T. Innate Lymphoid Cells: Emerging Insights in Development, Lineage Relationships, and Function. *Annu. Rev. Immunol.* 2012;30(1):647–675.
108. Constantinides MG, McDonald BD, Verhoef PA, Bendelac A. A committed precursor to innate lymphoid cells. *Nature*. 2014;508(7496):397–401.
109. Seillet C, Rankin LC, Groom JR, et al. Nfil3 is required for the development of all innate lymphoid cell subsets. *J. Exp. Med.* 2014;211(9):1733–1740.
110. Geiger TL, Abt MC, Gasteiger G, et al. Nfil3 is crucial for development of innate lymphoid cells and host protection against intestinal pathogens. *J. Exp. Med.* 2014;211(9):1723–1731.
111. Caligiuri M a. Human natural killer cells. *Bone*. 2008;112(3):461–469.
112. Hoyler T, Klose CSN, Souabni A, et al. The Transcription Factor GATA-3 Controls Cell Fate and Maintenance of Type 2 Innate Lymphoid Cells. *Immunity*. 2012;37(4):634–648.
113. Mjösberg J, Bernink J, Golebski K, et al. The Transcription Factor GATA3 Is Essential for the Function of Human Type 2 Innate Lymphoid Cells. *Immunity*. 2012;37(4):649–659.
114. Zhong C, Cui K, Wilhelm C, et al. Group 3 innate lymphoid cells continuously require the transcription factor GATA-3 after commitment. *Nat. Immunol.* 2015;17(2):2–8.
115. Loza MJ, Zamai L, Azzoni L, Rosati E, Perussia B. Expression of type 1 (interferon gamma) and type 2 (interleukin-13, interleukin-5) cytokines at distinct

stages of natural killer cell differentiation from progenitor cells. *Blood*. 2002;99(4):1273–1281.
116. Chan A, Hong D-L, Atzberger A, et al. CD56bright human NK cells differentiate into CD56dim cells: role of contact with peripheral fibroblasts. *J. Immunol.* 2007;179:89–94.
117. Simonetta F, Pradier A, Roosnek E. T-bet and Eomesodermin in NK Cell Development, Maturation, and Function. *Front. Immunol.* 2016;7(June):1–6.
118. Scoville SD, Mundy-Bosse BL, Zhang MH, et al. A Progenitor Cell Expressing Transcription Factor RORγt Generates All Human Innate Lymphoid Cell Subsets. *Immunity*. 2016;44(5):1–11.
119. Montaldo E, Teixeira-Alves LG, Glatzer T, et al. Human RORgt+CD34+ cells are lineage-specified progenitors of group 3 RORgt+ innate lymphoid cells. *Immunity*. 2014;41(6):988–1000.
120. Woll PS, Martin CH, Miller JS, Kaufman DS. Human Embryonic Stem Cell-Derived NK Cells Acquire Functional Receptors and Cytolytic Activity. *J. Immunol.* 2005;175(8):5095–5103.
121. Woll PS, Grzywacz B, Tian X, et al. Human embryonic stem cells differentiate into a homogeneous population of natural killer cells with potent in vivo antitumor activity. *Blood*. 2009;113(24):6094–101.
122. Hermanson DL, Bendzick L, Pribyl L, et al. Induced Pluripotent Stem Cell-Derived Natural Killer Cells for Treatment of Ovarian Cancer. *Stem Cells*. 2016;34(1):93–101.
123. Ni Z, Knorr DA, Clouser CL, et al. Human pluripotent stem cells produce natural killer cells that mediate anti-HIV-1 activity by utilizing diverse cellular mechanisms. *J. Virol.* 2011;85(1):43–50.
124. Geller MA, Knorr DA, Hermanson DA, et al. Intraperitoneal delivery of human natural killer cells for treatment of ovarian cancer in a mouse xenograft model. *Cytotherapy*. 2013;15(10):1297–1306.
125. Martin C, Woll P, Zhenya N, Zuniga-Pfucker J, Kaufman DS. Differences in lymphocyte developmental potential between human embryonic stem cell and umbilical cord blood–derived hematopoietic progenitor cells. *Blood*. 2008;112(7):2730–2737.
126. Knorr DA, Ni Z, Hermanson DL, et al. Clinical-Scale Derivation of Natural Killer Cells From Human Pluripotent Stem Cells for Cancer Therapy. *Stem Cells Transl. Med.* 2013;274–283.
127. Denman CJ, Senyukov V V., Somanchi SS, et al. Membrane-bound IL-21 promotes sustained Ex Vivo proliferation of human natural killer cells. *PLoS One*. 2012;7(1):e30264.
128. Hahn ME. Aryl hydrocarbon receptors: diversity and evolution. *Chem. Biol. Interact.* 2002;141(1-2):131–160.
129. Julliard W, Fechner JH, Mezrich JD. The Aryl Hydrocarbon Receptor Meets Immunology: Friend or Foe? A Little of Both. *Front. Immunol.* 2014;5(October):1–6.
130. Smith BW, Rozelle SS, Leung A, et al. The aryl hydrocarbon receptor directs

hematopoietic progenitor cell expansion and differentiation. *Blood*. 2013;122(3):376–85.
131. Iain AM, Andrew DP, Gary HP. Aryl hydrocarbon receptor ligands in cancer: friend and foe. *Nat. Rev. Cancer*. 2014;14(12):801–814.
132. Tsuji N, Fukuda K, Nagata Y, et al. The activation mechanism of the aryl hydrocarbon receptor (AhR) by molecular chaperone HSP90. *FEBS Open Bio*. 2014;4:796–803.
133. Cox MB, Miller C a. Cooperation of heat shock protein 90 and p23 in aryl hydrocarbon receptor signaling. *Cell Stress Chaperones*. 2004;9(1):4–20.
134. Schneider AJ, Branam AM, Peterson RE. Intersection of AHR and Wnt Signaling in Development, Health, and Disease. *Int. J. Mol. Sci.* 2014;15(10):17852–17885.
135. Simones T, Shepherd DM. Consequences of AhR activation in steady-state dendritic cells. *Toxicol. Sci.* 2011;119(2):293–307.
136. Jin G-B, Moore AJ, Head JL, Neumiller JJ, Lawrence BP. Aryl hydrocarbon receptor activation reduces dendritic cell function during influenza virus infection. *Toxicol. Sci.* 2010;116(2):514–22.
137. Quintana FJ, Basso AS, Iglesias AH, et al. Control of T(reg) and T(H)17 cell differentiation by the aryl hydrocarbon receptor. *Nature*. 2008;453(7191):65–71.
138. Frericks M, Meissner M, Esser C. Microarray analysis of the AHR system: tissue-specific flexibility in signal and target genes. *Toxicol. Appl. Pharmacol.* 2007;220(3):320–32.
139. Mezrich JD, Fechner JH, Zhang X, et al. An interaction between kynurenine and the aryl hydrocarbon receptor can generate regulatory T cells. *J. Immunol.* 2010;185(6):3190–8.
140. Veldhoen M, Hirota K, Westendorf AM, et al. The aryl hydrocarbon receptor links TH17-cell-mediated autoimmunity to environmental toxins. *Nature*. 2008;453(7191):106–9.
141. Boitano AE, Wang J, Romeo R, et al. Aryl Hydrocarbon Receptor Antagonists Promote the Expansion of Human Hematopoietic Stem Cells. *Science (80-. ).* 2010;329(5997):1345–1348.
142. Wagner JE, Brunstein CG, Boitano AE, et al. Phase I/II Trial of StemRegenin-1 Expanded Umbilical Cord Blood Hematopoietic Stem Cells Supports Testing as a Stand-Alone Graft. *Cell Stem Cell*. 2015;18(1):144–155.
143. Singh KP, Garrett RW, Casado FL, Gasiewicz T a. Aryl hydrocarbon receptor-null allele mice have hematopoietic stem/progenitor cells with abnormal characteristics and functions. *Stem Cells Dev.* 2011;20(5):769–84.
144. Hirabayashi Y, Inoue T. Aryl hydrocarbon receptor biology and xenobiotic responses in hematopoietic progenitor cells. *Biochem. Pharmacol.* 2009;77(4):521–35.
145. Lindsey S, Papoutsakis ET. The Evolving Role of the Aryl Hydrocarbon Receptor (AHR) in the Normophysiology of Hematopoiesis. *Stem Cell Rev. Reports*. 2012;8:1223–1235.
146. Mulero-Navarro S, Fernandez-Salguero PM. New Trends in Aryl Hydrocarbon Receptor Biology. *Front. Cell Dev. Biol.* 2016;4(May):1–14.

147. Boisset J-C, van Cappellen W, Andrieu-Soler C, et al. In vivo imaging of haematopoietic cells emerging from the mouse aortic endothelium. *Nature*. 2010;464(7285):116–20.
148. Mikkola HKA. The journey of developing hematopoietic stem cells. *Development*. 2006;133(19):3733–3744.
149. Jagannathan-Bogdan M, Zon LI. Hematopoiesis. *Development*. 2013;140(12):2463–2467.
150. Rafii S, Kloss CC, Butler JM, et al. Human ESC-derived hemogenic endothelial cells undergo distinct waves of endothelial to hematopoietic transition. *Blood*. 2013;121(5):770–780.
151. Eilken HM, Nishikawa S-I, Schroeder T. Continuous single-cell imaging of blood generation from haemogenic endothelium. *Nature*. 2009;457(7231):896–900.
152. Antas VI, Al-Drees MA, Prudence AJA, Sugiyama D, Fraser ST. Hemogenic endothelium: A vessel for blood production. *Int. J. Biochem. Cell Biol.* 2013;45(3):692–695.
153. Zambidis ET, Peault B, Park TS, Bunz F, Civin CI. Hematopoietic differentiation of human embryonic stem cells progresses through sequential hematoendothelial , primitive , and definit. *Blood*. 2008;106(3):860–870.
154. Lie-A-Ling M, Marinopoulou E, Li Y, et al. RUNX1 positively regulates a cell adhesion and migration program in murine hemogenic endothelium prior to blood emergence. *Blood*. 2014;124(11):e11–20.
155. Hirose SI, Takayama N, Nakamura S, et al. Immortalization of erythroblasts by c-MYC and BCL-XL enables large-scale erythrocyte production from human pluripotent stem cells. *Stem Cell Reports*. 2013;1(6):499–508.
156. Kobar L, Yates F, Oudrhiri N, et al. Human induced pluripotent stem cells can reach complete terminal maturation: In vivo and in vitro evidence in the erythropoietic differentiation model. *Haematologica*. 2012;97(12):1795–1803.
157. Choi K-D, Vodyanik M a, Togarrati PP, et al. Identification of the hemogenic endothelial progenitor and its direct precursor in human pluripotent stem cell differentiation cultures. *Cell Rep.* 2012;2(3):553–67.
158. Vodyanik M, Bork J, Thomson J, Slukvin I. Human embryonic stem cell – derived CD34+ cells : efficient production in the coculture with OP9 stromal cells and analysis of lymphohematopoietic potential. *Blood*. 2005;105(2):617–626.
159. Chadwick K, Wang L, Li L, et al. Cytokines and BMP-4 promote hematopoietic differentiation of human embryonic stem cells. *Blood*. 2003;102(3):906–915.
160. Knorr DA, Bock A, Brentjens RJ, Kaufman DS. Engineered human embryonic stem cell-derived lymphocytes to study in vivo trafficking and immunotherapy. *Stem Cells Dev.* 2013;22(13):1861–9.
161. Ni Z, Knorr DA, Kaufman DS. Hematopoietic and Natural Killer Cell Development from Human Pluripotent Stem Cells. *Embryonic Stem Cell Immunobiol. Methods Protoc. Methods Mol. Biol.* 2013;1029:33–41.
162. Melichar H, Li O, Ross J, et al. Comparative study of hematopoietic differentiation between human embryonic stem cell lines. *PLoS One*. 2011;6(5.):
163. Chen B, Mao B, Huang S, Zhou Y. Human Embryonic Stem Cell-Derived

Primitive and Definitive Hematopoiesis. 2014;
164. Kennedy M, D'Souza SL, Lynch-Kattman M, Schwantz S, Keller G. Development of the hemangioblast defines the onset of hematopoiesis in human ES cell differentiation cultures. *Blood*. 2007;109(7):2679–87.
165. Shalek AK, Satija R, Adiconis X, et al. Single-cell transcriptomics reveals bimodality in expression and splicing in immune cells. *Nature*. 2013;498(7453):236–40.
166. Tan SYS, Krasnow MA. Developmental origin of lung macrophage diversity. *Development*. 2016;1318–1327.
167. Yvernogeau L, Gautier R, Khoury H, et al. An in vitro model of hemogenic endothelium commitment and hematopoietic production. *Development*. 2016;1302–1312.
168. Björklund ÅK, Forkel M, Picelli S, et al. The heterogeneity of human CD127(+) innate lymphoid cells revealed by single-cell RNA sequencing. *Nat. Immunol.* 2016;17(4):451–60.
169. Ferrell PI, Adlakha M, Kaufman DS. RUNX1c Expression Identifies an Enriched Subpopulation of Hematopoietic Progenitor Cells Derived From Human Pluripotent Stem Cells. *Submitted*. 2014;Submitted.:
170. Ng ES, Davis R, Stanley EG, Elefanty AG. A protocol describing the use of a recombinant protein-based, animal product-free medium (APEL) for human embryonic stem cell differentiation as spin embryoid bodies. *Nat. Protoc.* 2008;3(5):768–776.
171. Satija R, Farrell JA, Gennert D, Schier AF, Regev A. Spatial reconstruction of single-cell gene expression data. *Nat. Biotechnol.* 2015;33(5):495–502.
172. Macosko EZ, Basu A, Satija R, et al. Highly Parallel Genome-wide Expression Profiling of Individual Cells Using Nanoliter Droplets. *Cell*. 2015;161(5):1202–1214.
173. Wurtzel O, Cote LE, Poirier A, et al. A Generic and Cell-Type-Specific Wound Response Precedes Regeneration in Planarians. *Dev. Cell*. 2015;35(5):632–645.
174. Camp JG, Badsha F, Florio M, et al. Human cerebral organoids recapitulate gene expression programs of fetal neocortex development. *Proc. Natl. Acad. Sci. U. S. A.* 2015;112(51):15672–7.
175. Patro R, Duggal G, Kingsford C. Salmon: Accurate, Versatile and Ultrafast Quantification from RNA-seq Data using Lightweight-Alignment. *bioRxiv*. 2015;021592.
176. Søreide K. Receiver-operating characteristic curve analysis in diagnostic, prognostic and predictive biomarker research. *J. Clin. Pathol.* 2009;62(1):1–5.
177. Anderson H, Patch TC, Reddy PNG, et al. Hematopoietic stem cells develop in the absence of endothelial cadherin 5 expression. *Blood*. 2015;126(26):2811–2820.
178. Nikolova-Krstevski V, Yuan L, Le Bras A, et al. ERG is required for the differentiation of embryonic stem cells along the endothelial lineage. *BMC Dev. Biol.* 2009;9(1):72.
179. Choi KD, Vodyanik MA, Togarrati PP, et al. Identification of the Hemogenic Endothelial Progenitor and Its Direct Precursor in Human Pluripotent Stem Cell

Differentiation Cultures. *Cell Rep.* 2012;2(3):553–567.
180. Chen MJ, Li Y, De Obaldia ME, et al. Erythroid/myeloid progenitors and hematopoietic stem cells originate from distinct populations of endothelial cells. *Cell Stem Cell*. 2011;9(6):541–552.
181. Lu S-J, Luo C, Holton K, et al. Robust generation of hemangioblastic progenitors from human embryonic stem cells. *Regen. Med.* 2008;3(5):693–704.
182. Lu S, Feng Q, Caballero S, et al. Generation of functional hemangioblasts from human embryonic stem cells. 2007;4(6):501–509.
183. Kennedy M, D'Souza SL, Lynch-Kattman M, Schwantz S, Keller G. Development of the hemangioblast defines the onset of hematopoiesis in human ES cell differentiation cultures. *Blood*. 2007;109(7):2679–2687.
184. Zambidis ET, Sinka L, Tavian M, et al. Emergence of human angiohematopoietic cells in normal development and from cultured embryonic stem cells. *Ann. N. Y. Acad. Sci.* 2007;1106:223–232.
185. Nakajima H, Ito M, Smookler DS, et al. TIMP-3 recruits quiescent hematopoietic stem cells into active cell cycle and expands multipotent progenitor pool. *Blood*. 2010;116(22):4474–4482.
186. Nakajima H, Shibata F, Fukuchi Y, et al. Immune suppressor factor confers stromal cell line with enhanced supporting activity for hematopoietic stem cells. *Biochem. Biophys. Res. Commun.* 2006;340(1):35–42.
187. Yokota T, Oritani K, Butz S, et al. The endothelial antigen ESAM marks primitive hematopoietic progenitors throughout life in mice. *Blood*. 2009;113(13):2914–2923.
188. Ooi a GL, Karsunky H, Majeti R, et al. The adhesion molecule esam1 is a novel hematopoietic stem cell marker. *Stem Cells*. 2009;27(3):653–661.
189. Yuan L, Sacharidou A, Stratman AN, et al. RhoJ is an endothelial cell-restricted Rho GTPase that mediates vascular morphogenesis and is regulated by the transcription factor ERG. *Blood*. 2011;118(4):1145–1153.
190. Leszczynska K, Kaur S, Wilson E, Bicknell R, Heath VL. The role of RhoJ in endothelial cell biology and angiogenesis. *Biochem. Soc. Trans.* 2011;39(6):1606–1611.
191. McLaughlin F, Ludbrook VJ, Cox J, et al. Combined genomic and antisense analysis reveals that the transcription factor Erg is implicated in endothelial cell differentiation. *Blood*. 2001;98(12):3332–3339.
192. Wilson E, Leszczynska K, Poulter NS, et al. RhoJ interacts with the GIT-PIX complex and regulates focal adhesion disassembly. *J. Cell Sci.* 2014;127(Pt 14):3039–51.
193. Kim AD, Melick CH, Clements WK, et al. Discrete Notch signaling requirements in the specification of hematopoietic stem cells. *EMBO J.* 2014;33(20):2363–73.
194. Hadland BK, Huppert SS, Kanungo J, et al. A requirement for Notch1 distinguishes 2 phases of definitive hematopoiesis during development. *Blood*. 2004;104(10):3097–3105.
195. Chen JY, Miyanishi M, Wang SK, et al. Hoxb5 marks long-term haematopoietic stem cells and reveals a homogenous perivascular niche. *Nature*.

2016;530(7589):223–227.
196. Lin F, Wang N, Zhang TC. The role of endothelial-mesenchymal transition in development and pathological process. *IUBMB Life*. 2012;64(9):717–723.
197. James D, Nam H, Seandel M, et al. Expansion and maintenance of human embryonic stem cell – derived endothelial cells by TGFb inhibition is Id1 dependent. *Nat Biotechnol*. 2010;28(2):161–6.
198. Li Z, Hu S, Ghosh Z, Han Z, Wu JC. Functional characterization and expression profiling of human induced pluripotent stem cell- and embryonic stem cell-derived endothelial cells. *Stem Cells Dev.* 2011;20(10):1701–10.
199. Vodyanik MA, Thomson JA, Slukvin II. Leukosialin (CD43) defines hematopoietic progenitors in human embryonic stem cell differentiation cultures. *Blood*. 2006;108(6):2095–105.
200. Chung NC, Storey JD. Statistical significance of variables driving systematic variation in high-dimensional data. *Bioinformatics*. 2015;31(4):545–554.
201. Toscano MG, Navarro-Montero O, Ayllon V, et al. SCL/TAL1-mediated transcriptional network enhances megakaryocytic specification of human embryonic stem cells. *Mol. Ther.* 2015;23(1):158–70.
202. Woll PS, Morris JK, Painschab MS, et al. Wnt signaling promotes hematoendothelial cell development from human embryonic stem cells. *Blood*. 2008;111(1):122–31.
203. Slukvin II. Deciphering the hierarchy of angiohematopoietic progenitors from human pluripotent stem cells. *Cell Cycle*. 2013;12(5):720–7.
204. Choi K-D, Vodyanik M, Slukvin II. Hematopoietic differentiation and production of mature myeloid cells from human pluripotent stem cells. *Nat. Protoc.* 2011;6(3):296–313.
205. Ditadi A, Sturgeon CM, Tober J, et al. Human Definitive Haemogenic Endothelium and Arterial Vascular Endothelium Represent Distinct Lineages. *Nat. Cell Biol.* 2015;17(5):580–591.
206. Singh KP, Wyman A, Casado FL, Garrett RW, Gasiewicz TA. Treatment of mice with the Ah receptor agonist and human carcinogen dioxin results in altered numbers and function of hematopoietic stem cells. *Carcinogenesis*. 2009;30(1):11–19.
207. Boitano AE, Wang J, Romeo R, et al. Aryl hydrocarbon receptor antagonists promote the expansion of human hematopoietic stem cells. *Science*. 2010;329(5997):1345–8.
208. Martin CH, Woll PS, Ni Z, Zúñiga-Pflücker JC, Kaufman DS. Differences in lymphocyte developmental potential between human embryonic stem cell and umbilical cord blood-derived hematopoietic progenitor cells. *Blood*. 2008;112(7):2730–7.
209. La Motte-Mohs RN, Herer E, Zúñiga-Pflücker JC. Induction of T-cell development from human cord blood hematopoietic stem cells by Delta-like 1 in vitro. *Blood*. 2005;105(4):1431–9.
210. Alter G, Malenfant JM, Altfeld M. CD107a as a functional marker for the identification of natural killer cell activity. *J. Immunol. Methods*. 2004;294(1-

2):15–22.
211. Alter G, Martin MP, Teigen N, et al. Differential natural killer cell-mediated inhibition of HIV-1 replication based on distinct KIR/HLA subtypes. *J. Exp. Med.* 2007;204(12):3027–36.
212. Ni Z, Knorr DA, Bendzick L, Allred J, Kaufman DS. Expression of chimeric receptor CD4ζ by natural killer cells derived from human pluripotent stem cells improves in vitro activity but does not enhance suppression of HIV infection in vivo. *Stem Cells*. 2013;1021–1031.
213. Ng ES, Davis R, Stanley EG, Elefanty AG. A protocol describing the use of a recombinant protein-based, animal product-free medium (APEL) for human embryonic stem cell differentiation as spin embryoid bodies. *Nat. Protoc.* 2008;3(5):768–76.
214. Tian X, Hexum MK, Penchev VR, et al. Bioluminescent imaging demonstrates that transplanted human embryonic stem cell-derived CD34(+) cells preferentially develop into endothelial cells. *Stem Cells*. 2009;27(11):2675–85.
215. Bai H, Gao Y, Arzigian M, et al. BMP4 regulates vascular progenitor development in human embryonic stem cells through a Smad-dependent pathway. *J. Cell. Biochem.* 2010;109(2):363–374.
216. Bai H, Liu Y, Xie Y, et al. Definitive Hematopoietic Multipotent Progenitor Cells Are Transiently Generated From Hemogenic Endothelial Cells in Human Pluripotent Stem Cells. *J. Cell. Physiol.* 2016;231(5):1065–1076.
217. Choi K, Yu J, Smuga-otto K, et al. Hematopoietic and endothelial differentiation of human induced pluripotent stem cells. *Stem Cells*. 2009;27(3):559–567.
218. Dore LC, Crispino JD. Transcription factor networks in erythroid cell and megakaryocyte development. *Blood*. 2011;118(2):231–239.
219. Soza-ried C, Hess I, Netuschil N, Schorpp M, Boehm T. Essential role of c-myb in de fi nitive hematopoiesis is evolutionarily conserved. *Proc. Natl. Acad. Sci.* 2010;107:17340–17308.
220. Ferreira R, Ohneda K, Yamamoto M, Philipsen S. GATA1 function, a paradigm for transcription factors in hematopoiesis. *Mol. Cell. Biol.* 2005;25(4):1215–27.
221. Lohmann F, Bieker JJ. Activation of Eklf expression during hematopoiesis by Gata2 and Smad5 prior to erythroid commitment. *Development*. 2008;135(12):2071–2082.
222. Zhou L. AHR Function in Lymphocytes: Emerging Concepts. *Trends Immunol.* 2016;37(1):17–31.
223. Yagi R, Zhong C, Northrup DL, et al. The transcription factor GATA3 is critical for the development of all IL-7Ra-expressing innate lymphoid cells. *Immunity*. 2014;40(3):378–388.
224. Gori JL, Chandrasekaran D, Kowalski JP, et al. Efficient generation, purification, and expansion of CD34+ hematopoietic progenitor cells from nonhuman primate induced pluripotent stem cells. *Blood*. 2012;120(13):35–45.
225. Flaveny C, Reen RK, Kusnadi A, Perdew GH. The mouse and human Ah receptor differ in recognition of LXXLL motifs. *Arch. Biochem. Biophys.* 2008;471(2):215–223.

226. Flaveny CA, Murray IA, Perdew GH. Differential gene regulation by the human and mouse aryl hydrocarbon receptor. *Toxicol Sci*. 2010;114(2):217–225.
227. Forgacs AL, Dere E, Angrish MM, Zacharewski TR. Comparative analysis of temporal and dose-dependent TCDD-elicited gene expression in human, mouse, and rat primary hepatocytes. *Toxicol. Sci.* 2013;133(1):54–66.
228. White J, Dalton S. Cell cycle control of embryonic stem cells. *Stem Cell Rev*. 2005;1(2):131–138.
229. Neganova I, Zhang X, Atkinson S, Lako M. Expression and functional analysis of G1 to S regulatory components reveals an important role for CDK2 in cell cycle regulation in human embryonic stem cells. *Oncogene*. 2009;28(1):20–30.
230. Barta T, Dolezalova D, Holubcova Z, Hampl A. Cell cycle regulation in human embryonic stem cells: links to adaptation to cell culture. *Exp. Biol. Med. (Maywood)*. 2013;238(3):271–5.
231. Kawajiri K, Kobayashi Y, Ohtake F, et al. Aryl hydrocarbon receptor suppresses intestinal carcinogenesis in ApcMin/+ mice with natural ligands. *Proc. Natl. Acad. Sci. U. S. A*. 2009;106(32):13481–6.
232. Singh KP, Bennett J a, Casado FL, et al. Loss of aryl hydrocarbon receptor promotes gene changes associated with premature hematopoietic stem cell exhaustion and development of a myeloproliferative disorder in aging mice. *Stem Cells Dev.* 2014;23(2):95–106.
233. Roeven MWH, Thordardottir S, Kohela A, et al. The Aryl Hydrocarbon Receptor Antagonist StemRegenin1 Improves In Vitro Generation of Highly Functional Natural Killer Cells from CD34 $^{+}$ Hematopoietic Stem and Progenitor Cells. *Stem Cells Dev.* 2015;24(24):2886–2898.
234. Wagage S, Pritchard GH, Dawson L, et al. The group 3 innate lymphoid cell defect in aryl hydrocarbon receptor deficient mice is associated with T cell hyperactivation during intestinal infection. *PLoS One*. 2015;10(5):1–13.
235. Sonnenberg GF, Artis D. Innate lymphoid cells in the initiation, regulation and resolution of inflammation. *Nat. Med.* 2015;21(7):698–708.
236. Karrich JJ, Cupedo T. Group 3 innate lymphoid cells in tissue damage and graft-versus-host disease pathogenesis. *Curr. Opin. Hematol.* 2016;23(4):410–415.
237. Miller CL, Eaves CJ. Long-Term Culture-Initiating Cell Assays for Human and Murine Cells. *Methods Mol. Med.* 2002;63:123–141.
238. Petzer a L, Hogge DE, Landsdorp PM, Reid DS, Eaves CJ. Self-renewal of primitive human hematopoietic cells (long-term-culture-initiating cells) in vitro and their expansion in defined medium. *Proc. Natl. Acad. Sci. U. S. A.* 1996;93(4):1470–1474.
239. Ferrell, Patrick I, Xi Jiafei, Ma Chao, Adlakha, Mitali KD. The RUNX1 124 Enhancer and P1 Promoter Identify a Unique Subpopulation of Hematopoietic Progenitor Cells Derived from Human Pluripotent Stem Cells. *Stem Cells*. 2015;33:1759–1770.
240. Kaufman DS. Toward clinical therapies using hematopoietic cells derived from human pluripotent stem cells. *Blood*. 2009;114(17):3513–3523.
241. Timmins NE, Nielsen LK. Blood cell manufacture: current methods and future

challenges. *Trends Biotechnol.* 2009;27(7):415–422.
242. Liu Y, Wang Y, Gao Y, et al. Efficient generation of megakaryocytes from human induced pluripotent stem cells using food and drug administration-approved pharmacological reagents. *Stem Cells Transl. Med.* 2015;4(4):309–19.
243. Feng Q, Shabrani N, Thon JN, et al. Scalable generation of universal platelets from human induced pluripotent stem cells. *Stem Cell Reports*. 2014;3(5):817–831.
244. Hermanson DL, Kaufman DS. Utilizing chimeric antigen receptors to direct natural killer cell activity. *Front. Immunol.* 2015;6(APR):1–6.
245. Glienke W, Esser R, Priesner C, et al. Advantages and applications of CAR-expressing natural killer cells. *Front. Pharmacol.* 2015;6(FEB):1–7.

# APPENDIX

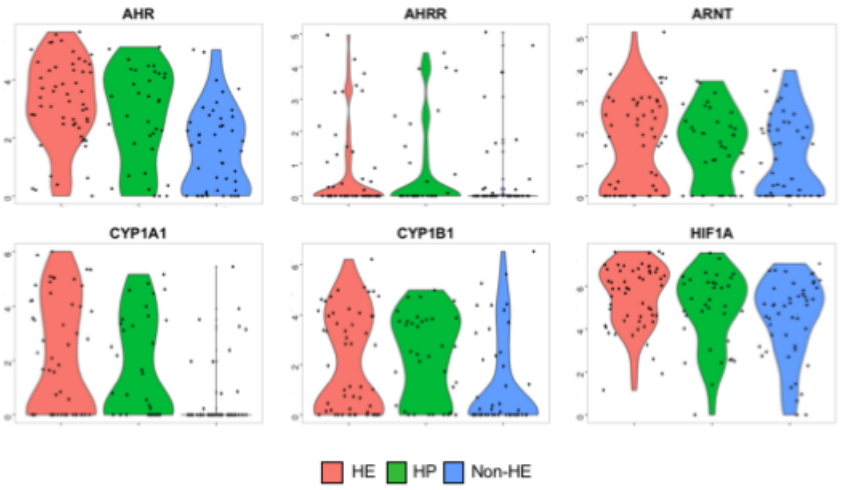


**Appendix 1. Violin plots of AHR-related genes in single hESC-derived hemato-endothelial cells.** Log-transformed FPKM gene expression of hESC-derived HE, non-HE, and HP, as described in Chapter 2. Here, *AHR* and *AHR* downstream effector targets (notably *CYP1A1* and *CYP1B1*) are enriched in hESC-derived HE and HP as compared to non-HE.